

Final Report Compilation for Building Integrated Photovoltaics



TECHNICAL REPORT

October 2003
P-500-03-096-A16



Gray Davis, Governor

CALIFORNIA ENERGY COMMISSION

Prepared By:

Architectural Energy Corporation
Vernon A. Smith
Boulder, CO

*National Institute of Standards and
Technology*

A. Hunter Fanney
Gaithersburg, MD

CEC Contract No. 400-99-011

Prepared For:

Christopher Scruton
Contract Manager

Nancy Jenkins

PIER Buildings Program Manager

Terry Surles

PIER Program Director

Robert L. Therkelsen

Executive Director

DISCLAIMER

This report was prepared as the result of work sponsored by the California Energy Commission. It does not necessarily represent the views of the Energy Commission, its employees or the State of California. The Energy Commission, the State of California, its employees, contractors and subcontractors make no warrant, express or implied, and assume no legal liability for the information in this report; nor does any party represent that the uses of this information will not infringe upon privately owned rights. This report has not been approved or disapproved by the California Energy Commission nor has the California Energy Commission passed upon the accuracy or adequacy of the information in this report.

Acknowledgements

Hunter Fanney, Brian Dougherty, Mark Davis, Eric R. Weise, and Kenneth R. Henderson with NIST conducted this research project. Fred Porter and Vernon Smith with Architectural Energy Corporation provided simulation support for the economic assessment study.

Preface

The Public Interest Energy Research (PIER) Program supports public interest energy research and development that will help improve the quality of life in California by bringing environmentally safe, affordable, and reliable energy services and products to the marketplace.

The Program's final report and its attachments are intended to provide a complete record of the objectives, methods, findings and accomplishments of the Energy Efficient and Affordable Commercial and Residential Buildings Program. This attachment is a compilation of reports from Project 5.1, ***Building Integrated Photovoltaics***, providing supplemental information to the final report (Commission publication #P500-03-096). The reports, and particularly the attachments, are highly applicable to architects, designers, contractors, building owners and operators, manufacturers, researchers, and the energy efficiency community.

This document is one of 17 technical attachments to the final report, consolidating seven research reports from Project 5.1:

- [*Building Integrated Photovoltaic Test Facility \(Mar 2001\)*](#)
- [*Measured Performance Of Building Integrated Photovoltaic Panels \(Feb 2002\)*](#)
- [*Short-Term Characterization Of Building Integrated Photovoltaic Panels \(Feb 2002\)*](#)
- [*Measured Versus Predicted Performance Of Building Integrated Photovoltaics \(Oct 2002\)*](#)
- [*Evaluating Building Integrated Photovoltaic Performance Models \(Oct 2002\)*](#)
- [*Measured Performance Of A 35 Kilowatt Roof Top Photovoltaic System \(May 2003\)*](#)
- [*Economic Assessment of Building Integrated Photovoltaics in California \(Aug 2003\)*](#)

The Buildings Program Area within the Public Interest Energy Research (PIER) Program produced this document as part of a multi-project programmatic contract (#400-99-011). The Buildings Program includes new and existing buildings in both the residential and the nonresidential sectors. The program seeks to decrease building energy use through research that will develop or improve energy-efficient technologies, strategies, tools, and building performance evaluation methods.

For the final report, other attachments or reports produced within this contract, or to obtain more information on the PIER Program, please visit www.energy.ca.gov/pier/buildings or contact the Commission's Publications Unit at 916-654-5200. The reports and attachments, as well as the individual research reports, are also available at www.archenergy.com.

Abstract

Project 5.1, Building Integrated Photovoltaics.

The project was conducted by NIST using laboratory and field tests at its headquarters in Gaithersburg, MD, to develop a validated design algorithm to predict the energy production of building-integrated photovoltaic panels.

- Performance and environmental data were collected for one year on four different BIPV technologies (single-crystalline, poly-crystalline, silicon film, and triple junction amorphous silicon panels), mounted in insulated and uninsulated configurations.
- The results of validated models were used to predict the energy savings possible by using curtain-wall photovoltaic products that are integrated for buildings in high growth areas of California.
- Insulation behind PV panels degrades power production slightly in three out of the four cell technologies tested. The fourth technology showed a very slight improvement in power output due to the insulation.
- The simulations demonstrated that shading will result in a significant reduction in power production from curtain wall BIPV products. In addition, the vertical orientation will adversely affect power production compared to roof-mounted PV systems, particularly during the summer.

This document is a compilation of seven technical reports from the research.

BUILDING INTEGRATED PHOTOVOLTAIC TEST FACILITY

A. Hunter Fanney

ASME Fellow

Building and Fire Research Laboratory
National Institute of Standards and Technology
Gaithersburg, Maryland

Brian P. Dougherty

ASME Member

Building and Fire Research Laboratory
National Institute of Standards and Technology
Gaithersburg, Maryland

ABSTRACT

The widespread use of building integrated photovoltaics appears likely as a result of the continuing decline in photovoltaic manufacturing costs, the relative ease in which photovoltaics can be incorporated within the building envelope, and the fact that buildings account for over 40 percent of the U.S. energy consumption. However, designers, architects, installers, and consumers need more information and analysis tools in order to judge the merits of building-integrated solar photovoltaic products. In an effort to add to the knowledge base, the National Institute of Standards and Technology (NIST) has undertaken a multiple-year project to collect high quality experimental performance data. The data will be used to validate computer models for building integrated photovoltaics and, where necessary, to develop algorithms that may be incorporated within these models. This paper describes the facilities that have been constructed to assist in this effort. The facilities include a mobile tracking photovoltaic test facility, a building integrated photovoltaic “test bed”, an outdoor aging rack, and a meteorological station.

INTRODUCTION

The photovoltaic (PV) power generation market is currently experiencing rapid growth. Worldwide PV module shipments increased 38 percent in 1997 and 29 percent in 1998, as shown in Figure 1. This rapid growth is expected to continue. The international photovoltaic industry is projected to grow at a rate of around 20 percent per year over the next 15 years. It is anticipated that by the year 2010 annual PV shipments could reach 1,600 MW (1999, PV Insider's Report).

Industry analysts estimate that solar power is a \$2 billion business today. The vast majority of present photovoltaic sales are for applications such as navigational signals, call boxes,

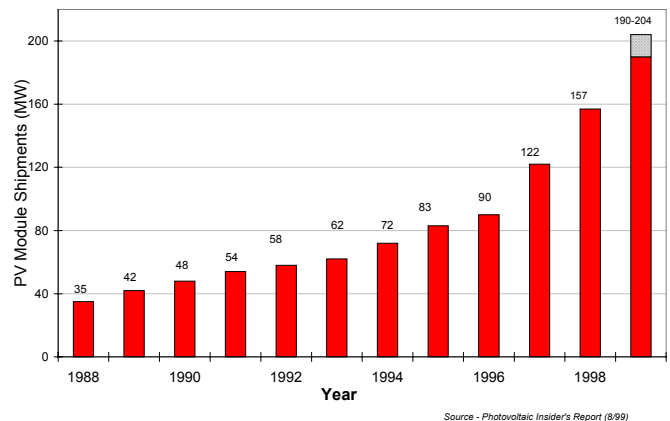


Figure 1 Annual Worldwide PV Module Shipments

telecommunication centers, consumer products, and off-grid electrification projects. More recently, small grid-interactive rooftop installations have started contributing to the demand for PV products. Building-integrated photovoltaic installations will be aided if more information and better design and analysis tools are made available to the building industry and the buying public.

Several factors support the growing interest in building integrated photovoltaic systems. Increased concerns over global warming, President Clinton's *Million Solar Roofs* program, legislation that requires utilities to buy excess energy generated by on-site, distributed power sources, and that 40 percent of U.S. energy consumption is attributed to buildings are all providing incentives to incorporate photovoltaics into buildings.



Figure 2 Building Integrated Photovoltaic Examples
(Source, Paul Maycock)

Figure 2 provides two examples of building integrated photovoltaic products. Residential roofing products are commercially available that incorporate amorphous and crystalline cell technologies. Crystalline cells can be incorporated into fenestration elements, and photovoltaic spandrel panels are available for use in curtain wall applications.

A survey of 900 building professionals in the United Kingdom found that 88 percent would consider the use of integrated photovoltaic building products if there was greater evidence of the performance and reliability of these products (Schoen, 1999). Forty nine percent of the survey respondents noted that they would only consider building integrated products after they had seen them utilized in demonstration sites. Although a similar survey has not been conducted within the U.S., it is anticipated that the results would be comparable.

The Building and Fire Research Laboratory at NIST hopes to accelerate the deployment of building photovoltaics by providing high quality experimental data for the development, validation, and improvement of computer simulation tools. These computer simulation tools will be used to predict the electrical and, in some cases, thermal performance of building integrated photovoltaics. The combination of experimental data and validated computer simulation tools will play a crucial role in economic decisions concerning the future use of photovoltaics in buildings.

APPROACH

Although there are several computer tools for predicting the electrical performance of photovoltaic products, there is a lack of experimental data that can be used to determine how close the predicted results agree with measured performance. Data, if available, are generally limited to a measurement of the total energy delivered by the photovoltaic system. The lack of measured meteorological data and electrical performance data during various meteorological conditions, incident angles, and panel temperatures limits the ability to compare predicted to measured results. As a result of conversations with researchers at Sandia National Laboratory, the National Renewable Energy Laboratory, the Florida Solar Energy Center, and the University of Wisconsin, it became apparent that providing performance

data would fill a void without replicating any current or planned activities. NIST confirmed the need for building integrated photovoltaic performance data by subsequent conversations with manufacturers of photovoltaic cells and of building integrated photovoltaic panels. In addition to supplying the needed data, NIST's building integrated "test bed" will provide the first opportunity to compare the performance of building integrated photovoltaic panels using various cell technologies under identical operating conditions.

One of the existing computer simulation tools used to predict the performance of photovoltaic modules and/or building integrated photovoltaics is PVSIM, an electrical simulation model for photovoltaic cells, modules, and arrays, developed by King et al. (1997) at Sandia National Laboratory. The University of Wisconsin Solar Energy Laboratory has developed PHANTASM (PHotovoltaic ANalysis and TrAnsient Simulation Method) (1999) to study the potential benefits of building integrated photovoltaics. The model uses photovoltaic performance data typically supplied by the manufacturer. ENERGY-10 (2000) computes the annual energy consumption of a user defined building based on hour-by-hour calculations. The program is especially helpful in comparing various design options such as additional insulation, energy efficient lights, daylighting, and passive solar energy. Future versions of ENERGY-10 will include building integrated photovoltaics as a design option. Ultimately these and other models will be used to predict the annual performance and economics of building integrated photovoltaics.

The overall approach being taken at NIST to validate and refine these models is shown in Figure 3. The approach includes short-term characterization of building integrated photovoltaic panels, long-term performance measurements, validation and refinement of the computer simulation models, and studies to document the performance changes that amorphous silicon exhibits as a result of exposure.

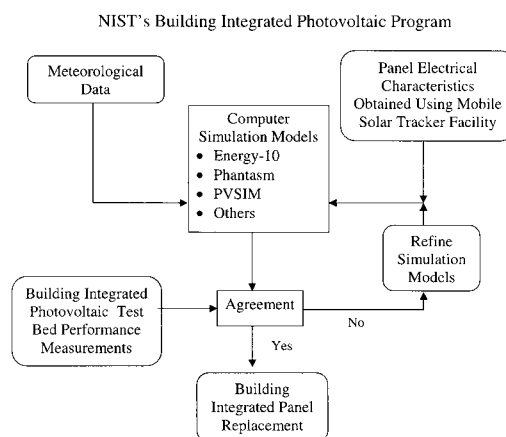


Figure 3 Building Integrated Photovoltaic Program

In order to accurately predict the electrical output of building integrated photovoltaic products, computer simulation models require a number of input parameters. These parameters will be obtained from short-term tests using a mobile solar tracking facility. For example, the model advocated by King (1997) requires the following parameters:

- Influence of solar angle-of-incidence
- Influence of solar spectrum
- Temperature coefficients for the open circuit voltage and maximum power voltage
- Temperature coefficients for the short circuit current and the maximum power current
- Module operating temperature as a function of ambient temperature, wind velocity, and solar radiation

The long-term performance of building integrated photovoltaic panels will be measured “in-situ” using a “test bed” that is located within the south wall of a building located on the NIST campus in Gaithersburg, MD. The facility will provide comparisons between different building integrated photovoltaic panels when exposed to identical meteorological conditions. Comparisons based on energy production, operating temperature, heat flux, and characteristic current versus voltage (IV) curve traces will be available. This “test bed” initially consists of crystalline, polycrystalline, amorphous, and silicon film building integrated photovoltaic products. Two identical panels of each photovoltaic cell technology, one insulated and one un-insulated, are installed.

Using the short-term characterization results, obtained from the solar tracker facility, and the measured long-term performance of the “in-situ” building integrated photovoltaic products, NIST researchers will exercise the currently available simulation models and compare predicted to measured results. The meteorological data will be provided by the combination of a rooftop meteorological station and a south wall meteorological station. NIST researchers will work closely with the models’ authors to improve and refine them in order to obtain acceptable agreement with measured results.

An additional challenge in the validation of predictive models for amorphous silicon building integrated photovoltaic products are changes in electrical performances attributed to outdoor exposure. In order to explore the magnitude of the performance change over time, an aging facility has been constructed. The amorphous panels installed at this facility will be initially characterized using the mobile solar tracking facility prior to exposure on the aging facility. The panels will be installed on the aging facility and removed on a periodic basis for additional testing on the mobile tracking facility. The resulting information will be used to determine the radiation and/or temperature exposure required before steady-state performance is achieved.

EXPERIMENTAL FACILITIES

Mobile Solar Tracking Facility

The mobile solar tracking facility is used to characterize the electrical performance of building integrated photovoltaic panels (Figure 4). Software has been developed for the mobile solar tracker that allows the user to select from the following tracking modes:

- Azimuth and Elevation Tracking
- Azimuth Tracking
- Elevation Tracking
- Azimuth Tracking with User Selected Offset
- Elevation Tracking with User Selected Offset
- User Selected Incident Angle Tracking



Figure 4 NIST's Mobile Solar Tracking Facility

In addition to the various tracking modes, the software is used to move the tracker to a fixed position, facilitate aligning the tracker with regard to true south, and setting limits on the tracker movement to preclude damage to the tracker and/or building integrated photovoltaic panels. Stepping motors in combination with spool drive systems permit movements as small as 0.1° and 0.2° in azimuth and elevation, respectively. A servo-controller interfaces the stepping motors to a personal computer.

Deployment begins by positioning the tracker in the direction of true south and then manually leveling it. The tracker is then aligned to magnetic south using a digital magnetic compass. Once magnetic south is established true south is established using the magnetic declination. Experience has shown that this technique results in misalignments of 1° or less. Final alignment is achieved by using the diopter incorporated within a pyrheliometer. The azimuth and elevation angles of the sun are computed on a real time basis using equations set forth by Duffie and Beckman (1991). Design specifications for the tracking facility are given in Table 1.

Table 1 NIST Mobile Solar Tracker Facility Specifications

Azimuth Range	+/- 135° from center
Elevation Range	90° from horizontal
Pointing Accuracy	+/- 0.1° in wind up to 11 m/s
Maximum Backlash	0.05°
Slew Rate	2° to 10° per second, user defined
Survival Wind Speed	18 m/s
Maximum Collector Weight	140 kg
Platform Tilt Adjustment	Leveling Jacks, 0.1E Resolution
Weight (Unloaded)	900 kg
Tracking Communications	RS-232 interface

The mobile solar tracking facility incorporates meteorological instruments, a solar spectroradiometer, a data acquisition system, and a single-channel photovoltaic curve tracer. Precision spectral pyranometers are used to measure total (beam plus diffuse) solar radiation. The pyranometer's detectors, optically black thermopile sensors, are independent of radiation wavelength over the solar energy spectrum. Two instruments are used to provide redundant measurements. A pyrliometer is used to measure the beam component of solar radiation. The detector, a multi-junction thermopile, coated optically black, is positioned at the end of a collimating tube. The operature angle of the instrument, 5.7°, receives radiation from the sun and an area of the circumsolar sky two orders of magnitude larger than that of the sun. Long-wave radiation greater than 3 μm is measured using a precision infrared radiometer.

A three-cup anemometer assembly is used to measure wind speed. The wind sensor has a speed threshold of 0.2 m/s and has a maximum speed of 55 m/s. The wind direction sensor consists of a counter-balanced, lightweight vane and a precision, low torque, potentiometer yielding a voltage output proportional to wind direction. The ambient temperature is measured using a perforated tip, type-T thermocouple sensor enclosed in a naturally ventilated multi-plate radiation shield.

The output signals of the meteorological instruments and thermocouples attached to the building integrated photovoltaic panels are measured using a data acquisition system. The data acquisition system incorporates a 6 ½ - digit multi-meter, IEEE 488 and RS 232 interfaces, and multiplexing relay cards that can accommodate up to 60 transducers. It can be used to measure voltage, resistance, current, and frequency. Although the multiplexer cards have built-in thermocouple reference junctions, improved accuracy is obtained through the use of an electronic ice point reference. The reference temperature is established by the physical equilibrium of ice and water within a sealed vessel.

Spectral radiation data from 300 to 1100 nm is obtained using a spectroradiometer with selectable scan intervals of 1, 2,

5, or 10 nm. The optical receptor has a 180° field of view. A filter wheel is used to filter out light that is not in the same region of the spectrum as that being measured. Operation of the filter wheel is controlled by an internal microprocessor. The polychromatic radiation transmitted through the filter wheel is dispersed into narrow wavebands by a monochromator. After emerging from the monochromator, the radiant power is received by a silicon photodiode detector that produces a current proportional to the amount of radiation. The current signal is amplified, converted to a voltage, and passed through an analog-to-digital converter.

The solar tracker's photovoltaic array tester measures and records the current versus voltage (IV) characteristics of photovoltaic panels. The tester is capable of measuring panels or groups of panels with power outputs ranging from 10 watts to 36 kilowatts. Irradiance from a reference cell and a thermocouple attached to the panel are recorded and used to normalize the data to a user-selected irradiance and temperature. In addition to sweeping the panel IV curve and storing the measured values, the curve tracer calculates the values of maximum output power, open circuit voltage, short circuit current, and fill factor.

Building Integrated Photovoltaic Test Bed

The building integrated photovoltaic test bed was created by removing five adjacent windows from the south wall of a building located on NIST's Gaithersburg, MD campus. All five windows are part of a high-bay laboratory and exposed to identical indoor environmental conditions. The original window framing system was modified to facilitate the installation and removal of building integrated photovoltaic test specimens. The front of each panel is recessed 8 mm from the frame's outer surface. An exterior view of the "test bed" and the eight building integrated photovoltaic panels chosen for the initial evaluation are shown in Figure 5. A horizontal aluminum shelf was added to partition each window into two test cells. One lower test cell was further divided by adding a vertical aluminum partition. The end product is a south wall test bed composed of 11 test cells.

Building integrated photovoltaic panels selected for the "test bed" include custom-made panels using crystalline, polycrystalline, and silicon film cells as well as commercially available amorphous silicon modules. Specifications for the building integrated photovoltaic panels are given in Table 2. Three of the five window openings have the horizontal shelf positioned at the vertical midpoint of the opening. Two identical panels, utilizing crystalline, polycrystalline, or silicon film cells, are installed, one above the other, in the resulting six openings. The upper panels are not insulated. The lower panels are insulated with 10.2 cm of extruded polystyrene. Each of these six panels are 1.38 m by 1.18 m. For the remaining two windows, the horizontal shelf is positioned below the vertical midpoint. Tandem, commercially available, amorphous silicon PV modules, having overall measurements of 1.37 m by 1.48 m, are installed in the upper test cells of both

Table 2 Building Integrated Photovoltaic Panel Specifications

Cell Efficiency (%)	13	8.7	12	6.9
Cell Technology	Single Crystalline	Silicon Film	Poly Crystalline	Tri Junction Amorphous
Cell Dimensions (mm)	125 x 125	150 x 150	125 x 125	120 x 350
Number of Cells	72	56	72	44
Total Cost	\$1324	\$995	\$1123	\$578
Price per Watt	\$8.71	\$10.70	\$8.44	\$4.52
Rated Power Output (W)	152	93	133	128
Glazing Covered by PV Cells (%)	72	82	72	92

windows. The east amorphous silicon panel is insulated with 10.2 cm of extruded polystyrene insulation. The west amorphous silicon panel is un-insulated.

Two of the three remaining test cells are allocated to instrumentation. A black, 1.38 m x 0.87 m plexiglass panel accommodates up to three precision spectral pyranometers, one precision infrared radiometer, and two radiatively shielded type-T thermocouples. An ultrasonic wind sensor, used to measure the magnitude and direction of air movement in a vertical plane is mounted in the second test cell.

The final test cell contains a scaled-down version of the single crystalline building integrated photovoltaic panel specified in Table 2. The backside of this panel is not insulated.

In an effort to investigate the thermal performance of building integrated PV panels, heat flux transducers were attached to the four panels having backside insulation and to the scaled-down, un-insulated PV panel. Heat flux transducers were not added to the un-insulated, paired panels because of concerns that the transducer may alter each panel's electrical performance due to changes induced in the panel's temperature profile. Finite element calculations revealed that the addition of the heat flux transducer to the un-insulated panels would alter the temperature of adjacent cells by as much as 1°C. Similar analysis for the insulated panels showed virtually no impact on cell-to-cell temperature variation. As a hedge, the scaled-down PV panel was added and instrumented with a heat flux transducer to provide some data on the thermal performance of un-insulated PV panels.

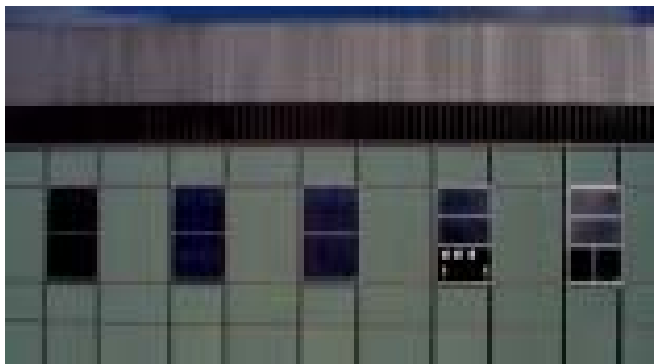


Figure 5 Building Integrated Photovoltaic Testbed

Heat flux transducers having active areas of 250 mm x 250 mm and 305 mm x 305 mm are being used. These transducers, which have total areas twice their active areas, were selected because they completely cover an integer number of photovoltaic cells. In addition to the noted installations on PV panels, a heat flux transducer was also mounted on the curtain wall that separates each of the test cells. The heat flux transducers were calibrated using the NIST 1-meter guarded hot plate prior to installation (Zarr, TBP).

As summarized in Table 3, multiple temperature sensors are installed on each PV panel. Sensor locations include the rear of each panel and, where applicable, the rear face of the heat flux transducer and the rear face of the attached insulation. Figure 6 depicts the setup used on the insulated panels. The panels utilizing crystalline, polycrystalline, and silicon film cells, in addition, were fabricated with two sensors embedded within each panel to measure actual cell temperature. All of the noted temperature sensors are foil-type, type-T thermocouples. Each temperature sensor was individually calibrated prior to installation.

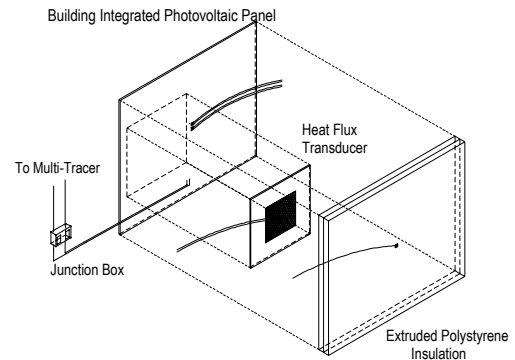


Figure 6 Instrumentation Schematic

Two instrumentation systems are used to monitor the building integrated photovoltaic test bed. The test bed data acquisition system, identical to one used on the mobile solar tracking facility, is used to measure the output signals of the outdoor meteorological instruments (with the exception of one precision spectral pyranometer and an outdoor ambient temperature sensor), the heat flux transducers, the panel temperature sensors (Table 3), and two radiatively shielded indoor ambient temperature sensors. This data acquisition system scans the sensors and records the data every five minutes. The second data acquisition system is a custom built photovoltaic measurement system and is referred to as a multi-tracer.

The multi-tracer simultaneously loads and collects electrical performance data on multiple PV panels. The multi-tracer can operate with a maximum of 14 panels connected while dissipating up to 2400 watts. User selectable load options include: (1) peak power tracking, (2) fixed voltage operation, (3) user specified voltage profile, and (4) unloaded or open

Table 3 Location of Panel Temperature Sensors

Temperature Sensor Location	Custom-built PV panel	Commercial PV Panel
Embedded Behind PV Cell: Connected	X	
Embedded Behind PV Cell: Disconnected (Spare)	X	
Indoor-Side of Test Panel: Connected to Test Bed DAS	X	X
Indoor-Side of Test Panel: Connected to Multi-Tracer	X	X
Rear Face of Heat Flux Transducer	X ¹	X ¹
Rear Face of Backside Insulation	X ²	X ²
¹ For PV panels where a heat flux transducer is installed.		
² For PV panels installed with backside insulation		

circuited. For NIST's initial long-term studies, peak power tracking is being used. When operated in this mode, the multi-tracer maintains the power output of each PV panel within 0.2% of the maximum power output by making continuous load setting adjustments (Raydec, 1998).

The multi-tracer samples panel temperature, current, and voltage every 15 seconds and then integrates the readings, along with instantaneous power, over time before recording mean values of each parameter to disk. A user-specified averaging interval of 5 minutes is used for the eight paired "test bed" PV panels. In a follow-up data reduction step, the mean power quantities are used to determine daily energy production. A digital power analyzer, connected between the multi-tracer and a PV panel, provides a redundant measurement for the 5-minute-interval and daily energy produced by one test panel.

The multi-tracer also collects current versus voltage (IV) traces. Presently, the multi-tracer is configured to record an IV trace for each PV panel every five minutes if the measured irradiance exceeds a threshold value of 5 W/m². The multi-tracer typically requires less than 45 seconds to complete the eight IV traces of the paired panels. The IV data associated with each panel is saved to a unique data file. The file contains up to 257 IV data pairs along with irradiance, panel temperature, and outdoor ambient temperature measurements recorded before and after collecting the IV data. Also included in each file is the short circuit current, open circuit voltage, peak power, current at peak power, voltage at peak power, fill factor, system efficiency, aperture efficiency, a time stamp, and several other parameters that contribute to providing a stand-alone summary of the panels instantaneous electrical performance. Overall, the test bed provides extensive electrical and thermal data for characterizing the performance of building integrated photovoltaic panels.

Meteorological Station

The computer simulation tools require meteorological data in order to predict the electrical performance of building integrated photovoltaic panels. This data is being provided by two meteorological stations, a complete rooftop station and the test bed meteorological station previously described.

The roof top meteorological station, Figure 7, incorporates an automated solar tracker and instruments to measure solar radiation, ambient temperature, and wind conditions. Two pyrheliometers are mounted on an automated solar tracker and are used to measure the solar radiation's beam component. The automated solar tracker is a two-axis azimuth/elevation device programmed to align the solar radiation instruments with the normal incidence of the sun. The tracking is achieved using a computer program that calculates the solar position for the time and location and subsequently transmits pulses to electronic drives, which operate two stepping motors. In addition to the pyrheliometers, a precision spectral pyranometer and shading disk are also mounted on the automated solar tracker. The shading disk is positioned such that the precision spectral pyranometer on the tracker is continuously shaded, providing a measurement of the of solar radiation's diffuse component.

A pair of redundant precision spectral pyranometers, mounted on a horizontal surface near the automated solar tracker, is used to measure global solar radiation. Long-wave radiation, beyond 3 μ m, is measured using a precision infrared radiometer. Wind speed and direction are measured using a three-cup anemometer and wind direction sensor. A sheathed type-T thermocouple sensor, enclosed in a naturally ventilated multi-plate radiation shield, is used to measure ambient temperature. The output signals from the meteorological station's instruments are measured using a data acquisition system identical to the one used on the solar tracking facility. A personal computer interfaced to the data acquisition system permits viewing of real time and historical weather data by means of a local area network.

**Figure 7 Roof Top Meteorological Station**

Aging Facility

A series of indoor and outdoor stability studies, Hof et al. (1996), Klotz et al. (1988), von Roedern and Kroposki (1996), have shown that the electrical performance of amorphous silicon degrades with solar and/or temperature exposure. This shift in performance presents an additional challenge in attempting to predict the annual energy production of building integrated photovoltaic panels that utilize amorphous silicon. Parameters obtained from the initial short-term tests to characterize the panels may not be appropriate for long-term performance predictions.

In order to assess the magnitude of performance changes as a result of exposure, data are being gathered on three amorphous silicon panels mounted on an outdoor exposure rack, Figure 8. The exposure rack faces true south and has a tilt angle of 40°, which is the rack's incremental setting that is closest to the site's latitude, 39°. The three amorphous silicon panels exposed on the rack are identical to those being evaluated within the building integrated photovoltaic test bed. Each panel and its associated backside insulation, if used, is supported by a 6.4 mm thick piece of aluminum plate that extends 100 mm beyond the panel's perimeter. In order to subject the panels to three different temperatures during outdoor exposure, one panel is attached directly to the aluminum plate, whereas extruded insulation having nominal thicknesses of 25 mm and 102 mm is placed between the second and third panels, and the aluminum plates, respectively.

A calibrated type-T thermocouple is attached to the center of each panel's rear surface. A precision spectral pyranometer is used to measure the incident radiation on the aging rack. An ultraviolet radiometer is used to measure radiation present between 295 and 385 μm . Located in close proximity to the aging rack are a radiation-shielded thermocouple and a wind station to measure ambient temperature and wind conditions. The output signals from the thermocouples and meteorological instruments are measured using a data acquisition system and electronic ice point reference cell identical to those previously described for the mobile solar tracking facility.

Figure 8 Aging Facility



The electrical performance of the three panels was initially measured using the mobile solar tracking facility. At periodic

intervals, the panels will be removed and re-characterized on the tracking facility to determine the magnitude, if any, of performance changes due to exposure.

The computer used with this facility, as well as the computers used in all of the other building-integrated photovoltaic test facilities are automatically time synchronized with the NIST atomic clock.

SUMMARY

The widespread use of building integrated photovoltaics appears likely as a result of the rapid growth that photovoltaics is experiencing, the relative ease in which photovoltaics can be incorporated within a building, and the fact that buildings account for over 40 percent of the United States' energy consumption. Obstacles to the proliferation of building integrated photovoltaics include the lack of validated computer simulations to predict the electrical performance of building integrated photovoltaics and an insufficient database on how well these products perform. Economic decisions regarding the use of building integrated photovoltaics are dependent upon the availability of accurate simulation tools and the availability of product performance data, especially under representative field installation conditions. NIST's Building and Fire Research Laboratory hopes to accelerate the deployment of building integrated photovoltaics by providing high quality experimental data for the development, validation, and improvement of computer simulation tools.

A mobile photovoltaic solar tracking facility, a building integrated photovoltaic "test bed", an outdoor aging rack, and meteorological stations have been constructed to assist in this effort. The mobile solar tracking test facility is used to capture the effects of specific parameters, such as incident angle, panel temperature, and solar spectrum, on the panel's electrical performance. The building integrated photovoltaic "test bed" is used to conduct side-by-side comparisons of building integrated wall panels. The outdoor aging rack is used, in conjunction with the mobile tracking facility, to investigate the magnitude of electrical performance changes in amorphous silicon panels as a result of exposure to outdoor conditions. The meteorological stations are equipped to measure solar radiation, wind, and temperature conditions during the performance monitoring of the building integrated photovoltaic panels.

Building integrated photovoltaic panel characteristics obtained using the mobile solar tracking facility and the measured meteorological data will be used in conjunction with simulation tools to predict the electrical performance of building photovoltaics installed in the test bed. The predicted performance will be compared to measured data from the building integrated photovoltaic test bed in order to evaluate the prediction capabilities of the simulation tools.

ACKNOWLEDGEMENTS

The authors would like to acknowledge Gerald Ceasar of NIST's Advanced Technology Premium Power Program and the California Energy Commission for providing financial support for this project. Gratitude is extended to the following NIST personnel who have assisted the authors: Stanley T. Morehouse for his role in fabricating the various facilities described within this paper; Mark Davis and Daniel Vennetti for developing the software used to operate the mobile solar tracking test facility; Daniel Vennetti and Susan Fioravante for collecting and reducing experimental data; William Healy for development of the web based meteorological software; and Paula Svincek for manuscript preparation.

REFERENCES

- 1999, "Markets: Worldwide PV Module Output Heading for Record 190-204 MW Range in 1999", *"Photovoltaic Insider's Report"*, Vol. XVIII No. 8, pg's 1 & 6.
- 1999, Photovoltaic Analysis and TrAnsient Simulation Method (PHANTASM), Building Integrated Photovoltaic Simulation Software, Solar Energy Laboratory, University of Wisconsin, Madison, WI.
- Duffie, J.A., and Beckman, W.A., 1991, *"Solar Engineering of Thermal Processes"*, 2nd. Ed., John Wiley and Sons, New York, pp. 768-794.
- ENERGY-10, V1.3, 2000, "A Tool for Designing Low Energy Buildings", Sustainable Buildings Energy Council, Washington, D.C.
- Hof, C., Ludi, M., Goetz, M., Fischer, D., Shah, A., 1996, "Long Term Behaviour of Passively Heated or Cooled A-SI:H Modules", *Proceedings of the 25th IEEE Photovoltaics Specialists Conference 1996*, Washington, D.C., May 13-17, 1996, pp. 1057-1060
- King, D.L., Dudley, J.K., and Byoson, W.E., "PVSIM: A Simulation Program for Photovoltaic Cells, Modules, and Arrays", *Proceedings of the 26th IEEE Photovoltaics Specialists Conference*, Anaheim, CA, 9/29/97-10/3/97.
- King, D.L., "Photovoltaic Module and Array Performance Characterization Methods for All system Operating Conditions", *Proceedings of the National Renewable Energy Laboratory/Sandia National Laboratory Photovoltaics Program Review Meeting*, November 18-22, Lakewood, CO, AIP Press, New York, 1997.
- Klotz, F.H., Massano, G., Sarno, A. Zavarese, L., 1988, "Determination and Analysis of the Performance and Degradation of a Si Modules Using Outdoor, Simulator and Open-Circuit-Voltage-Decay (OCVD) Measurements", *Proceedings of the 20th IEEE Photovoltaics Specialists Conference 1988*, Las Vegas, NV, September 26-30, 1988, Vol 1, pp. 301-306.
- Maycock, P., *"Photovoltaics in Buildings"*, Slide Kit PV-8.
- Raydec, "Photovoltaic Operations and Maintenance Manual", Version 4.0, November 1998.
- Schoen, T. J., 1999, "Information", *Renewable Energy World*, Vol. 2, No. 5, p. 84.
- von Roedern, B., and Kroposki, B., "Can the Staebler-Wronski Effect Account for the Long-Term Performance of a-SI PV Arrays?", *NREL/SNL Photovoltaics Program Review, Proceedings of the 14th Conference-A Joint Meeting*, AIP 394, pp. 313-322.
- Zarr, R.R., Martinez-Fuentes, V., , Filliben, J.J., and Dougherty, B.P., "Calibration of Thin Heat Flux Sensors for Building Applications Using ASTM C1130", *ASTM Journal of Testing and Evaluation*, To Be Published.

MEASURED PERFORMANCE OF BUILDING INTEGRATED PHOTOVOLTAIC PANELS

A. Hunter Fanney

Heat Transfer and Alternative Energy Systems Group
National Institute of Standards and Technology
Gaithersburg, Maryland

Brian P. Dougherty

Heat Transfer and Alternative Energy Systems Group
National Institute of Standards and Technology
Gaithersburg, Maryland

Mark W. Davis

Heat Transfer and Alternative Energy Systems Group
National Institute of Standards and Technology
Gaithersburg, Maryland

ABSTRACT

The photovoltaic industry is experiencing rapid growth. Industry analysts project that photovoltaic sales will increase from their current \$1.5 billion level to over \$27 billion by 2020, representing an average growth rate of 25 % [1]. To date, the vast majority of sales have been for navigational signals, call boxes, telecommunication centers, consumer products, off-grid electrification projects, and small grid-interactive residential rooftop applications.

Building integrated photovoltaics, the integration of photovoltaic cells into one of more of the exterior surfaces of the building envelope, represents a small but growing photovoltaic application. In order for building owners, designers, and architects to make informed economic decisions regarding the use of building integrated photovoltaics, accurate predictive tools and performance data are needed. A building integrated photovoltaic test bed has been constructed at the National Institute of Standards and Technology to provide the performance data needed for model validation. The facility incorporates four identical pairs of building integrated photovoltaic panels constructed using single-crystalline, polycrystalline, silicon film, and amorphous silicon photovoltaic cells. One panel of each identical pair is installed with thermal insulation attached to its rear surface. The second paired panel is installed without thermal insulation. This experimental configuration yields results that quantify the effect of elevated cell temperature on the panels' performance for different cell technologies.

This paper presents the first set of experimental results from this facility. Comparisons are made between the electrical performance of the insulated and non-insulated panels for each of the four cell technologies. The monthly and overall conversion efficiencies for each cell technology are presented and the seasonal performance variations discussed. Daily efficiencies are presented for a selected month. Finally, hourly plots of the power output and panel temperatures are presented and discussed for the single-crystalline and amorphous silicon panels.

INTRODUCTION

More than two-thirds of the electricity in the United States is consumed by residential and commercial buildings [1]. The incorporation of photovoltaics into buildings, referred to as building integrated photovoltaics (BIPV) offers an aesthetically pleasing means of displacing centrally located utility generated power with distributed renewable energy. Building integrated photovoltaics replace conventional building elements such as roof tiles, asphalt shingles, façade elements, and shading devices with photovoltaic modules that perform the same functions but also provide electrical power.

In addition to concerns over first costs, a barrier to the wide spread proliferation of BIPV is the lack of performance data. A survey of 900 building professionals in the United Kingdom found that 88 % would consider the use of integrated photovoltaic building products if there was greater evidence of the performance and reliability of these products [2]. Forty nine percent of the survey respondents noted that they would only consider building integrated products after they had seen them

utilized in demonstration sites. Although a similar survey has not been conducted within the U.S., it is anticipated that the results would be comparable. An additional barrier to BIPV implementation is the lack of predictive performance tools to quantify the achievable energy savings. These predictive tools are needed by building owners, architects, and designers in order to make decisions concerning the economic viability of BIPV.

NIST's Building and Fire Research Laboratory hopes to accelerate the deployment of BIPV by addressing the need for performance data and validated performance models. A "test-bed" located in Gaithersburg, MD, will provide side-by-side comparisons of BIPV panels using different cell technologies and levels of thermal insulation. The resulting data will be compared to predictive models being developed by others including PVSIM [3], PHANTASM (PHotovoltaic ANalysis and TrAnsient Simulation Method) [4], Energy-10 [5], and IV Tracer [6].

APPROACH

NIST's Building Integrated Photovoltaic program is shown schematically in Fig. 1. The program consists of short-term testing to characterize the electrical performance of BIPV panels that utilize various cell technologies, modeling to predict the annual energy production of the characterized panels, and long-term performance monitoring of the BIPV panels under real world conditions.

In order to accurately predict the electrical output of BIPV systems, the panel's electrical response to various parameters must be known. The number of required electrical characteristics varies with the simulation model being used. For example, the model advocated by King [7] requires the following parameters:

- Influence of solar angle-of-incidence
- Influence of solar spectrum
- Temperature coefficients for the open circuit voltage and maximum power voltage
- Temperature coefficients for the short circuit current and the maximum power current
- Module operating temperature as a function of ambient temperature, wind velocity, and solar radiation

These parameters will be obtained from short-term tests using a mobile solar tracking facility [8]. The electrical characteristics obtained from the solar tracker and measured meteorological data will be supplied to simulation models. The predicted electrical energy produced by the various BIPV technologies will be compared to the measurements from NIST's BIPV "test-bed", the subject of this paper. In addition to providing validation data, the BIPV test-bed will provide side-by-side comparisons of various cell technologies under real world conditions. Discrepancies between measured and

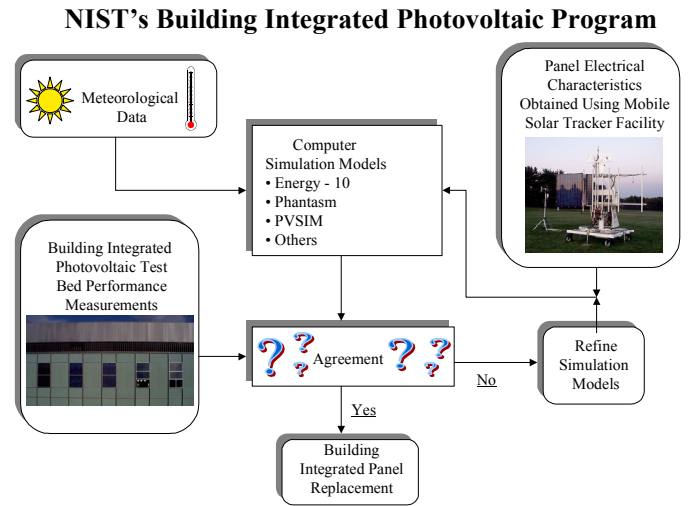


Figure 1

modeled results will be reported to the authors of the simulation models. The end result will be predictive performance tools that can be used with confidence to assess the energy savings potential of BIPV.

BUILDING INTEGRATED PHOTOVOLTAIC TEST FACILITY

A facility has been built to provide experimental data needed to validate and improve predictive performance tools for building integrated photovoltaic panels. This building integrated photovoltaic "test bed" is located on the south wall of NIST's Building Research building, Fig. 2. This facility was created by removing five adjacent windows and modifying the framing system to facilitate the installation and removal of building integrated photovoltaic panels. A moveable horizontal shelf partitions each opening into two test cells, permitting up to ten panels to be tested simultaneously. Each panel's front surface is mounted as close to the front surface of the surrounding framework as possible in order to minimize shading.



Figure 2 Photovoltaic BIPV Test-Bed

Table 1 Building Integrated Photovoltaic Panel Specifications				
Cell Technology	Single Crystalline	Poly Crystalline	Silicon Film	Triple-Junction Amorphous
Panel Dimensions (m x m)	1.38 x 1.18	1.38 x 1.18	1.38 x 1.18	1.37 x 1.48
Front Cover	6 mm glass	6 mm glass	6 mm glass	Tefzal
Encapsulant	EVA	EVA	EVA	
Backsheet/Color	Tedlar/Charcoal	Tedlar/Charcoal	Tedlar/Charcoal	Stainless Steel
Cell dimensions (mm x mm)	125 x 125	125 x 125	150 x 150	119 x 340
Number of Cells (in series)	72	72	56	44
Adjacent Cell Spacing (mm)	2	2	2	
Vertical Border Width(mm)	100	100	51	8
Top Border Height(mm)	72	72	55	11
Bottom Border(mm)	70	70	29	5
Recessed Distance to PV Cell (mm)	12	12	12	9
Glazing Covered by PV Cells %	63	69	80	88
Total Cost (\$)	1324	1123	995	578
Price/Watt(\$/W)	8.66	8.43	10.75	4.52
Rated Power (W)	153	133	93	128
Cell Area (m ²)	1.020	1.128	1.341	1.780
Aperture Area (m ²)	1.682	1.682	1.682	2.108
Coverage Area (m ²)	1.160	1.160	1.371	1.815

The eight BIPV panels selected for the initial one-year study include custom-fabricated single-crystalline, polycrystalline, and silicon film panels and commercially available amorphous silicon modules. Specifications for each panel are given in Table 1. Two identical custom fabricated panels are installed, one above the other, in six of the test cells. Tandem, commercially available, amorphous silicon modules are installed in the upper area of two openings. The lower areas of these two openings are allocated to meteorological instrumentation and a building integrated photovoltaic panel used exclusively for heat flux measurements. Extruded polystyrene insulation, having a thickness of 10.2 cm and a thermal resistance of 3.46 m²·K/W [9], is attached to the rear surface of the lower custom fabricated panels and to one set of the amorphous silicon modules.

The custom made panels were fabricated by a firm that specializes in BIPV panels for commercial and residential applications. Design considerations included incorporating borders that would minimize shading on the cells, the use of readily available cells, and cell interconnections that result in an electrical configuration compatible with monitoring equipment. A representative panel's cross section is shown in Fig. 3. Individual amorphous silicon cells were not available for incorporation within a custom fabricated panel. Fortunately, commercially available triple-junction amorphous modules were available that could easily be incorporated

within the test facility. Each of the two amorphous silicon panels within the test facility consists of two modules. It should be noted that the costs given in Table 1 reflect the fact that the amorphous panels were "off-the-shelf" items whereas the other BIPV panels were custom fabricated.

INSTRUMENTATION

Validation of predictive computer simulation tools requires measurement of each building integrated photovoltaic panel's electrical performance and meteorological conditions coincident with the electrical measurements. In addition to these measurements, temperatures associated with each panel and the heat flux through selected panels are measured.

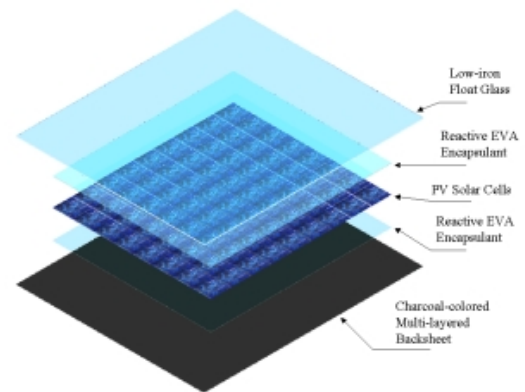


Figure 3 BIPV Panel Cross Section

The electrical performance of each building integrated photovoltaic panel is measured using a multi-curve tracer. This instrument continuously operates each panel within 0.2 % of its maximum power point [10]. While max power tracking, the multi-tracer is set up to measure, every 15 s, the instantaneous voltage and current from which power is derived. The multi-curve tracer also records the incident irradiance, using a precision spectral radiometer, rear panel temperature, and outdoors ambient temperature as part of the 15 s scans. Every 5 min, the 15 s readings are averaged and saved. In addition to these data, the multi-curve tracer obtains a current versus voltage (IV) trace for each panel every five minutes when the irradiance is above a minimum threshold of 15 W/m². The short circuit current, open circuit voltage, peak power, current at peak power, voltage at peak power, fill factor, and electrical efficiency are automatically computed. Incident irradiance, rear panel temperature, and outdoor temperature are recorded before and after each I-V trace.

One objective of NIST's BIPV Program is to measure the thermal performance of the building integrated photovoltaic panels. This is being done through the use of heat flux transducers attached to selected panels. The resulting measurements will be compared to predicted heat fluxes that would have occurred if conventional building materials were used. The actual heat flux measurements will be the subject of a subsequent publication and are not discussed within this paper. During the design of the test facility, a finite element analysis revealed that the use of heat flux transducers on non-insulated panels could alter the cell temperatures under the heat flux transducer as much as 1 °C relative to the surrounding cells. The researchers were concerned that the resulting non-uniform temperature distribution would alter the panel's electrical performance. For this reason, heat flux transducers were only attached to the insulated panels as the thermal resistance of the heat flux transducer is small compared to the thermal insulation. In order to measure the heat flux that occurs through the non-insulated panels, an extra non-insulated panel with an attached heat flux transducer was added to the facility. This panel is identical in construction to the paired single-crystalline BIPV panels, with the exception of its smaller size. The sole purpose of this extra panel is to measure the heat flux through a non-insulated BIPV panel. The electrical measurements from this extra panel will not be used for validating electrical performance algorithms.

Multiple foil-type, type-T thermocouples are installed on each building integrated photovoltaic panel. These sensors are located on the rear of each panel, the rear face of the heat flux transducer (if present), and the rear surface of the attached insulation. During fabrication of the single-crystalline, polycrystalline, and silicon film panels, thermocouples were attached to the rear surface of two cells within each panel. Each temperature sensor was individually calibrated prior to installation.

Predictive simulation tools require meteorological data in order to predict the electrical performance of building integrated photovoltaic panels. Two meteorological stations, a complete roof top station and a "test-bed" meteorological station are providing this data. The roof top meteorological station incorporates an automated solar tracker and instruments to measure solar radiation, ambient temperature, and wind conditions. The automated solar tracker is a two-axis azimuth/elevation device programmed to align the solar radiation instruments with the normal incidence of the sun. Two pyrheliometers are mounted on the automated solar tracker and are used to measure the solar radiation's beam component. A precision spectral pyranometer and shading disk are also mounted on the automated solar tracker. The shading disk is positioned such that the precision spectral pyranometer on the tracker is continuously shaded, providing a measurement of the solar radiation's diffuse component.

A pair of redundant precision spectral pyranometers, mounted on a horizontal surface near the automated solar tracker, is used to measure global solar radiation. Long-wave radiation, beyond 3 μm , is measured using a precision infrared radiometer. Wind speed and direction are measured using a three-cup anemometer and wind direction sensor. A sheathed type-T thermocouple sensor, enclosed in a naturally ventilated multi-plate radiation shield, is used to measure ambient temperature. The output signals from the meteorological station's instruments are measured using a data acquisition system.

The "test bed" meteorological station consists of two precision spectral pyranometers, one precision infrared radiometer, and two radiatively shielded type-T thermocouples, and an ultrasonic wind sensor. The ultrasonic wind sensor is used to measure the magnitude and direction of air movement over to the panels. All of the instruments are mounted on the building's vertical façade, adjacent to the BIPV panels. This set of meteorological instruments provides data at the actual BIPV site and eliminates and any errors that may arise when attempts are made to predict the radiation on a vertical surface from the horizontal measurements collected from the roof top facility. Additional information on these meteorological stations and the test facilities are provided in reference [8].

EXPERIMENTAL RESULTS

Prior to installing the heat flux transducers and thermal insulation, the BIPV panels were monitored to determine if performance differences existed between the two panels of each cell technology. During a 29 day monitoring period (November 9 - December 7, 1999) the differences in delivered energy between the two panels of each technology was less than 2.0 %. Specifically, the measured differences were (0.7,

0.3 and 1.8) % for the single-crystalline, polycrystalline, silicon-film, and amorphous silicon panel sets. The performance differences observed during this initial comparison period were assumed to exist throughout the year and so were used to normalize the results recorded after one of each paired panel was insulated. The expanded uncertainty, using a confidence level of 95 %, associated with the energy measurements presented in this paper is ± 1.2 %.

The limited pre-insulation data suggests that custom made BIPV panels can be manufactured without significant differences in panel to panel performance. It is interesting to note that the technology with the greatest panel to panel difference is 1.8 %, is amorphous silicon. Unlike the other technologies, which were custom manufactured, the amorphous silicon panels represent “off the shelf” modules.

The efficiency of the building integrated photovoltaic panels in converting the incident solar radiation into electrical energy is referred to as the conversion efficiency,

$$\eta_c = \frac{\int_o^\tau P_o d\tau}{A \int_o^\tau H_T d\tau} \quad (1)$$

where

A is a representative area, m^2 ,

H_T is the incident solar radiation, W/m^2 ,

P_o is the panels electrical power output, W

and τ is the time interval selected for monitoring, h .

Unlike other variables in Eq. 1, the selection of an appropriate area is somewhat subjective for the building integrated photovoltaic panels. For example, the area of each cell within a panel times the number of cells yields an area referred to as the cell area. The aperture area is defined as the sunlit opening in the building wall prior to adding the sashing used for mounting the BIPV panels. A third area, referred to in this paper as the coverage area, is defined as the portion of the panel covered by the cells including the areas associated with the spaces between cells. The areas associated with each cell technology are given in Table. 1.

Figure 4 gives the overall efficiency of the building integrated photovoltaic panels from January 4 through December 31, 2000. The expanded uncertainty associated with the efficiency results is ± 2.4 %. The coverage area was used to compute the efficiencies in Fig. 4. There are two efficiencies plotted for each building integrated photovoltaic panel in Fig. 4. The bars in the foreground are computed using sunrise to sunset measurements of the incident irradiance and power output. The background bars are the efficiencies of the various panels computed only during the middle of each day when shading along the vertical sides of the panels was not

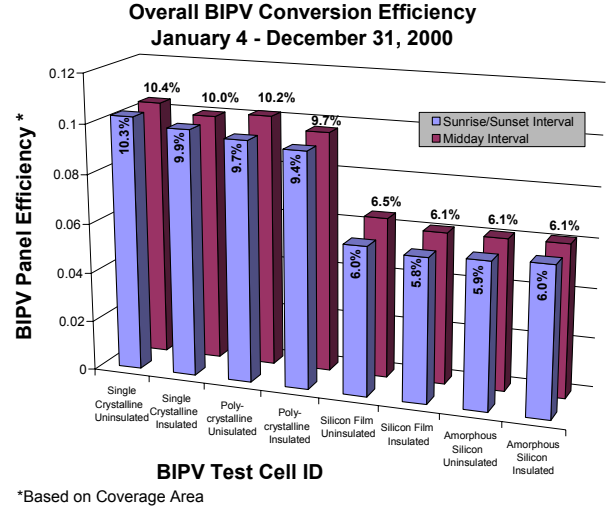


Figure 4

present on any cells within any of the BIPV panels. The panels in which shading is most problematic in this particular installation, and thus acts as a limiting case, are those that utilize the amorphous silicon cells. This is due to the small borders, 8 mm on its vertical sides and 11 mm along the horizontal top edge, that exist between the cells within amorphous silicon panels and the exterior sash that secures the panel, Table 1. The BIPV panels are recessed from the front of the surrounding mullions approximately 6 mm in order to accommodate the exterior retaining sash. Figure 5 shows the hours and the accompanying incident angle during which no shading along the vertical sides of the amorphous silicon panel occurs. This interval, hereafter referred to as the “mid-day interval,” is one of two data collection intervals – the other being sunrise to sunset – used for analysis in this paper. It is interesting to note that at the summer solstice, June 21, the

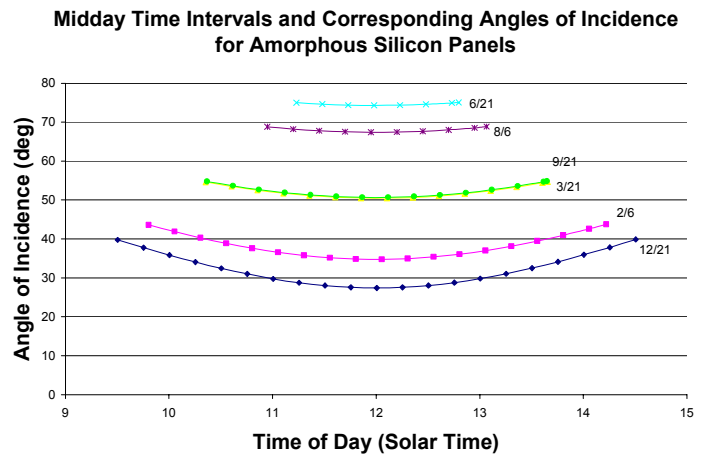


Figure 5

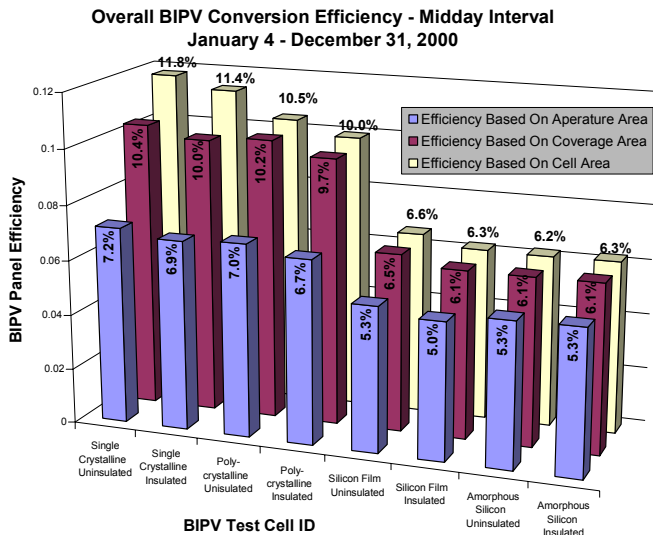


Figure 6

midday interval (when the cells within amorphous silicon panels are un-shaded along their vertical sides) is less than 2 h and the incident angles during this interval all exceed 70°.

Figure 5 does not account for hours when minimal shading occurs along the upper edge of the amorphous silicon panels. If included, the result is several days bracketing the summer solstice where before the vertical shading stops, the horizontal shading starts, and then in the afternoon, the vertical shading on the opposite side of the panel starts before the horizontal shading ends. For the worst case – solar noon on the summer solstice – the shading on the upper edge of the amorphous silicon panels is 21 mm. Given this relatively minor worst case of upper edge shading on the comparatively large individual amorphous silicon cells, plus the researchers' desire to have middle-of-the-day performance comparisons for every day of the year, the decision to define the time interval in terms of periods of no shading along the vertical sides of the

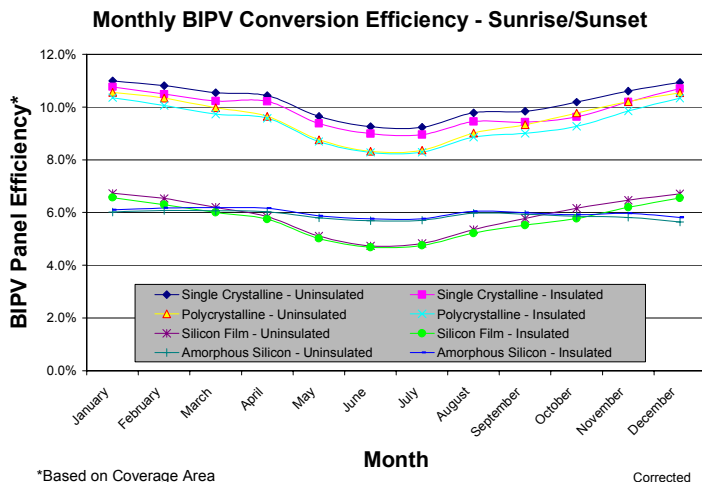


Figure 7

amorphous silicon panels was made. The potential for upper edge shading was considered when designing the custom-made BIPV panels and, as a result, the upper row of cells in the single-crystalline, poly-crystalline, and silicon film panels are never shaded due to the upper, horizontal exterior sash.

The highest overall conversion efficiency (sunrise to sunset) was achieved using single-crystalline cells. The insulated single-crystalline panel efficiency was 3.8 % lower than the non-insulated panel, 9.9 % versus 10.3 %, Fig. 4. The polycrystalline panels differed by 3.1 %: 9.7 % for the insulated panel compared to 9.4 % for the non-insulated panel. The non-insulated and insulated silicon film panels converted 6.0 % and 5.8 % of the incident solar energy into electrical energy, a 3.3 % difference. Finally, Fig. 4 shows that the addition of insulation to an amorphous silicon panel improved the panels' efficiency from 5.9 % to 6.0 %.

As previously noted, selection of the area used in computing efficiency is somewhat subjective. Figure 6 shows the overall conversion efficiency of the building integrated photovoltaic panels using the three areas previously discussed, cell area, coverage area, and aperture area. The values in Fig. 6 corresponds to the mid-day interval that was defined above. The relative areas vary depending upon a number of design choices. For example, although the single crystalline and polycrystalline BIPV panels have identical border areas and cell spacing (Table 1), the fact that the single crystalline cells have diagonal rather than square corners results in significantly different efficiencies depending upon which area is used, cell or coverage. In the case of the polycrystalline panels, which utilize square cells, the difference in cell and coverage area efficiencies is small. These results show the clear need to identify the area that is used when presenting efficiency results.

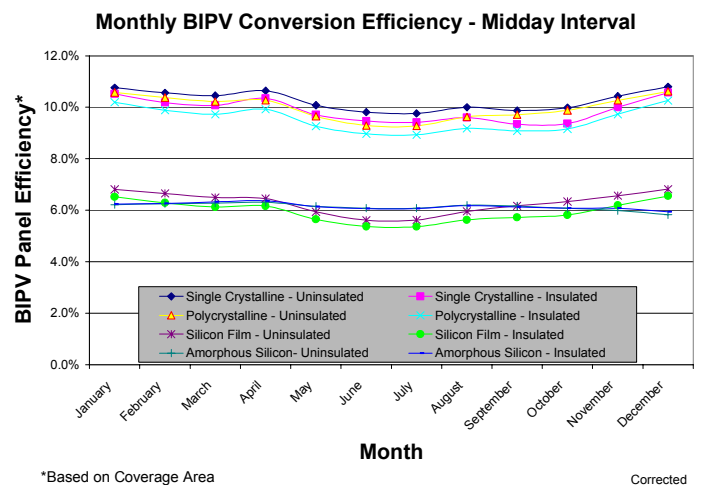
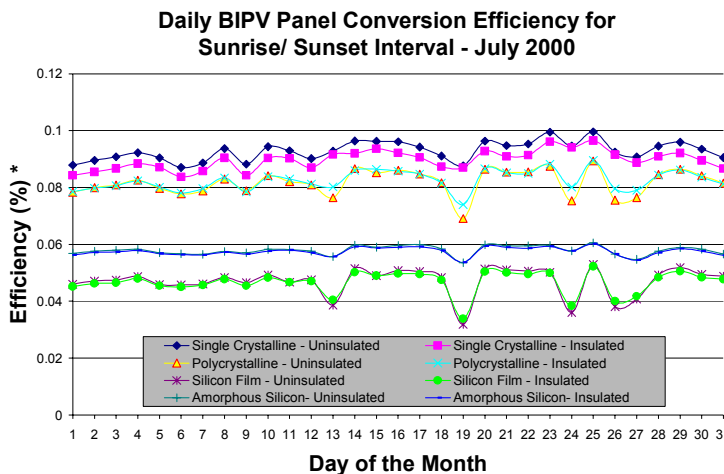


Figure 8

The monthly building integrated photovoltaic conversion for both the insulated and non-insulated panels is shown in Fig. 7. With the exception of the amorphous silicon panels, the highest conversion efficiency was obtained during the month of January. The monthly variation in efficiency is primarily attributed to variations in the incident angle, which varies from 27.4° at solar noon on December 21 to a value of 74.3° at solar noon on June 21. Variations in cell temperatures and shading on the cells due to the surrounding mullions are also responsible, to a lesser extent, for the monthly variations. It is interesting to note that the monthly conversion efficiencies of the amorphous silicon panels are relatively constant from month to month compared to the remaining panels. This behavior is attributed to the fact that amorphous silicon panels are less affected by the angle of incidence relative to the other cell technologies [11].

Figure 8 shows the monthly conversion efficiencies computed using only the data captured during the mid-day intervals. The monthly efficiency of the single-crystalline, polycrystalline, and silicon film panels decreases from January through March in a near linear manner. The amorphous silicon BIPV panel conversion efficiencies slightly increase during this time interval. After April, the efficiencies decline until June. The BIPV panel efficiencies for June and July are almost equivalent. During August all of the efficiencies improved relative to July. The efficiencies decrease slightly in September and, with the exception of the amorphous silicon panels, improve each month through December.

Comparing Figures 7 and 8, the conversion efficiencies are comparable for the months of January through April, September through December. The greatest differences are observed for the months of May through August. It is believed that these larger differences are due to the greater angles of incident between the BIPV panels and the sun that occurs



*Based on Coverage Area

Figure 9

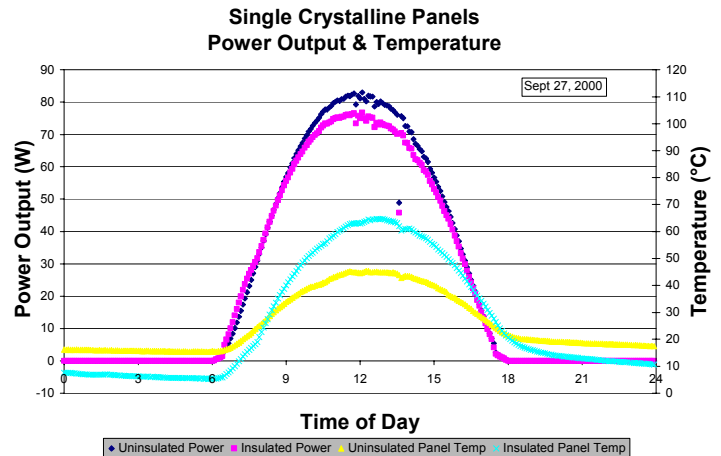


Figure 10

during the central hours of the days during these months, Fig. 5. Consistent with monthly results previously discussed, the difference in conversion efficiency between the sunrise to sunset results, Fig. 7, and the results for the mid-day intervals, Fig. 8, is much less significant for the amorphous silicon panels than is exhibited by the other cell technologies.

Further comparison of Figures 7 and 8 shows that the difference between the insulated and non-insulated panels is more pronounced in Fig. 8. This is a result of the panel operating temperatures. During the mid-day hours, the difference between the insulated and non-insulated panel temperatures are greater, resulting in a greater performance shift. This phenomenon will be discussed in greater detail when the hourly performance results are presented.

The daily conversion efficiency for a representative month, July 2000, is plotted in Fig. 9. On a daily basis, the

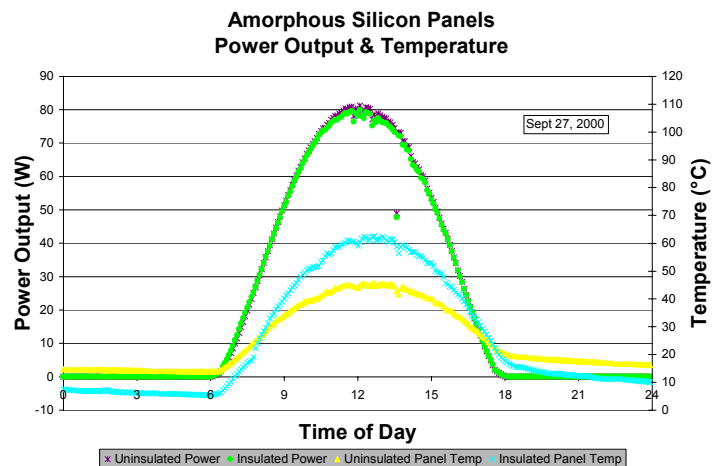


Figure 11

Table 2

Monthly and Cumulative BIPV Panel Performance														
		Jan 2000	Feb 2000	Mar 2000	Apr 2000	May 2000	Jun 2000	Jul 2000	Aug 2000	Sep 2000	Oct 2000	Nov 2000	Dec 2000	Total
Panel Energy Production Sunrise to Sunset (Wh)	Single Crystalline - U	11795	12197	12289	6628	6745	6520	7185	7626	10119	14243	10036	11985	105384
	Single Crystalline - I	11556	11833	11925	6491	6552	6332	6967	7367	9694	13463	9644	11725	101827
	Poly Crystalline - U	11332	11662	11624	6130	6124	5859	6509	7029	9596	13668	9653	11546	99187
	Poly Crystalline - I	11116	11349	11341	6084	6075	5833	6452	6904	9262	12956	9317	11327	96688
	Silicon Film – U	8538	8711	8541	4390	4217	3947	4443	4938	7024	10186	7235	8698	72170
	Silicon Film - I	8334	8399	8273	4318	4146	3904	4372	4810	6718	9543	6928	8487	69745
	Amorphous - U	10117	10734	11064	5995	6345	6272	6954	7295	9548	12822	8613	9681	95757
	Amorphous - I	10252	10894	11287	6130	6431	6353	7029	7381	9647	12954	8832	9977	97191
Panel Energy Density * Production Sunrise to Sunset (Wh/m2)	Single Crystalline - U	10171	10518	10597	5715	5816	5622	6195	6576	8726	12282	8654	10334	90871
	Single Crystalline - I	9965	10204	10283	5598	5650	5460	6008	6353	8359	11609	8316	10110	87804
	Poly Crystalline - U	9771	10056	10023	5286	5281	5053	5613	6061	8275	11786	8324	9956	85528
	Poly Crystalline - I	9585	9786	9779	5246	5238	5030	5563	5953	7987	11172	8034	9767	83374
	Silicon Film – U	6226	6353	6228	3201	3076	2878	3240	3601	5122	7429	5276	6343	52631
	Silicon Film - I	6077	6125	6033	3149	3023	2847	3188	3508	4899	6960	5052	6189	50862
	Amorphous - U	5573	5913	6095	3302	3495	3455	3831	4018	5260	7063	4745	5333	52750
	Amorphous - I	5648	6001	6218	3377	3542	3500	3872	4066	5314	7136	4865	5496	53540
Average Backside Panel Temperature Sunrise to Sunset (°C)	Single Crystalline - U	27.0	27.7	26.7	23.7	27.0	28.7	29.6	30.9	31.7	32.9	30.0	26.9	28.7
	Single Crystalline - I	28.8	31.0	29.0	24.2	29.9	31.9	33.2	35.1	37.4	40.3	35.6	28.7	32.2
	Poly Crystalline - U	26.9	27.7	26.7	23.8	27.1	28.8	29.7	31.0	31.8	33.0	30.1	26.8	28.7
	Poly Crystalline - I	28.3	30.5	28.8	24.0	29.7	31.8	33.0	34.9	37.1	39.9	35.0	28.1	31.9
	Silicon Film – U	27.4	28.1	27.1	23.8	27.3	29.0	29.9	31.3	32.2	33.6	30.6	27.3	29.0
	Silicon Film - I	29.1	31.0	29.4	24.2	30.0	32.0	33.3	35.2	37.5	40.4	35.5	28.8	32.3
	Amorphous - U	23.3	24.8	24.9	22.5	26.5	28.5	29.2	30.3	30.7	31.1	27.2	23.3	26.9
	Amorphous - I	23.7	26.5	26.4	22.2	28.3	30.7	32.0	33.6	34.9	37.0	30.8	23.8	29.3
Average Outdoor Ambient Temp (°C) **		3.5	8.5	13.2	17.2	21.5	24.8	24.9	25.3	22.1	18.9	11.2	2.6	16.1
Average Indoor Ambient Temp (°C) **		21.9	22.0	22.2	22.2	23.4	24.5	24.9	25.6	25.0	23.8	22.1	20.5	23.2
Vertical Solar Insolation (Wh/m2) **		92563	97282	100528	54806	60274	60742	67132	67241	88704	120599	81580	94485	985939
Complete Days of BIPV Electrical Performance Data (days)		28	29	31	23	28	30	31	29	27	31	26	31	344
Average Daily Insolation (Wh/m2)		3306	3355	3243	2383	2153	2025	2166	2319	3285	3890	3138	3048	2866

* Based on coverage area

** Evaluated using data collected between sunrise and sunset

U denotes Uninsulated

I denotes Insulated

differences between the insulated and non-insulated panels for each of the crystalline technologies remain relatively constant except when poor solar conditions exist. During the days in which the incident solar energy was low, (July 13, 19, 24, 26, and 27), the difference between the paired single-crystalline panels diminishes, whereas the performance difference for the paired polycrystalline panels increases. The silicon film appears to exhibit the same behavior as the polycrystalline panels but to a lesser extent. There is essentially no difference between the insulated and non-insulated amorphous silicon panels. It is interesting to note the relative performance of the insulated and non-insulated panels for an individual day. Figure 10 shows the insulated single-crystalline and non-insulated single-crystalline cell temperatures for September 27. The expanded uncertainty of the temperature measurements using a confidence level of 95 %, is ± 0.3 °C. At 12:55, the insulated panel is 19.8 °C higher than the non-insulated panel. This was an extremely clear day with the exception of a few minutes around 14:30. The power output of these two modules, also shown in Fig. 10, closely coincide prior to 9:20 and after 16:45. During the central part of the day, the non-insulated panel outperforms the insulated panel. At 12:55 this difference is approximately 9 %. The uncertainty associated with the power measurements is ± 1.2 %, assuming a 95 % confidence level. For the same day the recorded backside panel temperatures and power outputs for the amorphous silicon panels are plotted in Fig. 11. Although the amorphous panel is 17 °C higher at solar noon, the power outputs are essentially identical.

Table 2 summarizes the monthly and cumulative energy production, energy density, operating temperatures, and meteorological conditions for each BIPV panel. The cumulative energy production ranged from a high of 105.4 kW·h for the non-insulated single-crystalline panel to a low of 69.7 kW·h for the insulated silicon film panel. Due to the variations in coverage area, a more meaningful comparison is the energy density. The energy density is computed by dividing the cumulative energy production by the coverage area of each panel. The cumulative energy density ranged from a high of 90.9 kW·h/m² for the non-insulated crystalline panel to a low of 50.8 kW·h/m² for the insulated silicon film panel.

The addition of insulation to the rear of crystalline, polycrystalline, and silicon film panels resulted in declines in energy production of 3.3, 2.5, and 3.4 %, respectively. Unlike the other BIPV panels, the insulated amorphous silicon panel outperformed the non-insulated panel by 1.5 %. The results in Table 2 show that for a south-facing vertical façade at the latitude of the test-bed, 39.1°, BIPV energy production will be at its greatest magnitude during the winter months.

SUMMARY

Among the barriers to the widespread proliferation of building integrated photovoltaics is the lack of performance data and validated performance models. A building integrated photovoltaic “test-bed” has been constructed that will address these barriers. The facility, placed into operation in January 2000, is capable of providing side-by-side performance comparisons of up to eight panels.

Eight BIPV panels are currently installed within the test-bed. The panels include custom fabricated single-crystalline, polycrystalline, and silicon film panels as well as commercially available amorphous silicon modules. An insulated and non-insulated panel of each cell technology is installed. This paper contains the first twelve months of performance results, January through December, collected at NIST’s BIPV “test-bed”.

The selection of the area used to compute efficiency is subjective and can have a dramatic impact on reported results. The potential BIPV system owner must take great care in using a consistent area when comparing BIPV conversion efficiencies. Three areas are discussed in this paper: cell, coverage, and aperture. Unlike cell area, which is fixed by the cell’s manufacturer, and aperture area, which is dependent upon the building’s design, the coverage area can vary significantly dependent upon the panel’s design. For example, an architect may elect to use large spaces between cells and transparent materials in the BIPV’s panel construction to provide day-lighting as well as electrical power. The variation in reported efficiency resulting from area selection can be tremendous. The conversion efficiency of the non-insulated single-crystalline panel in this study could be reported as (7.2, 10.4, or 11.8) %, as a result of using the aperture, coverage, or cell area in computing efficiency.

During the twelve months that the panels have been monitored, the measured mid-day efficiencies for the non-insulated panels are (10.4, 10.2, 6.5 and 6.1) % for the single-crystalline, polycrystalline, silicon film, and amorphous silicon panels, respectively. The non-insulated single-crystalline, polycrystalline, and silicon-film panels outperformed the insulated panels. The midday performance differential was 3.8 % for the single-crystalline, 4.9 % for the polycrystalline panels, and 6.1 % for the panels constructed using silicon film. By comparison, the insulated amorphous silicon panel conversion efficiency was identical to the paired un-insulated panel.

The single-crystalline, polycrystalline, and silicon film panels were most efficient during January and least efficient during the months of June and July. The month-to-month variation in efficiency is attributed primarily to the large variations in incident angle. The incident angle between the sun and BIPV panels varied from a low of 27.4° on December

21 to 74.3° on June 21 for these vertical south-facing panels. Placement of the panels on a horizontal roof would have resulted in incident angles of 62.6° and 15.7°, respectively, on these dates.

The data summarized in this paper should be of interest to building owners, photovoltaic cell manufacturers, and fabricators of BIPV panels. In subsequent publications [12] the hourly data will be compared to the computer predictions.

ACKNOWLEDGEMENTS

The authors would like to acknowledge Gerald Ceasar of NIST's Advanced Technology Premium Power Program and the California Energy Commission for providing financial support for this project. Also recognized for their contributions are Jake Brown of Solar Building Systems for his assistance in the design and fabrication of the BIPV panels. Gratitude is extended to the following NIST personnel who have assisted the authors: Stanley T. Morehouse for his role in fabricating the various facilities described within this paper; Robert Zarr for calibrating the heat flux transducers, Daniel Vennetti for calibrating the various instruments associated with the BIPV facility and preparing the graphics; Michael Christopher, along with Daniel Vennetti, for transforming the experimental data generated by the BIPV "test-bed" into useful formats; and Paula Svincek for manuscript preparation.

REFERENCES

[1] Cook, G., David, R., Gwinner, D. & Hicks, A. *Photovoltaics; Energy for the New Millennium*. 1-17. 1-1-2000. NREL, Golden, CO, Department of Energy

[2] Schoen, T.J., 1999, "Information", *Renewable Energy World*, **2**, No. 5, p. 84.

[3] King, D.L., Dudley, J.K, and Byoson, W.E., 1997, "PVSIM: A Simulation Program for Photovoltaic Cells, Modules, and Arrays", *Proceedings of the 26th IEEE Photovoltaics Specialists Conference*, Anaheim, CA.

[4] 1999, Photovoltaic Analysis and TrAnsient Simulation Method (PHANTASM), Building Integrated Photovoltaic Simulation Software, Solar Energy Laboratory, University of Wisconsin, Madison, WI.

[5] ENERGY-10, V1.3, 2000, "A Tool for Designing Low Energy Buildings", Sustainable Buildings Energy Council, Washington, D.C.

[6] IV Curve Tracer, Solar Design Studio, v4.0, Maui Solar Energy Software Corp., Haiku, I, October 2000.

[7] King, D.L., 1997, "Photovoltaic Module and Array Performance Characterization methods for all System Operating Conditions", *Proceedings of NREL/SNL Photovoltaics Program Review Meeting*, Nov. 18-22, 96, Lakewood, CO, AIP Press, New York, 1997.

[8] Fanney, A.H. and Dougherty, B.P., 2000, "Building Integrated Photovoltaic Test Facility", *Proceedings of the 2000 International Solar Energy Conference*, June 16-21, 00, Madison, WI, ASME, New York 2000.

[9] NIST R-Matic Test Report R000420 B, April 20, 2000

[10] Raydec, 1988, "Photovoltaic Operations and Maintenance Manual", Ver. 4.0.

[11] King, D.L, Kratochvil, J.A., & Boyson, W.E., "Measuring Solar Spectral and Angle-of-Incidence Effects on Photovoltaic Modules and Solar Irradiance Sensors", *26th IEEE Photovoltaic Specialists Conference, Anaheim, CA, 9/97*.

[12] Davis, M.W., Fanney, A.H., and Dougherty, B.P., "Prediction of Building Integrated Photovoltaic Cell Temperatures", Submitted to *Proceedings of Forum 2001, Solar Energy: The Power to Choose*, April 21-25, 2001, ASES, Washington, DC, 2001.

SHORT-TERM CHARACTERIZATION OF BUILDING INTEGRATED PHOTOVOLTAIC PANELS

A. Hunter Fanney

Heat Transfer and Alternative
Energy Systems Group
National Institute of Standards and Technology
Gaithersburg, Maryland 20899

Mark W. Davis

Heat Transfer and Alternative
Energy Systems Group
National Institute of Standards and Technology
Gaithersburg, Maryland 20899

Brian P. Dougherty

Heat Transfer and Alternative
Energy Systems Group
National Institute of Standards and Technology
Gaithersburg, Maryland 20899

ABSTRACT

Building integrated photovoltaics, the integration of photovoltaic cells into one or more exterior building surfaces, represents a small but growing part of today's \$2 billion dollar photovoltaic industry. A barrier to the widespread use of building integrated photovoltaics (BIPV) is the lack of validated predictive simulation tools needed to make informed economic decisions. The National Institute of Standards and Technology (NIST) has undertaken a multi-year project to compare the measured performance of BIPV panels to the predictions of photovoltaic simulation tools.

The existing simulation models require input parameters that characterize the electrical performance of BIPV panels subjected to various meteorological conditions. This paper describes the experimental apparatus and test procedures used to capture the required parameters. Results are presented for custom fabricated mono-crystalline, polycrystalline, and silicon film BIPV panels and a commercially available triple junction amorphous silicon panel.

INTRODUCTION

The National Institute of Standards and Technology (NIST) has undertaken a multi-year project to validate and improve, if needed, computer simulation tools used to predict the energy production of building integrated photovoltaic panels [1]. These tools will enable building owners and designers to accurately quantify the economic savings associated with building integrated photovoltaic panels.

Among the models available for predicting the performance of photovoltaic systems are PV-Design Pro [2], developed jointly by Maui Solar Software Corporation and Sandia National Laboratories (SNL), and PHotovoltaic ANalysis and TrAnsient Simulation Method (PHANTASM) [3] developed by the University of Wisconsin's Solar Energy Laboratory. Researchers at SNL have also developed PVMOD, a model used within SNL to predict the performance of a wide variety of photovoltaic systems.

Input parameters required by these models include the photovoltaic panels' current and voltage at maximum power conditions, open circuit voltage, short circuit current, number of cells in series within a module, and the temperature coefficients associated with the short circuit current and open circuit voltage. The PHANTASM model also requires the nominal operating cell temperature, the glazing material's solar transmittance, the photovoltaic cell's solar absorptance, and the electrical band-gap of the photovoltaic material. Additional PV-Design Pro input parameters include the maximum power voltage and current temperature coefficients and the polynomials that are used to predict the panel's electrical performance response to changes in incident angle and absolute air mass.

NIST has constructed an outdoor solar tracking test facility to obtain the needed parameters. This paper describes the experimental apparatus, test procedures used to obtain the various parameters, and the resulting measurements. Results are compared to data, if available, from manufacturers and the Sandia National Laboratories.

Table 1 Building Integrated Photovoltaic Panel Specifications

Cell Technology	Mono Crystalline	Poly Crystalline	Silicon Film	Triple-Junction Amorphous
Panel Dimensions (m x m)	1.38 x 1.18	1.38 x 1.18	1.38 x 1.18	1.37 x 1.48
Front Cover	6 mm glass	6 mm glass	6 mm glass	2 mm Tefzal
Encapsulant	EVA	EVA	EVA	EVA
Backsheet/Color	*Tedlar/Charcoal	Tedlar/Charcoal	Tedlar/Charcoal	Stainless Steel
Cell dimensions (mm x mm)	125 x 125	125 x 125	150 x 150	119 x 340
Number of Cells (in series)	72	72	56	44
Adjacent Cell Spacing (mm)	2	2	2	
Vertical Border Width (mm)	100	100	51	8
Top Border Height (mm)	72	72	55	11
Bottom Border (mm)	70	70	29	5
Recessed Distance to PV Cell (mm)	12	12	12	9
Glazing Covered by PV Cells %	63	69	80	88
Total Cost (\$)	1324	1123	995	578
Price/Watt(\$/W)	8.66	8.43	10.75	4.52
Rated Power (W)	153	133	93	128
Cell Area (m ²)	1.020	1.128	1.341	1.780
Aperture Area (m ²)	1.682	1.682	1.682	2.108
Coverage Area (m ²)	1.160	1.160	1.371	1.815

EXPERIMENTAL APPARATUS

BIPV Panel Description

The panels selected for characterization include custom-fabricated mono-crystalline, polycrystalline, and silicon film BIPV panels and a commercially available triple-junction amorphous silicon module, Table 1. The selected panels are duplicates of those installed in NIST's BIPV "test bed" [4]. The custom fabricated panels were made to NIST specifications by a firm that specializes in BIPV panels for commercial and residential applications. Design considerations included incorporating borders that minimize shading on the cells, the use of readily available cells, and cell interconnections that resulted in electrical configuration compatible with the monitoring equipment.

The rated power values listed in Table 1 for the monocrystalline, polycrystalline, and silicon film panels are based upon 'flash tests' performed by the fabricator. The amorphous silicon BIPV panel rating is taken from the manufacturer's literature. Three different areas are listed in Table 1, cell, aperture, and coverage. Cell area is defined as the number of cells within a panel times the area of each individual cell. The aperture area is the sunlit opening in the building wall prior to adding the sashing required to mount the BIPV panels. Coverage area is the portion of each panel covered by cells including the spaces between adjacent cells.

With the exception of the triple-junction amorphous panels, which was commercially available, the costs listed in Table 1 are the per panel costs based on producing four panels using

each cell technology. The triple-junction amorphous panel was constructed using two commercially available modules connected in series. It should be noted that the costs given in Table 1 reflect the fact that the amorphous panels were off-the-shelf items whereas the other panels were custom fabricated.

Solar Tracking Test Facility

A mobile solar tracking facility is used to characterize the electrical performance of building integrated photovoltaic panels, Fig. 1. Software has been developed for the mobile solar tracker that allows the user to select the following tracking modes:

- Azimuth and Elevation Tracking
- Azimuth Tracking
- Elevation Tracking
- Azimuth Tracking with User Selected Offset
- Elevation Tracking with User Selected Offset
- User Selected Incident Angle Tracking

The mobile solar tracking facility incorporates meteorological instruments, a data acquisition system, and a photovoltaic curve tracer. Precision spectral pyranometers are used to measure total (beam plus diffuse) solar radiation. Two instruments are used to provide redundant measurements. A pyrheliometer is used to measure the beam component of solar radiation. Long-wave radiation, greater than 3 μm , is measured using a precision infrared radiometer. Spectral radiation data from 300 nm to 1100 nm is obtained using a

* Certain trade names and company products are mentioned in the test or identified in an illustration in order to adequately specify the experimental procedure and equipment used. In no case does such an identification imply recommendation or endorsement by the National Institute of Standards and Technology, nor does it imply that the products are necessarily the best available for the purpose.

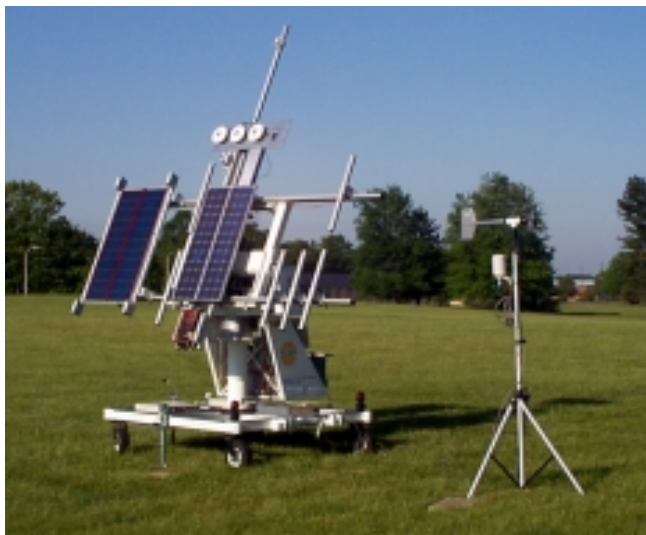


Figure 1 NIST's Mobile Solar Tracking Facility

spectroradiometer with selectable scan intervals of 1 nm, 2 nm, 5 nm, or 10 nm.

A three-cup anemometer and wind vane assembly is used to measure wind speed and direction. Ambient temperature is measured using a perforated tip, type-T thermocouple sensor enclosed in a naturally ventilated multi-plate radiation shield.

The output signals of the meteorological instruments and thermocouples associated with the building integrated photovoltaic panels are measured using a data acquisition system. The data acquisition system incorporates a 6 1/2 - digit multimeter, IEEE 488 and RS 232 interfaces, and multiplexing relay cards that can accommodate up to 60 transducers. Although the multiplexer cards have built-in thermocouple reference junctions, improved accuracy is obtained through the use of an electronic ice point reference.

The solar tracker incorporates an IV curve tracer to capture the electrical performance of the panel being evaluated. The curve tracer is programmed to sweep the panel's IV curve and store the resulting values every minute. Although the curve tracer incorporates two voltage ranges (60 V and 600 V) and two current ranges (10 A and 100 A), to date, the lower current and voltage ranges have been used resulting in voltage and current resolutions of 14 mV and 2.4 mA, respectively.

The solar tracking test facility is powered by means of an on-board uninterruptible power supply (UPS) capable of operating the equipment for approximately 14 h. For multiple day tests, the UPS is charged through the use of a portable generator.

TEST PROCEDURES

The simulation models' input parameters are obtained using the solar tracking facility and various test procedures. A description of each input parameter and the test procedure used to obtain it follows.

Temperature Coefficients

Temperature coefficients are used to quantify the relationship between various electrical characteristics of a photovoltaic device and its operating temperature. The computer simulation models use temperature coefficients to translate the electrical output of a photovoltaic panel at a given reference temperature to the electrical output at the panel's operating temperature. Temperature coefficients for the short-circuit current, the open circuit voltage, maximum power current, and maximum power voltage are measured for each building integrated photovoltaic panel.

Open-circuit voltage and short-circuit current temperature coefficients are addressed within ASTM E 1036M[5]. The correction factors within this test method are determined from a matrix of open-circuit voltage and short-circuit current values that result from measurements of the device over a range of operating temperatures and incident irradiances. The test procedure states that the measurements should be made over temperature and irradiance ranges of 0 °C to 80 °C and 800 W/m² to 1000 W/m², respectively.

Although ASTM E 1036M suggests that the measurements be made using a pulsed indoor solar simulator, the temperature coefficients for this study were determined outdoors using the NIST mobile solar tracking facility. Outdoor, as opposed to indoor, testing was selected for a number of reasons. A temperature controlled pulsed indoor solar simulator, sufficient in size to test the 1.38 m x 1.18 m panels, was not available. Outdoor testing eliminated the need to adjust the electrical output of the cells to take into account solar spectrum differences between an indoor solar simulator and outdoor test conditions. Finally, results could be compared to similar panels previously tested outdoors at Sandia National Laboratories [6].

The methodology proposed by Sandia National Laboratories [7] for outdoor testing was utilized. Each building integrated photovoltaic panel is mounted on an extruded polystyrene insulation board having a nominal thermal resistance of 3.5 m² · K/W. Prior to testing, the panel is shaded with a reflective cover positioned approximately 75 mm above the photovoltaic panel.

During the tests, the mobile solar tracker facility is operated in the full tracking mode, resulting in the sun's rays being perpendicular to the panel's surface throughout the test. The instrumentation and IV curve tracer are started and the cover used to shade the panel is removed. The IV curve tracer measures the electrical output every minute until the panel approaches a steady-state temperature. The temperatures of the BIPV panel are measured at five locations on the back surface of each BIPV panel. The thermocouples attached to the rear of two centrally located cells with the custom fabricated BIPV panels provide additional temperature measurements.

The tests are conducted when the absolute air mass is as close as possible to the reference value of 1.5, minimizing the need to correct the test data using the air mass function. The measured short-circuit current and maximum power current are

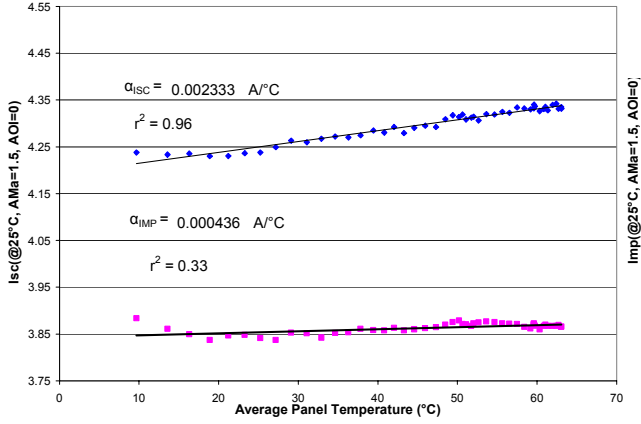


Figure 2. Polycrystalline BIPV Panel Isc and Imp Versus Panel Temperature

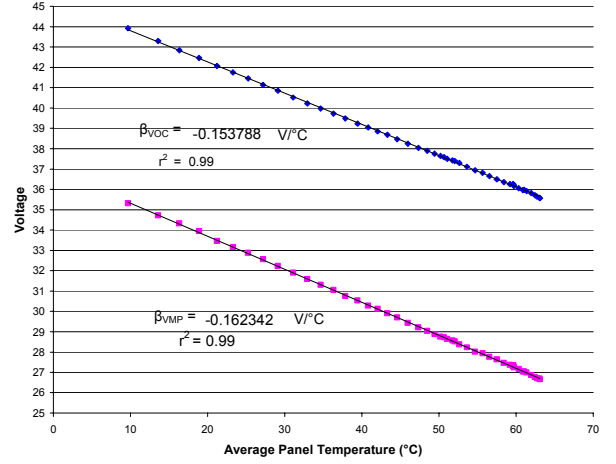


Figure 3. Polycrystalline BIPV Panel Voc and Vmp Versus Temperature

adjusted by multiplying by the ratio of the reference irradiance, E_o , (1000 W/m^2) to the measured irradiance and by normalizing the data, using an air mass function, to an absolute air mass of 1.5. The adjusted Isc and Imp for each IV curve is plotted against the average panel temperature as shown in Fig. 2. The slopes of the resulting regressions are the temperature coefficients for Isc and Imp.

The temperature coefficients for the open circuit and maximum power voltage are determined in a similar manner using the same set of IV curves. Unlike the short circuit current and maximum power current, the voltage values are assumed to be independent of the solar irradiance level and air mass. King et al. [7] found that there is typically less than a 5 % change in the voltage coefficients over a 10 fold change in irradiance – 100 W/m^2 to 1000 W/m^2 . The open circuit and maximum power voltage for each IV curve is plotted versus the panel's temperature. The slope of the linear regressions relating the open voltages to panel temperature are the voltage temperature coefficients, Fig. 3.

Air Mass Function

The air mass function used in the IV Curve Tracer photovoltaic model is an attempt to capture the influence of the solar energy's spectral distribution on the conversion efficiency of the photovoltaic cells. The solar spectrum is influenced by a number of factors including the absolute air mass, precipitable water content, turbidity, clouds, aerosol particle size distribution, particulate matter, and ground reflectance [8]. The magnitude of the solar spectrum's effect on the photovoltaic cell's performance depends upon the type of cell technology being utilized. King [9] has found that under clear sky conditions, the majority of the solar spectral influence can be taken into account by considering only the air mass. The relationship between the photovoltaic panel's short circuit current and absolute air mass is defined as the air mass function.

The air mass function for each of the building integrated photovoltaic panels was measured using the methodology proposed by King et al. [10]. The tracking facility is operated in a manner that maintains a zero angle of incidence throughout the day. The curve tracer and instrumentation used to measure the meteorological conditions and the photovoltaic panel's temperature are synchronized and started at sunrise. Data are collected every minute until sunset.

The short-circuit current associated with each IV curve is adjusted to a nominal temperature, T_r , of 25°C and nominal irradiance, E_o , of 1000 W/m^2 using the previously measured short-circuit temperature coefficient,

$$I_{sc}(T_r) = I_{sc}(T) + \frac{E}{E_o} \alpha_{Isc} (T_r - T) \quad (1)$$

The relative short circuit values are subsequently obtained by dividing the temperature adjusted current $I_{sc}(T_r)$ values by the temperature adjusted short circuit current measured at an absolute air mass of 1.5. The air mass is computed using the zenith angle of the sun, Z_s ,

$$AM = \left[\cos(Z_s) + 0.5057 \cdot (96.080 - Z_s)^{-1.634} \right]^{-1} \quad (2)$$

Finally, the absolute air mass is computed by multiplying the air mass value (Eq. 2) by the product of the atmospheric pressure at the test site, P , to the atmospheric pressure at sea level, P_o ,

$$AM_a = \frac{P}{P_o} AM \quad (3)$$

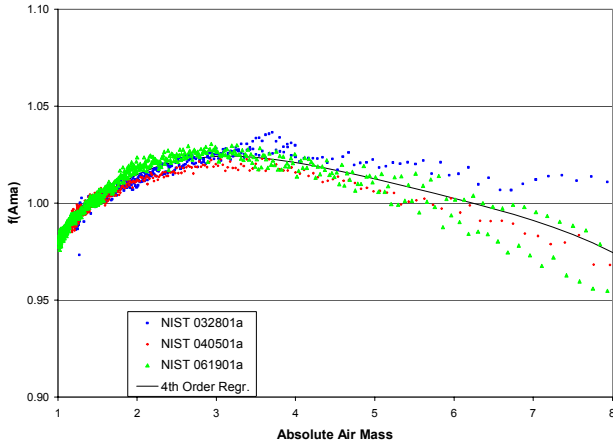


Figure 4. Polycrystalline BIPV Panel Air Mass Function

The relative short circuit current values versus the absolute air mass for the polycrystalline BIPV panel are plotted in Fig. 4 for three test days. A fourth order regression is used to determine the coefficients associated with the equation,

$$f(AM_a) = C + C_1 \cdot AM_a + C_2 \cdot AM_a^2 + C_3 \cdot AM_a^3 + C_4 \cdot AM_a^4 \quad (4)$$

It is interesting to note that the measured relative short-circuit current values for various days do not necessarily coincide. This is especially notable at air mass values greater than five. It is speculated that although “clear sky” test days were selected, the day-to-day variability in water content, turbidity, particulate matter, and other factors produced the data scatter. Fortunately, the amount of incident radiation available to a BIPV panel incorporated with a building during the hours at which high values of absolute air mass occur tends to be quite small, and thus, the uncertainty in the air mass function may have a small effect on daily energy production.

Incident Angle Function

The angle defined by the sun’s rays and a normal to the photovoltaic panel’s surface, is the angle of incidence or incident angle. The angle of incidence is computed using the sun’s azimuth and zenith angles, the slope and azimuth angles of the BIPV panel, and the panel’s geographical location [11]. The optical properties of the panel’s glazing material varies with incident angle. Under clear sky conditions, the “incident angle effect” can be quite pronounced for angles greater than 60°. Under uniform diffuse conditions, the angle of incidence does not affect the electrical output of the photovoltaic panel.

The effect of incident angle on the electrical performance of a photovoltaic panel is described by an empirically determined function, $f_2(AOI)$. The solar tracking facility is used to vary the incident angles of the BIPV panel while capturing its performance using the IV curve tracer. Data are collected at various incident angles with the greatest emphasis on incident angles greater than 60°. A normal incidence pyreheliometer,

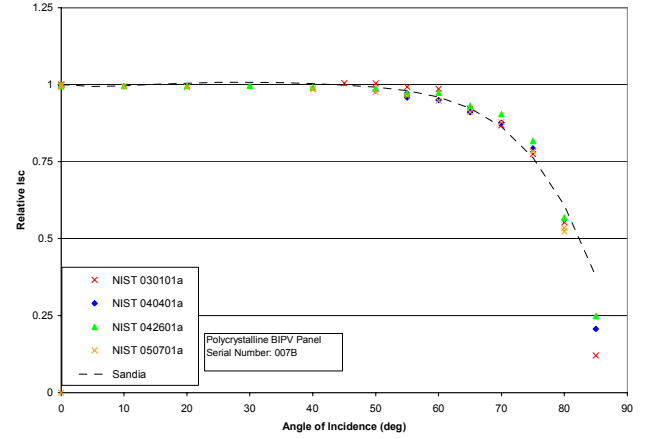


Figure 5 – Incident Angle Response for Polycrystalline BIPV Panel

part of NIST’s rooftop meteorological station [4] provides independent measurements of the beam irradiance during these tests. The diffuse irradiance in the plane of the BIPV panel is determined using the following equation

$$E_{diff} = E_{tpoa} - E_{dni} \cos \Theta \quad (5)$$

where E_{tpoa} is the total incident solar radiation, corrected for incident angle, measured in the plane of the BIPV panel using a precision spectral pyranometer, W/m^2

E_{dni} is the beam irradiance measured using a normal incident pyreheliometer tracking the sun, W/m^2

and Θ is the incident angle, deg

The incident angle function value for each measurement is computed using the procedure developed by King et al. [10],

$$f_2(AOI) = \frac{E_o I_{sc} (AM_a = 1.5, T = 25^\circ C) - E_{diff}}{E_{dni} \cos(\Theta)} \quad (6)$$

where E_o is the reference value of solar irradiance, $1000 W/m^2$

I_{sc} is the short circuit current of the BIPV panel at $AM_a=1.5$, $T=25^\circ C$, E_o , and $AOI=0$

and I_{sc} is the measured short circuit current at a given angle of incidence adjusted to the reference temperature and absolute air mass

Figure 5 is a plot of the resulting incident angle function values for the BIPV panel that incorporates polycrystalline cells. Values resulting from four test days are included. These results are in excellent agreement with measurements reported by King et al. [12].

Normal Operating Cell Temperature

The photovoltaic cells operating temperature is needed in order to translate the performance of the BIPV panels from the standard rating temperature of 25 °C to the panels' performance at operating temperatures. The PHANTASM model requires that the user input the nominal operating cell temperature (NOCT) of the photovoltaic panels whereas the PV-Design Pro model predicts cell operating temperature using an empirical correlation [2].

The procedure for determining NOCT temperature is outlined within Appendix A1 of ASTM Standard E 1036M [5]. NOCT is defined as the temperature of the solar cells when they are subjected to a solar irradiance of 800 W/m², a 1 m/s wind speed, and a surrounding ambient temperature of 20 °C. The photovoltaic panel is mounted such that it is normal to the sun at solar noon. The panels' temperature is measured for a period beginning at least 4 h before solar noon and continuing for at least 4 h after solar noon. During the test, the panel is not connected to an electrical load. The wind speed and direction, solar irradiance, and ambient temperature are monitored throughout the test. ASTM E 1036M specifies that the wind direction must be "predominantly either northerly or southerly."

The data are filtered to include only measurements consistent with wind speeds between 0.25 m/s and 1.75 m/s and with gusts less than 4 m/s for a period of at least 5 min prior to the measurement. The ambient temperature must be between 5 °C and 35 °C. The filtered data set is used to produce a plot of the difference between the photovoltaic cell's temperature and ambient temperature versus solar irradiance. Using this plot the NOCT is determined for an incident irradiance of 800 W/m² and 20 °C ambient temperature. Finally, a correction factor is added to this value to translate the measured NOCT from the test conditions to ambient conditions of 20 °C and 1 m/s.

Electrical Performance at Standard Rating Conditions

A required input to the computer simulation tools is the electrical performance of each BIPV panel at a specified set of test conditions, "Standard Reporting Conditions (SRC)." Typically an irradiance level of 1000 W/m², one of two standard solar spectral distributions, a cell temperature of 25 °C, and a 0° angle of irradiance have been specified. These conditions have been adopted in this paper as the standard rating conditions with the exception of the standard solar spectrum. In the values reported within this paper, the BIPV panels' performance at an absolute air mass of 1.5 is used in lieu of a standard solar spectrum.

Each BIPV panels' performance at this set of rating conditions is determined using the procedures developed by King et al. [9,12]. Using the mobile solar tracker to maintain the sun's rays perpendicular to the front surface of the panel (AOI = 0), the curve tracer is used to collect IV curves under clear sky conditions. The resulting short-circuit current values are corrected to an absolute air mass of 1.5 and a 25 °C cell

temperature using the previously determined air mass function and temperature coefficients. The resulting I_{sc} values are plotted versus the coincident solar irradiance striking the panel. A regression through the data is used to predict the short circuit current at of 1000 W/m², denoted I_{sco} .

In a similar manner, the measured maximum power current values are corrected to an absolute air mass of 1.5 and 25 °C cell temperature. The resulting values are plotted versus the effective irradiance. The effective irradiance is defined as,

$$E_e = \frac{I_{sc}(E, T_c = T_r, AM_a, AOI)}{I_{sco}} \quad (7)$$

where the numerator represents the temperature adjusted measured short-circuit current and the denominator is the short-circuit current of the panel at the standard rating conditions. The maximum power current corresponding to an effective irradiance of unity is the maximum power current at standard rating conditions, I_{mpo} .

The open circuit voltage and maximum power voltage measurements associated with each IV curve are plotted versus the natural logarithm of the effective irradiance values. Using a linear regression in the case of the open circuit voltage values, and a second order polynomial in the case of the maximum power voltage values, the open circuit voltage and maximum power voltage values are determined at an effective irradiance of 1.0.

TEST RESULTS

Results from tests conducted using the NIST solar tracking test facility are summarized in the following sections. In addition to the NIST results, the measurements are compared to data from the manufacturers and Sandia National Laboratories.

Temperature Coefficients

Table 2 is a compilation of the temperature coefficients, α_{isc} , α_{imp} , β_{voc} , and β_{vmp} measured in accordance with the previously described procedures. Two sets of units are associated with each coefficient. The test procedure produces results in units normally used within the photovoltaic industry, A/°C or V/°C. Unfortunately results presented in these units are not readily compared to temperature coefficients for panels that may use identical cells but differ in the number of cells or the manner in which the cells are interconnected.

In order to address this issue and to facilitate comparisons, the current and voltage temperature coefficients are divided by the corresponding current or voltage values (I_{sco} , I_{mpo} , V_{oco} , and V_{mpo}), at standard rating conditions. If the temperature coefficients of a BIPV panel using identical cells but having a different electrical configuration were needed, the normalized temperature coefficients, (1/°C) could be multiplied by the appropriate value (I_{sc} , I_{mp} , V_{oc} , and V_{mp}) of the panel for which the coefficients are desired.

Table 2 - Measured Temperature Coefficients

Monocrystalline BIPV Panel	Test Date		090501a	091101a	091501a	091501b	091701a	Average	Std. Deviation	
	α -Isc	A/°C	0.001868	0.001756	0.001776	0.001657	0.001707	0.001753	0.0000792	
		1/°C	0.000427	0.000401	0.000406	0.000379	0.000390	0.000401	0.0000181	
	α -Imp	A/°C	-0.001327	-0.001455	-0.001484	-0.001504	-0.001947	-0.001543	0.0002362	
		1/°C	-0.000335	-0.000367	-0.000375	-0.000380	-0.000492	-0.000390	0.0000596	
	β -Voc	V/°C	-0.157857	-0.149294	-0.146758	-0.155610	-0.152309	-0.152366	0.0045157	
		1/°C	-0.003677	-0.003478	-0.003419	-0.003625	-0.003548	-0.003549	0.0001052	
	β -Vmp	V/°C	-0.160084	-0.151999	-0.149460	-0.155116	-0.151231	-0.153578	0.0041731	
		1/°C	-0.004753	-0.004513	-0.004438	-0.004606	-0.004490	-0.004560	0.0001239	
Polycrystalline BIPV Panel	Test Date		030801a	042601a	050701a			Average	Std. Deviation	
	α -Isc	A/°C	0.002299	0.002502	0.002341			0.002380	0.0001071	
		1/°C	0.000541	0.000589	0.000551			0.000560	0.0000252	
	α -Imp	A/°C	0.000404	0.000161	-0.000031			0.000178	0.0002179	
		1/°C	0.000106	0.000042	-0.000008			0.000047	0.0000571	
	β -Voc	V/°C	-0.153788	-0.152396	-0.152209			-0.152798	0.0008626	
		1/°C	-0.003706	-0.003672	-0.003668			-0.003682	0.0000208	
	β -Vmp	V/°C	-0.162342	-0.157700	-0.157306			-0.159116	0.0028010	
		1/°C	-0.004928	-0.004787	-0.004775			-0.004830	0.0000850	
Silicon Film BIPV Panel	Test Date		062501a	062601a	070201a	070601a			Average	Std. Deviation
	α -Isc	A/°C	0.005756	0.004502	0.004182	0.004294			0.004683	0.0007273
		1/°C	0.001126	0.000880	0.000818	0.000840			0.000916	0.0001422
	α -Imp	A/°C	0.002037	0.001250	0.001467	0.001665			0.001605	0.0003344
		1/°C	0.000454	0.000279	0.000327	0.000371			0.000358	0.0000745
	β -Voc	V/°C	-0.129543	-0.132529	-0.129318	-0.128426			-0.129954	0.0017832
		1/°C	-0.004374	-0.004475	-0.004367	-0.004337			-0.004388	0.0000602
	β -Vmp	V/°C	-0.128977	-0.132790	-0.130170	-0.129611			-0.130387	0.0016744
		1/°C	-0.005568	-0.005732	-0.005619	-0.005595			-0.005629	0.0000723
Triple-Junction Amorphous BIPV Panel	Test Date		100501a	100501b	101101a	101501b	101501c	101501e	Average	Std. Deviation
	α -Isc	A/°C	0.005272	0.005403	0.004942	0.005852	0.006076	0.006094	0.005606	0.0004716
		1/°C	0.001187	0.001217	0.001113	0.001318	0.001368	0.001372	0.001263	0.0001062
	α -Imp	A/°C	0.006675	0.007014	0.006358	0.007392	0.007873	0.008773	0.007348	0.0008779
		1/°C	0.001848	0.001941	0.001760	0.002046	0.002179	0.002428	0.002034	0.0002430
	β -Voc	V/°C	-0.091300	-0.097684	-0.090912	-0.088250	-0.093312	-0.097150	-0.093102	0.0037149
		1/°C	-0.003943	-0.004218	-0.003926	-0.003811	-0.004030	-0.004195	-0.004021	0.0001604
	β -Vmp	V/°C	-0.049692	-0.052583	-0.045426	-0.042296	-0.049436	-0.046943	-0.047729	0.0036267
		1/°C	-0.003099	-0.003279	-0.002833	-0.002637	-0.003083	-0.002927	-0.002976	0.0002261

Table 3 - Summary of Measured Building Integrated Photovoltaic Panel

Silicon Film				Mono Crystalline			Polycrystalline			Triple Junction Amorphous			
Reference Cond.		Manufacturer	NIST	SNL	Manufacturer	NIST	SNL	Manufacturer	NIST	SNL	Manufacturer	NIST	SNL
P _{mpo}	(W)	125.94	103.96		149.60	133.40		128.10	125.78		64.02	57.04	
I _{sco}	(A)	5.80	5.11		4.80	4.37		4.00	4.25		4.80	4.44	
V _{oco}	(V)	30.66	29.61		43.40	42.93		42.60	41.50		23.80	23.16	
I _{mpo}	(A)	5.20	4.49		4.40	3.96		3.66	3.82		3.88	3.61	
V _{mpo}	(V)	24.22	23.17		34.00	33.68		35.00	32.94		16.50	16.04	
NOCT	(°C)	47	44		45			47			42		
Temperature Coefficients													
α _{isc}	(A/°C)	0.00400	0.00468		0.00206	0.00175		0.00260	0.00238		0.00480	0.00561	0.00424
α _{isc}	(1/°C)	0.000690	0.000916	0.000760	0.000429	0.000401	0.000370	0.000650	0.000560	0.000512	0.001000	0.001263	0.000850
α _{imp}	(A/°C)		0.00160			-0.00154			0.00018		0.00388	0.00735	0.00480
α _{imp}	(1/°C)		0.000358	0.000030		-0.000390	-0.000395		0.000047	-0.000148	0.001000	0.002034	0.001187
β _{Voc}	(V/°C)	-0.12600	-0.12995		-0.15400	-0.15237		-0.16000	-0.15280		-0.09044	-0.09310	-0.09767
β _{Voc}	(1/°C)	-0.004110	-0.004388	-0.004384	-0.003548	-0.003549	-0.004038	-0.003756	-0.003682	-0.003720	-0.003800	-0.004021	-0.004386
β _{Vmp}	(V/°C)		-0.13039			-0.15358			-0.15912		-0.05115	-0.04773	-0.05167
β _{Vmp}	(1/°C)		-0.005629	-0.005434		-0.004560	-0.005172		-0.004830	-0.004779	-0.003100	-0.002976	-0.003257
Coefficients for Air Mass and Angle of Incidence Functions													
f̂(A _{Ma})	Cnst		0.938110	0.928000		0.935823	0.938000		0.918093	0.913000		1.10044085	1.047
	A _{Ma}		0.062191	0.073144		0.054289	0.054228		0.086257	0.079168		-0.06142323	0.00082115
	A _{Ma} ²		-0.015021	-0.019427		-0.008677	-0.009903		-0.024459	-0.015975		-0.00442732	-0.0259
	A _{Ma} ³		0.001217	0.001751		0.000527	0.000730		0.002816	0.001306		0.000631504	0.0031736
	A _{Ma} ⁴		-0.000034	-0.000051		-0.000011	-0.000019		-0.000126	-0.000037		-1.9184E-05	-0.00011026
f̂(AOI)	Cnst		0.998980	1.000000		1.000341	1.000000		0.998515	1.000000		1.001845	1
	AOI		-0.006098	-0.002438		-0.005557	-0.002438		-0.012122	-0.002438		-0.005648	-0.00502
	AOI ²		8.117E-04	0.000310		6.553E-04	0.000310		1.440E-03	0.000310		7.254E-04	0.0005842
	AOI ³		-3.376E-05	-1.246E-05		-2.730E-05	-1.246E-05		-5.576E-05	-1.246E-05		-2.916E-05	-0.000023
	AOI ⁴		5.647E-07	2.112E-07		4.641E-07	2.112E-07		8.779E-07	2.112E-07		4.696E-07	3.826E-07
	AOI ⁵		-3.371E-09	-1.359E-09		-2.806E-09	-1.359E-09		-4.919E-09	-1.359E-09		-2.739E-09	-2.31E-09

The following values of uncertainty associated with the measurements in Table 3 represent the expanded uncertainty using a coverage factor of 2.

$$\begin{array}{ll}
 P_{mpo} - \pm 1 \% & \alpha_{isc} \pm 6 \% \\
 I_{sco} - \pm 1 \% & \alpha_{imp} \pm 20 \% \\
 V_{oco} - \pm 1 \% & \beta_{voc} \pm 1 \% \\
 I_{mpo} - \pm 1 \% & \beta_{vmp} \pm 1 \% \\
 V_{mpo} - \pm 1 \% &
 \end{array}$$

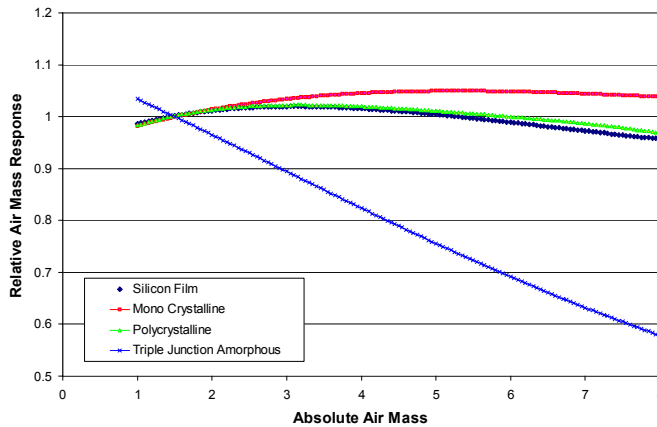


Figure 6 – Air Mass Response Function for BIPV Panels

For any given BIPV panel, test-to-test variations exist in the measured values, Table 2. The variations in temperature coefficients for current tend to be greater than those associated with voltage. The test-to-test variation is partially attributed to variations in spectral content, irradiance level, and temperature associated with outdoor testing [13].

It is interesting to note that although the short circuit current increases with temperature for all four panels, the maximum power current increases with temperature for the polycrystalline, silicon film, and triple junction amorphous panels while decreasing with temperature for the mono-crystalline panel.

The NIST measured temperature coefficients are compared to values within the manufacturer's literature and measurements at Sandia National Laboratories (SNL) for modules that incorporate identical cells within Table 3. The manufacturer's literature values were obtained from data sheets that accompanied the cells used in the fabrication of the custom BIPV panels, or from literature associated with a photovoltaic module using identical cells. Agreement between the manufacturer's data, NIST values, and measurements at SNL for the open circuit and maximum power voltage temperature coefficients is good. In general agreement between the three values of the temperature coefficients associated with short circuit and maximum power current is good with the exception of the NIST measured values associated with triple junction amorphous panel and the maximum power coefficients associated with the polycrystalline panel

Air Mass Functions

The measured air mass response for the monocrystalline, polycrystalline, silicon film, and triple junction amorphous silicon BIPV panels are shown in Fig. 6. It is interesting to note that the relative air mass response is similar for the BIPV panels that utilize the monocrystalline, polycrystalline, and silicon film cells. Air mass has a much greater effect on the triple junction amorphous BIPV panel than the other three panels. At an absolute air mass of six, the relative air mass response for the panel using the triple-junction amorphous

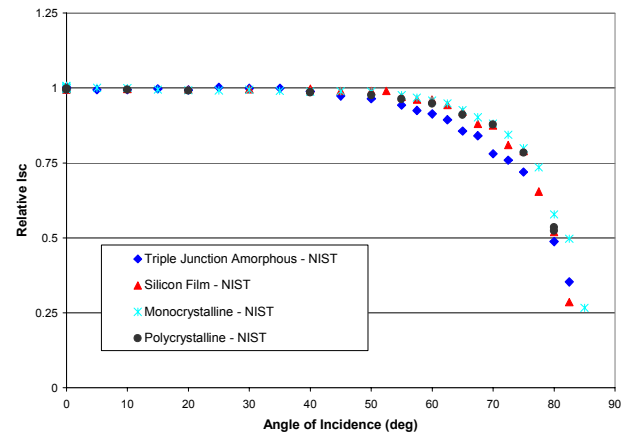


Figure 7 - Angle of Incidence Function for BIPV Panels

technology is approximately 70 % of that exhibited by the BIPV panels utilizing the other cell technologies. The significantly lower air mass response exhibited by the triple-junction amorphous panel, at air mass values greater than 1.5, is due to the fact that amorphous silicon cells are less responsive, compared to the other cell technologies, to the portion of the solar spectrum with wavelengths greater than 900 nm. As the absolute air mass increases, the solar spectrum contains a greater percentage of wavelengths above 900 nm resulting in the significant drop off exhibited in Fig. 6. Excellent agreement exists between the air mass functions measured at NIST and those published by Sandia National Laboratories (SNL) for modules that utilize the same cell technologies with the exception of the BIPV panel that incorporates polycrystalline cells, Fig. 6. The NIST measured results for the polycrystalline BIPV panel deviates from the SNL results as the absolute air mass increases. The reason for this discrepancy is unknown.

Incident Angle Functions

The coefficients resulting from a fifth order curve fit to the data sets in Fig. 7, to the incident angle for each BIPV panel are listed in Table 3. SNL data for modules utilizing identical cell technologies is included for comparison.

It is interesting to note that the incident angle response for the mono-crystalline, polycrystalline, and silicon film BIPV panels are almost identical. This is attributed to the fact that the glazing associated with these panels is identical, 6 mm low iron glass. The triple junction amorphous panel uses a two mil *Tefzel glazing and exhibits a somewhat different response to the angle of incidence.

Nominal Operating Cell Temperature

Table 4 summarizes the measured nominal operating cell temperatures (NOCT) of the BIPV panels. Two NOCT values are tabulated for each of the four cell technologies, one for an uninsulated panel and a second value for a panel with extruded polystyrene, having a nominal thickness and thermal resistance of 10.16 cm and 3.5 m²-K/W, respectively, attached to its rear

surface. These two test conditions were chosen to replicate the installation of the panels within NIST's BIPV "test bed" [1,4].

The measured NOCT values for the uninsulated BIPV panels using mono-crystalline, polycrystalline, and silicon film cells are within 1 °C of each other. Attachment of the insulation to the rear surface of each of these panels elevated the NOCT values by 21 °C to 23 °C. Since these three panels are identical, with the exception of the cell technology, it is not surprising that the resulting NOCT values are in close agreement. The triple junction amorphous panel is a commercially available module that bares little resemblance to the other three panels. Thus, the significantly different NOCT values for the triple-junction amorphous panel are not unexpected.

The uncertainty associated with the instrumentation used to measure the NOCT temperatures is estimated to be ± 0.4 °C. However, due to the inherent difficulties in measuring wind velocity and direction at the panel's surface in conjunction with the thermal mass associated with the panel, it is unlikely that the values in Table 4 represent true NOCT temperatures better than ± 0.3 °C

Electrical Performance at Standard Rating Conditions

The current and voltage values for each photovoltaic panel at standard rating conditions are given in Table 3. These values include the maximum power output (P_{mpo}), the current and voltage at the maximum power point (I_{mpo} and V_{mpo} , respectively) the short circuit current (I_{sco}) and the voltage at open circuit conditions (V_{oco}).

The custom fabricated BIPV panels are exact duplicates of the panels used within NIST's BIPV "test bed." The values listed in Table 3 are for a single triple-junction amorphous panel are for a single module, while the NIST BIPV "test bed" uses two of these connected in series. The amorphous silicon panel is an actual panel removed from the "test bed" after approximately 18 months of exposure.

The performance values in Table 3 denoted "Manufacturer" were derived in the following manner. Each of the manufacturers that provided cells for the custom fabricated BIPV panels also produces complete modules. Product information from the manufacturer's specification sheet for a module using the same cell technology and as close, as possible, the power rating of the BIPV panel was selected. The current, voltage, and power values from the module specification sheets were scaled appropriately for differences in the number of cells and electrical configuration. Close agreement between the NIST measurements for the BIPV modules and those derived from the specification sheets is not expected. Differences are attributed to variations in the glazings' solar transmittance, cell performance, and manufacturing procedures.

As expected, the current output of the silicon film panel is greater than that of the mono-crystalline or polycrystalline panels due to the larger cell size, 150 mm x 150 mm versus 125 mm x 125 mm. As a result of 72 cells being connected in series

Table 4 NOCT Summary (°C)

	Silicon Film	Mono- Crystalline	Poly Crystalline	Triple Junction Amorphous
Uninsulated Panel	43.0	43.7	43..3	37.9
Insulated Panel	64.7	66.7	65.5	55.3

for the mono-crystalline and polycrystalline panels, compared to 56 for the silicon film panel, the voltage measurements associated with these two panels are significantly higher than those for the silicon film panel.

SUMMARY

A series of tests to characterize the performance of three custom fabricated BIPV panels and one commercially available photovoltaic panel have been completed

Tests were conducted to determine the response of each panel to changes in cell temperature, absolute air mass and angle of incidence. The performance of each panel at Standard Rating Conditions was determined.

The measure temperature coefficients were generally in good agreement with data provided by the manufacturers and Sandia National Laboratories. The three custom fabricated BIPV panels exhibited similar responses to changes in absolute air mass and angle of incidence. The response of the fourth panel, the triple junction amorphous panel, to changes in absolute air mass and angle of incidence was distinctly different from the other three panels.

The nominal operating cell temperatures for the four panels were measured with and without thermal insulation attached to the panels' rear surface. The addition of insulation increased the NOCT temperatures by approximately 21 °C for the custom fabricated panels and 17 °C in the case of the triple junction amorphous silicon panel. The uninsulated and insulated amorphous panel's NOCT temperatures are approximately 5 °C and 10 °C less than the corresponding temperatures for the custom fabricated panels.

The parameters that have resulted from this work are being incorporated into the IV Curve Tracer and PHANTASM models. These models are being used to predict the annual performance of identical panels installed in NIST's BIPV "test bed."

ACKNOWLEDGMENTS

NIST's Building and Fire Research Laboratory and Advanced Technology Program as well as the California Energy Commission support this research. The assistance of David L. King and his colleagues at Sandia National Laboratories is greatly appreciated. They have provided continued and unwavering support throughout this project. Special thanks to Pete DeNapoli, Siemens Solar Systems, John Wolgemuth, BP/Solarex, and Jake Brown of Solar Building Systems for fielding numerous technical questions. Stanley Morehouse

constructed the solar tracker test facility used throughout this investigation. Stanley Morehouse, Daniel Vennetti, and David Frankford conducted the various tests described within this paper. The paper was typed and edited by Paula Svincek.

REFERENCES

- [1] Fanney, A.H., Dougherty, B.P., and Davis, M.W. 2001, "Measured Performance of Building Integrated Photovoltaic Panels," *ASME J. Solar Energy Engineering*, **123**, pp. 187-193.
- [2] 2000, PV-Design Pro, Solar Design Studio, v4.0, Maui Solar Energy Software Corp., Haiku, HI.
- [3] 1999, Photovoltaic Analysis and TrAnsient Simulation Method (PHANTASM), Building Integrated Photovoltaic Simulation Software, Solar Energy Laboratory, University of Wisconsin, Madison, WI
- [4] Fanney, A.H., and Dougherty, B.P., 2001, "Building Integrated Photovoltaic Test Facility," *ASME J. Solar Energy Engineering*, **123**, pp. 200-210.
- [5] ASTM "E 1036M, 2001, "Standard Test Methods for Electrical Performance of Nonconcentrator Terrestrial Photovoltaic Modules and Arrays Using Reference Cells," *Annual Book of ASTM Standards*, Vol. 12.02.
- [6] 2001, Database of Photovoltaic Module Performance Parameters, <http://www.sandia.gov/pv/pvc.htm>.
- [7] King, D.L., Kratochvil, J.A., and Boyson, W.E., 1997, "Temperature Coefficients for PV Modules and Arrays: Measurement Methods, Difficulties, and Results," *Proc. 26th IEEE Photovoltaic Specialists Conference*, Anaheim, CA, pp. 1183-1186.
- [8] Zanesco, and Krenzinger, 1993, "The Effects of Atmospheric Parameters on the Global Solar Irradiance and on the Current of a Silicon Solar Cell," *Progress in Photovoltaics: Research and Applications*, **1**, pp. 169-179.
- [9] King, D.L., 1996, "Photovoltaic Module and Array Performance Characterization Methods for all System Operating Conditions," *Proc. NREL/SNL Photovoltaics Program Review*, AIP Press, Lakewood, CO, 347-368.
- [10] King, D.L., Kratochvil, J.A., and Boyson, W.E., 1997, "Measuring Solar Spectral and Angle-of-Incidence Effects on Photovoltaic Modules and Solar Irradiance Sensors," *Proc. 26th IEEE Photovoltaic Specialists Conference*, Anaheim, CA, pp. 1113-1116.
- [11] Duffie, J.A., Beckman, W.A., 1991, *Solar Engineering of Thermal Processes*, John Wiley and Sons, New York.
- [12] King, D.L., Kratochvil, J.A., and Boyson, W.E., 1998, "Field Experience with a New Performance Characterization Procedure for Photovoltaic Arrays," *Proc. 2nd World Conference and Exhibition on Photovoltaic Solar Energy Conversion*, Vienna, Austria.
- [13] Emery et al., 1996, "Temperature Dependence of Photovoltaic Cells, Modules and Systems", *Proc. 25th PVSC*, Washington, DC, pp. 1275-1278.

MEASURED VERSUS PREDICTED PERFORMANCE OF BUILDING INTEGRATED PHOTOVOLTAICS

Mark W. Davis

Heat Transfer and Alternative Energy Systems Group
National Institute of Standards and Technology
Gaithersburg, Maryland 20899-8632

A. Hunter Fannery

Heat Transfer and Alternative Energy Systems Group
National Institute of Standards and Technology
Gaithersburg, Maryland 20899-8632

Brian P. Dougherty

Heat Transfer and Alternative Energy Systems Group
National Institute of Standards and Technology
Gaithersburg, Maryland 20899-8632

ABSTRACT

The lack of predictive performance tools creates a barrier to the widespread use of building integrated photovoltaic panels. The National Institute of Standards and Technology (NIST) has created a building integrated photovoltaic (BIPV) "test bed" to capture experimental data that can be used to improve and validate previously developed computer simulation tools. Twelve months of performance data have been collected for building integrated photovoltaic panels using four different cell technologies – crystalline, polycrystalline, silicon film, and triple-junction amorphous. Two panels using each cell technology were present, one without any insulation attached to its rear surface and one with insulation having a nominal thermal resistance value of $3.5 \text{ m}^2\cdot\text{K}/\text{W}$ attached to its rear surface. The performance data associated with these eight panels, along with meteorological data, were compared to the predictions of a photovoltaic model developed jointly by Maui Solar Software and Sandia National Laboratories (SNL), which is implemented in their IV Curve Tracer software [1]. The evaluation of the predictive performance tools was done in the interest of refining the tools to provide BIPV system designers with a reliable source for economic evaluation and system sizing.

INTRODUCTION

Predictive performance tools are an important factor in the success of any technology. An effective performance model would accurately predict the annual energy production given the orientation of the proposed photovoltaic system, typical weather conditions for the geographic region, the nominal performance of the specified BIPV technology, and the proposed coverage area of the BIPV application. The predicted energy production would subsequently be used to compute the energy and cost savings for different cell technologies and system orientations.

The benefits of these predictive tools are obvious. The ability to optimize the performance of BIPV applications allows consumers to maximize the cost effectiveness of the system before installing it.

Additionally, the predictive models can demonstrate whether or not a system will be economically feasible.

The accuracy of these tools is key in the overall customer satisfaction. If the predictive models significantly underpredict the amount of BIPV product required for applications, customers may assume that photovoltaics are not as effective as they truly are. Alternatively, predictive models that overpredict the amount of product needed result in poor economic decisions. Predictive tools that either underpredict or overpredict the size of BIPV systems contribute to negative customer satisfaction, which hamper the widespread use of the energy saving technology.

The National Institute of Standards and Technology created a building integrated photovoltaic test facility to evaluate BIPV products and predictive tools [2]. The facility includes a "test bed" for side-by-side testing of BIPV products, a solar tracking facility for short-term characterization of BIPV panels, and a rooftop meteorological station. During the calendar year 2000, four different cell technologies, crystalline, polycrystalline, silicon film, and triple-junction amorphous, were present in the "test bed." Two panels of each cell technology were installed, one panel without backside insulation and one with insulation attached to the rear surface of the panel. The 102 mm (4 in) thick extruded polystyrene insulation has a nominal R-value of $3.5 \text{ m}^2\cdot\text{K}/\text{W}$ (R-20). Twelve months of performance data was recorded at 5 min intervals, including power output, voltage, current, panel temperature, and meteorological data.

The solar tracking facility is used to characterize the electrical performance of the panels used in the "test bed." The performance at standard rating conditions, the temperature coefficients, the effect of air mass, and the effect of incident angle are measured for each panel. These parameters are required inputs to the computer simulation tools [3].

The rooftop meteorological station measures the total horizontal, horizontal diffuse, and the direct beam irradiance; the outdoor ambient temperature; and the wind speed and direction. The rooftop data are measured and stored at 5-minute intervals throughout the year. Additionally, a small meteorological station is located on the wall at

the “test bed.” This station measures the total irradiance in the plane of the panels, the wind speed in the plane of the panels, and the outdoor ambient temperature.

These facilities provide the measurements needed to evaluate BIPV predictive performance tools. The measured “test bed” performance [4] is compared to the performance predicted with the SNL PV model using characterization parameters from the tracking facility and the measured meteorological data. The SNL model is empirical in nature, and it requires many parameters specific to the model. The prediction of the panel’s temperature is a key component of any PV model. The temperature of the photovoltaic cells is predicted with IV Curve Tracer using an empirical model. A transient one-dimensional heat transfer model, developed at NIST [5], was substituted for the empirical model. Comparisons were made to predictions using the empirical model and measured data.

SANDIA ELECTRICAL PERFORMANCE MODEL

A number of publications have described the model developed by Sandia National Laboratories to predict the electrical output of photovoltaic panels [6, 7, 8, 9]. The equations presented in this paper represent SNL’s latest implementation of the model [10]. A premise of this performance model is that the I_{mp} , V_{oc} , and V_{mp} of a photovoltaic module can be described as functions of I_{sc} and the cell temperature. As shown in Eq. 1, the short-circuit current is assumed to be dependant on the beam and diffuse irradiance, air mass, incident angle, and panel temperature. Equations 2 – 6 are used to predict the remaining performance variables (open-circuit voltage, maximum power current, and maximum power voltage) using the short-circuit current. The effective irradiance, E_e , is defined as the ratio of the measured short-circuit current, which is adjusted to the reference temperature, T_o , to the short-circuit current at standard rating conditions. The remaining performance parameters are predicted using the effective irradiance and several empirical coefficients as well as the respective temperature coefficients.

$$I_{sc} = I_{sc_o} \cdot f_1(AM_a) \cdot \left(\frac{(E_b \cdot f_2(AOI) + f_d \cdot E_{diff})}{E_o} \right) \cdot (1 + \bar{\alpha}_{I_{sc}} \cdot (T_c - T_o)) \quad (1)$$

$$E_e = \frac{I_{sc}}{I_{sc_o} \cdot (1 + \bar{\alpha}_{I_{sc}} \cdot (T_c - T_o))} \quad (2)$$

$$I_{mp} = I_{mp_o} \cdot (C_0 \cdot E_e + C_1 \cdot E_e^2) \cdot (1 + \bar{\alpha}_{I_{mp}} \cdot (T_c - T_o)) \quad (3)$$

$$\delta(T_c) = \frac{n \cdot k \cdot (T_c + 273.15)}{q} \quad (4)$$

$$V_{oc} = V_{oc_o} + N_s \cdot \delta(T_c) \cdot \ln(E_e) + \beta_{V_{oc}} \cdot (T_c - T_o) \quad (5)$$

$$V_{mp} = V_{mp_o} + C_2 \cdot N_s \cdot \delta(T_c) \cdot \ln(E_e) + C_3 \cdot N_s \cdot (\delta(T_c) \cdot \ln(E_e))^2 + \beta_{V_{mp}} \cdot (T_c - T_o) \quad (6)$$

$$P_{mp} = V_{mp} \cdot I_{mp} \quad (7)$$

$$f(AM_a) = A0 + A1 \cdot AM_a + A2 \cdot AM_a^2 + A3 \cdot AM_a^3 + A4 \cdot AM_a^4 \quad (8)$$

$$f(AOI) = B0 + B1 \cdot AOI + B2 \cdot AOI^2 + B3 \cdot AOI^3 + B4 \cdot AOI^4 + B5 \cdot AOI^5 \quad (9)$$

A large number of performance parameters that are not provided by manufacturers are required. Temperature coefficients for the maximum power current and voltage, polynomials describing the effect of air mass and incident angles, and an empirical diode factor are a few of the less-common parameters that a system designer would need. However, the developers have provided these obscure values in a large database of parameters for some popular pre-fabricated panels. In the case of custom-fabricated BIPV panels, however, these parameters are not available. Once the parameters are acquired, the implementation of the model is simple, and several programs are available that utilize the SNL model, including IV Curve Tracer [1] and PV-Design Pro [11].

PANEL TEMPERATURE PREDICTION MODELS

The prediction of the panel temperature is an important part of the SNL electrical performance model. The temperature of the panel significantly affects the output voltage and, therefore, the power produced by the panel. The SNL model was run using its own cell temperature prediction method and the NIST cell temperature model. Each model predicts the panel temperature differently. In SNL’s model, the temperature on the rear surface of the panel is predicted using the incident irradiance, the ambient temperature, the wind speed, and several empirical coefficients as shown in Eq. (10). Then, using Eq. (11), the temperature at the PV cell, which is the temperature that truly governs the performance of the cell, is predicted using the panel temperature assuming a standard temperature difference between the two. The SNL model developers have provided empirical coefficients [10], Table 1, for three typical panel construction and application scenarios: glass-cell-tedlar panel in an open rack, glass-cell-glass panel mounted flat on a roof, and a glass-cell-glass panel in an open rack.

$$T_m = T_{amb} + E_{POA} \cdot \exp(a + b \cdot WS) \quad (10)$$

$$T_c = T_m + \frac{E_{POA}}{E_o} \Delta T \quad (11)$$

The NIST temperature model [5] uses the approximation of one-dimensional transient heat transfer to predict the temperature of the cell. It uses the beam and diffuse irradiance incident on the panel, the

Table 1. SNL thermal model parameters for several panel types and mounting schemes

Panel Type	Mount	a	b	ΔT
Glass/Cell/Glass	Open Rack	-3.473	-0.0595	2
Glass/Cell/Glass	Close Roof Mount	-2.976	-0.0471	3
Glass/Cell/Tedlar	Open Rack	-3.562	-0.0786	3

* Certain trade names and company products are mentioned in the text or identified in an illustration in order to adequately specify the experimental procedure and equipment used. In no case does such an identification imply recommendation or endorsement by the National Institute of Standards and Technology, nor does it imply that the products are necessarily the best available for the purpose.

Table 2 Measured electrical performance model parameters for Sandia photovoltaic model

Parameter		Monocrystalline	Polycrystalline	Silicon Film	Triple-Junction Amorphous
Isc	A	4.375	4.250	5.114	4.440
Impo	A	3.961	3.818	4.488	3.613
Voco	V	42.926	41.498	29.614	23.156
Vmpo	V	33.680	32.944	23.165	16.037
α -Isc	A/°C	0.001753	0.002380	0.004683	0.005606
	1/°C	0.000401	0.000560	0.000916	0.001263
α -Imp	A/°C	-0.001543	0.000178	0.001605	0.007348
	1/°C	-0.000390	0.000047	0.000358	0.002034
β -Voc	V/°C	-0.152366	-0.152798	-0.129954	-0.093102
	1/°C	-0.003549	-0.003682	-0.004388	-0.004021
β -Vmp	V/°C	-0.153578	-0.159116	-0.130387	-0.047729
	1/°C	-0.004560	-0.004830	-0.005629	-0.002976
Ns		72	72	56	11
A0		0.935823	0.918093	0.938110	1.100441
A1		0.054289	0.086257	0.062191	-0.061423
A2		-0.008677	-0.024459	-0.015021	-0.004427
A3		0.000527	0.002816	0.001217	0.000632
A4		-0.000011	-0.000126	-0.000034	-0.000019
B0		1.00034	0.99851	0.99898	1.00184
B1		-5.5575E-03	-1.2122E-02	-6.0977E-03	-5.6481E-03
B2		6.5530E-04	1.4398E-03	8.1173E-04	7.2543E-04
B3		-2.7299E-05	-5.5759E-05	-3.3758E-05	-2.9164E-05
B4		4.6405E-07	8.7794E-07	5.6466E-07	4.6957E-07
B5		-2.8061E-09	-4.9190E-09	-3.3714E-09	-2.7387E-09
C0		1.000	1.014	0.961	1.072
C1		0.003	-0.005	0.037	-0.098
C2		-0.538	-0.321	0.232	-1.846
C3		-21.408	-30.201	-9.429	-5.176
n		1.026	1.025	1.357	3.086

ambient temperature, the effective sky temperature in front and in back of the panel, the wind speed, and the electrical power produced by the panel. The photovoltaic panel is divided into several layers (backside insulation, PV cells, glazing, etc.) according to its construction, and the thickness, density, specific heat, and thermal conductivity are required for each layer. An implicit finite difference scheme is used to determine the temperature throughout the cross-section of the panel, and the cell temperature is calculated as the average of the temperatures in the PV cell layer. The method requires iteration of the temperatures at the two panel surfaces, which makes the NIST PV cell temperature model much more computationally intense than the

empirical model used by Sandia National Laboratories.

MODELING PARAMETERS

The SNL's electrical performance model and the NIST cell temperature model require parameters describing the important panel characteristics. Panel manufacturers provide some of these parameters, but each of the models require parameters that are not readily available. The electrical performance model by SNL requires the maximum power, open-circuit, and short-circuit performance ratings, which are normally provided by module manufacturers. The manufacturer's module specifications usually include the short-circuit

Table 3 NIST PV cell temperature model parameters

Layer		Monocrystalline	Polycrystalline	Silicon Film	Triple-Junction Amorphous
Parameter	Unit				
<i>Glazing</i>		<i>Glass</i>	<i>Glass</i>	<i>Glass</i>	<i>Tefzel</i>
Thickness	m	0.006	0.006	0.006	0.000051
Density	kg/m ³	2500	2500	2500	1750
Sp. Heat	J/kg K	840	840	840	1050
Th. Cond	W/m K	1.04	1.04	1.04	0.24
<i>Cell</i>		<i>Silicon</i>	<i>Silicon</i>	<i>Silicon</i>	<i>Silicon</i>
Thickness	m	0.00086	0.00038	0.00038	0.000001
Density	kg/m ³	2330	2330	2330	2330
Sp. Heat	J/kg K	712	712	712	712
Th. Cond	W/m K	148	148	148	148
<i>Backing/Substrate</i>		<i>Tedlar*/Mylar*</i>	<i>Tedlar*/Mylar*</i>	<i>Tedlar*/Mylar*</i>	<i>304SS</i>
Thickness	m	0.00017	0.00017	0.00017	0.000125
Density	kg/m ³	1475	1475	1475	7900
Sp. Heat	J/kg K	1130	1130	1130	477
Th. Cond	W/m K	0.14	0.14	0.14	14.9
<i>Insulation</i>		<i>Extruded Polystyrene</i>	<i>Extruded Polystyrene</i>	<i>Extruded Polystyrene</i>	<i>Extruded Polystyrene</i>
Thickness	m	0.1016	0.1016	0.1016	0.1016
Density	kg/m ³	55	55	55	55
Sp. Heat	J/kg K	1210	1210	1210	1210
Th. Cond	W/m K	0.0294	0.0294	0.0294	0.0294

current and open-circuit voltage temperature coefficients, which are also utilized by SNL's model, but the voltage and current temperature coefficients at the maximum power point that the SNL model requires are not always provided. Manufacturers do not supply the remaining parameters. As mentioned previously, SNL provides a database of empirical coefficients for some common PV panels. Unfortunately, three of the four cell technologies (six of the eight panels) were custom-made for the BIPV "test bed." Therefore all of the empirical parameters in Eqs. 1-7 were measured using the NIST Solar Tracking Facility [3], Table 2.

The thermal models also require a number of parameters. The parameters for the SNL thermal model were discussed previously, Table 1. For the purpose of modeling the NIST BIPV panels, the uninsulated panels will employ the open rack, glass/cell/Tedlar* parameters, and the insulated panels will use the close roof mounted glass/cell/glass parameters. While these parameters do not apply precisely to the mounting of the panels in the NIST BIPV "test bed", they are the most appropriate of the three options provided by the model developers.

thickness of the layer, density, specific heat, and thermal conductivity of each layer are required. The parameters used to model the eight panels are shown in Table 3. The monocrystalline, polycrystalline, and silicon film panels were custom fabricated. Therefore, the materials used in their construction were readily available for thickness measurements. The triple-junction amorphous panel is a pre-fabricated, and the thicknesses of the individual layers were obtained from the manufacturer. The properties for the Tefzel*, Tedlar*/Mylar*, and glass were obtained from specification sheets provided by the respective manufacturers. All of the other property data were obtained from commonly available material property tables.

MODEL IMPLEMENTATION

In order to compare the measurements made by the BIPV "test bed" with those predicted by the SNL model on an annual basis, the model needed to be applied at 5 min intervals over 1 year for eight different panels. IV Curve Tracer, which houses the SNL photovoltaic performance model, is used to trace a single I-V curve at specified

Table 4 Monthly SNL and SNL/NIST results for eight panels

	Monocrystalline								Polycrystalline							
	Uninsulated				Insulated				Uninsulated				Insulated			
	SNL		SNL/NIST		SNL		SNL/NIST		SNL		SNL/NIST		SNL		SNL/NIST	
	Diff (%)	R ²	Diff (%)	R ²	Diff (%)	R ²	Diff (%)	R ²	Diff (%)	R ²	Diff (%)	R ²	Diff (%)	R ²	Diff (%)	R ²
January	0.7	0.916	-5.1	0.924	-3.0	0.932	-5.3	0.930	0.6	0.919	-4.4	0.926	-4.8	0.938	-6.5	0.934
February	0.6	0.959	-4.6	0.961	-1.8	0.967	-4.2	0.964	0.2	0.958	-4.5	0.960	-4.1	0.967	-5.9	0.962
March	-1.4	0.971	-5.0	0.969	-3.1	0.972	-4.6	0.967	-1.7	0.969	-5.0	0.967	-5.8	0.969	-6.9	0.963
April	-5.0	0.973	-7.6	0.970	-6.2	0.973	-7.1	0.970	-4.5	0.972	-7.0	0.969	-9.0	0.968	-9.6	0.964
May	-6.3	0.964	-6.9	0.963	-5.9	0.966	-6.4	0.963	-6.8	0.961	-7.3	0.960	-10.4	0.957	-10.7	0.954
June	-5.3	0.962	-5.4	0.961	-4.5	0.964	-4.9	0.961	-6.6	0.957	-6.6	0.957	-10.2	0.952	-10.5	0.950
July	-5.7	0.939	-6.0	0.937	-4.9	0.942	-5.5	0.936	-7.1	0.932	-7.2	0.930	-10.4	0.930	-10.9	0.924
August	-2.8	0.948	-3.4	0.946	-2.3	0.950	-3.2	0.945	-3.6	0.945	-4.0	0.942	-6.8	0.945	-7.5	0.939
September	-1.4	0.940	-3.0	0.937	-1.6	0.942	-2.9	0.935	-2.2	0.937	-3.5	0.934	-5.3	0.939	-6.2	0.931
October	0.4	0.976	-2.5	0.977	0.4	0.980	-2.1	0.978	-0.3	0.976	-2.8	0.976	-2.4	0.981	-4.4	0.977
November	0.8	0.938	-3.8	0.942	-0.7	0.949	-3.1	0.945	1.1	0.943	-3.1	0.946	-2.6	0.958	-4.3	0.952
December	2.8	0.933	-3.9	0.943	-0.8	0.948	-3.5	0.947	3.0	0.939	-3.2	0.948	-2.5	0.958	-4.6	0.955
Total	-1.1	0.947	-4.6	0.951	-2.5	0.956	-4.2	0.953	-1.4	0.948	-4.5	0.951	-5.4	0.958	-6.8	0.953

	Silicon Film								Triple-Junction Amorphous							
	Uninsulated				Insulated				Uninsulated				Insulated			
	SNL		SNL/NIST		SNL		SNL/NIST		SNL		SNL/NIST		SNL		SNL/NIST	
	Diff (%)	R ²	Diff (%)	R ²	Diff (%)	R ²	Diff (%)	R ²	Diff (%)	R ²	Diff (%)	R ²	Diff (%)	R ²	Diff (%)	R ²
January	7.9	0.918	0.8	0.935	3.1	0.948	-0.3	0.947	-6.1	0.958	-7.2	0.957	-6.1	0.953	-6.6	0.953
February	6.7	0.954	0.4	0.963	3.1	0.965	-0.5	0.962	-3.8	0.971	-4.7	0.971	-4.3	0.971	-4.8	0.971
March	4.6	0.965	0.1	0.967	1.2	0.969	-1.2	0.963	-3.4	0.973	-4.0	0.973	-4.5	0.973	-4.8	0.972
April	3.6	0.970	0.1	0.969	0.1	0.972	-1.5	0.967	-2.0	0.975	-2.4	0.975	-3.0	0.976	-3.2	0.975
May	4.1	0.956	3.2	0.956	1.5	0.959	0.5	0.956	0.5	0.968	0.4	0.968	0.5	0.968	0.4	0.968
June	6.4	0.947	6.3	0.947	3.8	0.952	2.9	0.950	2.7	0.961	2.7	0.961	2.9	0.962	2.9	0.962
July	4.8	0.923	4.4	0.921	2.4	0.929	1.3	0.922	0.8	0.943	0.7	0.943	1.1	0.943	1.0	0.943
August	6.0	0.937	5.3	0.935	3.8	0.943	2.2	0.936	3.0	0.949	2.8	0.949	3.0	0.950	2.8	0.950
September	4.0	0.930	2.1	0.928	1.8	0.936	-0.2	0.928	-0.7	0.943	-1.1	0.943	-0.9	0.944	-1.1	0.944
October	4.5	0.974	1.0	0.977	3.4	0.979	-0.2	0.977	-0.6	0.984	-1.2	0.984	-1.1	0.983	-1.5	0.983
November	7.5	0.941	1.8	0.950	4.7	0.960	1.2	0.956	0.2	0.967	-0.7	0.968	-1.1	0.968	-1.6	0.968
December	10.0	0.937	2.0	0.955	5.1	0.964	1.2	0.964	1.2	0.970	-0.1	0.972	-0.2	0.968	-0.8	0.968
Total	6.2	0.945	1.8	0.954	3.0	0.960	0.3	0.957	-1.0	0.967	-1.7	0.967	-1.5	0.966	-1.9	0.966

As discussed previously, the NIST PV cell temperature divides the photovoltaic panel into layers according to its construction. The

input conditions. To simplify the use of the BIPV "test bed" meteorological data [4], the SNL model was implemented in a

FORTTRAN subroutine for use in the TRNSYS [12] frontend. The University of Wisconsin created TRNSYS as an object-oriented application that manages different FORTTRAN subroutines. TRNSYS also supplies radiation processors and data reader subroutines for transient applications such as this. The predicted electrical output using the FORTTRAN subroutine was compared to the predicted output using IV Curve Tracer. Additionally, a spreadsheet employing the SNL model was obtained from the model developers at Sandia National Laboratories. The spreadsheet had the ability to predict the electrical output of a module over a period of time using meteorological data supplied by the user. The accuracy of the FORTTRAN subroutine within TRNSYS as compared to the SNL model was verified by predicting 1 day's output of a BIPV "test bed" module using the SNL spreadsheet and the TRNSYS subroutine. The two applications agreed within 0.25 % over the day, which indicated successful implementation of the SNL model into FORTTRAN.

For the purpose of evaluating the accuracy of these models, the performance and meteorological data recorded during the testing period was divided into blocks of data that were considered suitable for evaluation of performance models. Records that were missing measurements or contained incorrect measurements were not used, and only days with all daylight records present were used in the final analysis. A total of 309 days were analyzed out of a possible 363 days of measured data.

The SNL model and the SNL model outfitted with the NIST PV cell temperature model were applied to the eight panels present in the BIPV "test bed" over the course of a year. The electrical output of the models was compared to the measured electrical output of each panel. At a 95 % confidence level, the expanded uncertainty of the measured energy output is $\pm 1.2\%$. Two methods were used to evaluate the quality of the predicted results. Most importantly, the measured accumulated energy was compared to the predicted energy. This

quantity is most easily comprehended in terms of a percent difference from the measured value. The second method of comparison was the statistical correlation coefficient, R^2 . Unlike the comparison of accumulated energy, the correlation coefficient compares the predicted output at each point. This provides a clearer picture of the precision of the model, but the energy output by the modules is the end goal.

RESULTS

Overall, the performance of the SNL photovoltaic performance model was found to be very good, Table 4. The greatest difference between the predicted and measured accumulated energy using the SNL model was 6.2 % in the case of the uninsulated silicon film module. The model agreed with the measured results to within 1.5 % for the remaining uninsulated panels. In the case of the insulated panels, the polycrystalline module resulted in the greatest difference (5.4 %) between the measured and predicted results. The remaining seven modules agreed within 3 % using the SNL model.

Incorporating the NIST temperature model within SNL's photovoltaic model produced mixed results. For the silicon film panel, the predicted energy improved for both the insulated (3.0 % to 0.3 %) and uninsulated panel (6.2 % to 1.8 %). However, the agreement between the measured and predicted results for the other three insulated panels was not as close as those obtained using the temperature model proposed by SNL.

Looking at the R^2 values, which more accurately indicate the precision of the predictions, the R^2 values for each uninsulated panel improved with the use of the NIST cell temperature model, and the R^2 values decreased for each of insulated panels. For both the insulated and uninsulated cases, the R^2 values of the triple-junction amorphous panels did not change between the two models.

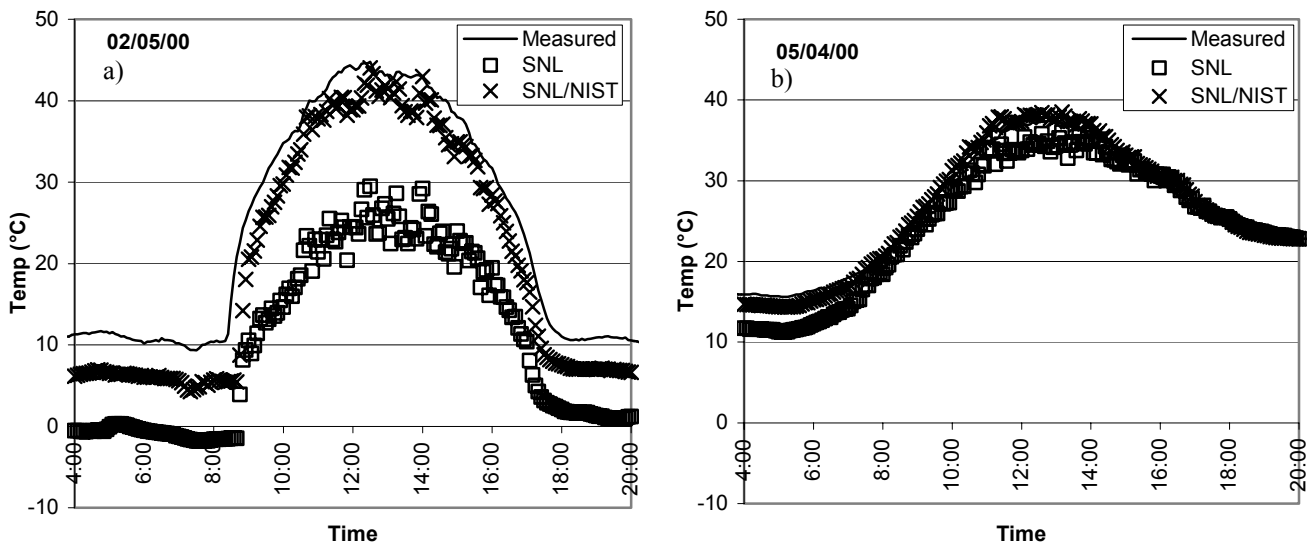


Figure 1 Measured and predicted cell temperatures for the uninsulated monocrystalline panel for a clear day in a) February and b) May

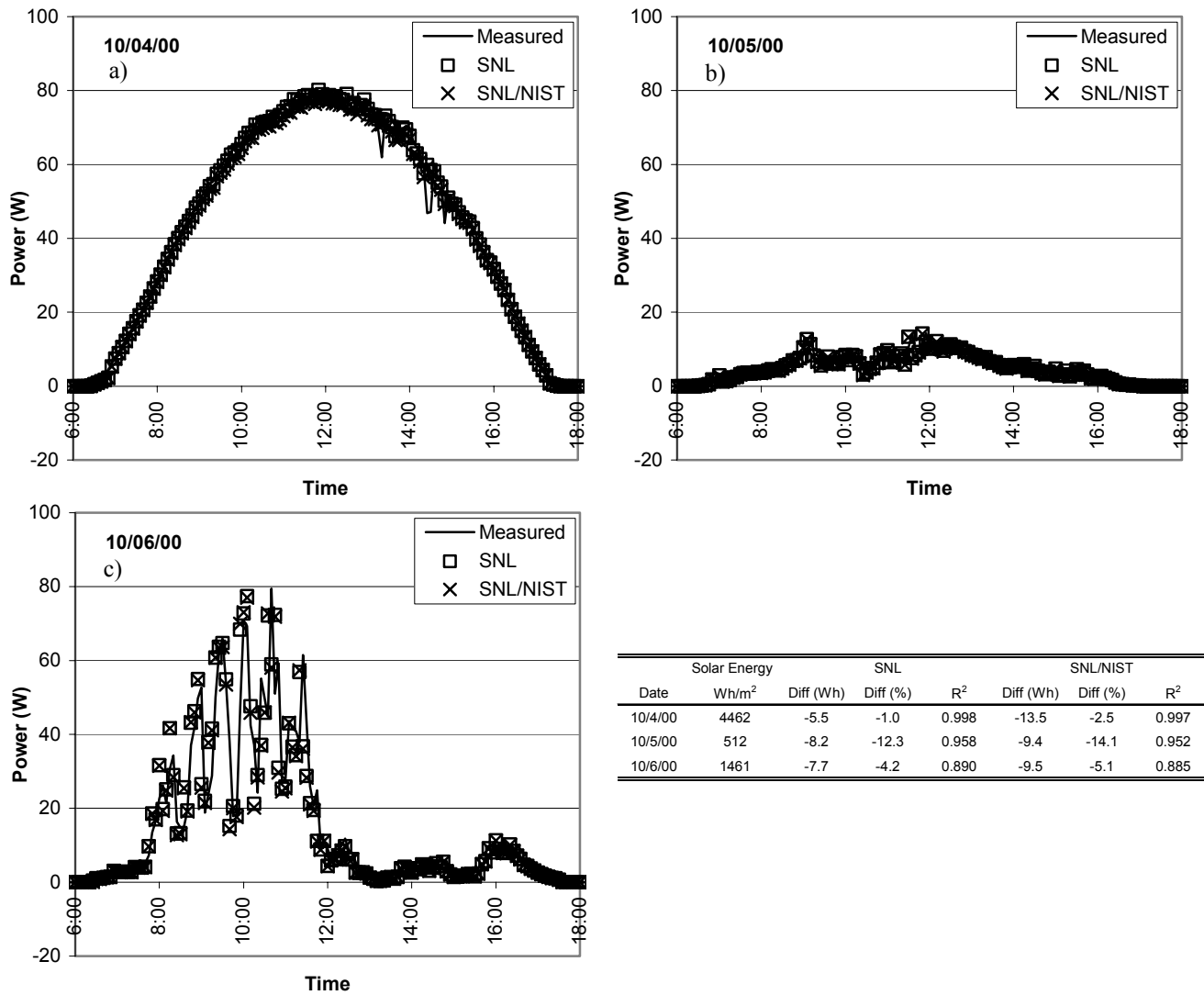


Figure 2 a) Predicted and measured results for the uninsulated monocrystalline module for a) clear, b) cloudy, and c) partly cloudy days

Although the electrical output predictions for the uninsulated panels were closer for the SNL model as opposed to the SNL/NIST model, the NIST temperature model more closely predicted the cell temperature. Figure 1 shows this for the uninsulated monocrystalline panel for two clear days with significantly different outdoor ambient temperatures. The average ambient temperature was 1.5 °C on February 5 and 19.5 °C on May 4. The expanded uncertainty for both the cell and ambient temperatures is ± 0.3 °C at a confidence level of 95 %. The average irradiance on February 5 and May 4 was 580 W/m² and 210 W/m², respectively, which explains the higher panel temperatures seen on the colder day. Similar results for cell temperature prediction were found for all four uninsulated modules. The difference between the models is greater during periods of cold ambient temperatures, Figure 1. This may be attributed to the fact that the SNL temperature model assumes both sides of the panel are subjected to the outdoor ambient temperature, but in reality, the rear side of the BIPV panels is exposed to controlled indoor conditions. The temperature prediction of both models for the insulated panels closely tracked the measured cell temperatures throughout the year.

It is interesting to note that if the temperature predicted by the SNL model was closer to the measured panel temperature, the SNL electrical performance model would not result in such good agreement. Figure 1 shows that the SNL temperature model underpredicts the uninsulated panel temperatures in the “test bed” during periods of cooler weather. Table 4 shows that the best agreement between the SNL model and the measured results was in those cooler months. In fact, during the warmer months when the NIST and SNL temperature model closely match in their temperature predictions, the differences between the SNL and SNL/NIST models are significantly less. For example, Table 4 shows that for the uninsulated monocrystalline panel, the SNL and SNL/NIST models result in a +0.6 % and -4.6 % difference, respectively, in the month of February. However, during the month of June, the differences between the measured results and the two models are almost equal (SNL: -5.3 %, SNL/NIST: -5.4 %). Except for the triple-junction amorphous panel, which is not as strongly affected by the temperature, similar trends occur for the other panels.

Considering the different methods used to measure the irradiance

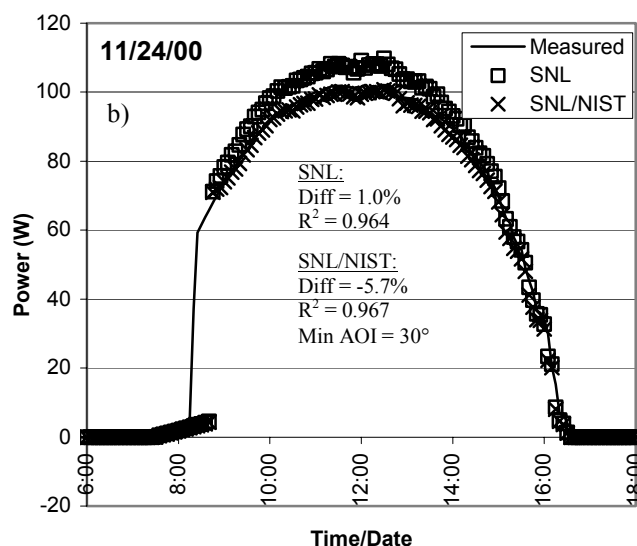
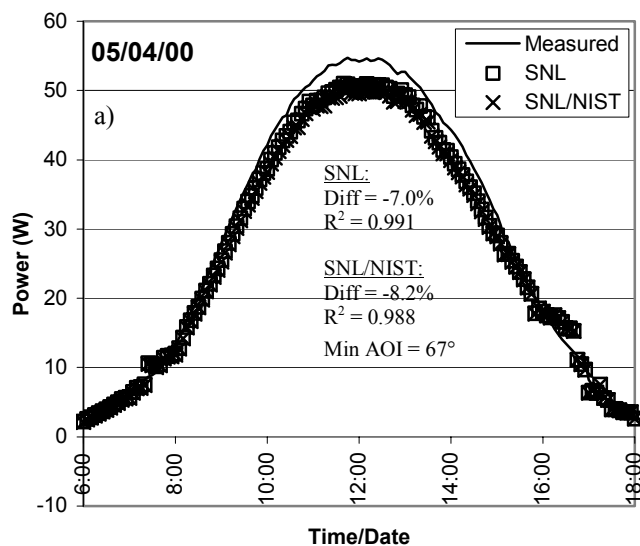


Figure 3 Measured and predicted power output for a clear day in a) May with a high incident angle and b) November with a low incident angle

and power output at each interval, the close agreement between the predicted and measured results is remarkable. The performance model uses the meteorological conditions recorded at 5 min intervals to predict the power output every 5 min. The accumulated energy is assumed to be the product of the power output and the time interval (5 min). The measured electrical energy is also calculated by multiplying the power and the time interval, but the instrument used at the BIPV “test bed” [1] measures the power at 15 s intervals and takes the average over the 5 min period. Thus, on days with quickly changing irradiance values, the predicted and measured values could vary significantly. Additionally, the measurement of the beam irradiance is not directly at the BIPV “test bed.” Therefore, on partly cloudy days, the beam irradiance at the “test bed” could be different than the measurement. Figures 2 a), b), and c) show measured and predicted power output on three days (clear, cloudy, and partly cloudy) for the uninsulated monocrystalline panel. The percent difference and R^2 values are significantly better for the clear day compared to both the partly cloudy and cloudy days. Although the solar energy was low on the cloudy day, it was relatively steady, which resulted in significantly better R^2 values for the cloudy day than those for the partly cloudy day. The absolute difference between the predicted and measured results for the two models on all three days is shown in the table in Figure 2. The magnitude of the Watt-hour difference remains approximately the same, but the delivered solar energy varies greatly between the three days. This would seem to indicate that the irradiance level itself does not produce errors in the predictions. The temperature prediction for both models is within 5 °C throughout the clear and cloudy days. Due to the quickly changing irradiance, the predicted temperatures on the partly cloudy day were not as close.

The better predictive performance of I-V Curve Tracer on clear days can also be seen in the compiled monthly data. Table 4 shows a dramatic decrease in the R^2 value during the months of July, August, and September for each of the panels. These three months were very cloudy at NIST. Alternatively, October of that year was extremely clear, and it resulted in the highest R^2 value for any month. There were nine clear days in October and only three in the July through

September period.

Another reason for poor performance during the summer months may be attributed to the high incident angle throughout the day. Figure 3 a) and b) show that the SNL model overpredicts the output power during the winter when the incident angle is relatively low and underpredicts on days when the angle is high. As shown previously, the SNL electrical performance model includes a polynomial function, $f_2(\text{AOI})$, to adjust the transmittance of the glass and absorptance of the PV cells to account for the effect of the incident angle. Additionally, the pyranometer readings are adjusted with respect to the incident angle. The temperatures of the module on these two days are within 6 °C at their peak.

Visually, the SNL/NIST model provides an excellent fit for the measured data on November 24, but the percent difference and R^2 values on this day are worse than those for May 4. This discrepancy is due to the early morning shading that occurs in the winter months. A large building lies due East of the BIPV “test bed” and casts a shadow on the test site in the morning. The irradiance measurements are made on the eastern end of the “test bed” below the panels. Therefore, the pyranometers are shaded for a longer period than the modules, especially the monocrystalline modules. Figure 3 b) shows a large underprediction in the early morning that would be expected in this situation.

CONCLUSION

The photovoltaic model proposed by Sandia National Laboratories was evaluated with respect to the measured electrical output of eight BIPV modules in NIST’s BIPV “test bed.” Additionally, the SNL electrical performance model was coupled with the NIST cell temperature model and compared to the measured results. The agreement of both models to the measured data was well within 7% on an annual basis compiling all eight modules. The SNL model resulted in a closer monthly and annual predicted energy output when compared to the SNL model using the NIST cell temperature model. However, it was shown that the NIST cell temperature model more closely predicted the cell temperatures. This discrepancy results

from a general underprediction of the power output using the SNL electrical performance model. Additionally, the model performs better on clear days when the irradiance is steady. The model may also underpredict at high incident angles. Overall, annual energy output predictions within 7 % of the measured results are quite remarkable.

NOMENCLATURE

A0–A4	= coefficients for the air mass function, $f_1(AM_a)$
a, b	= empirical coefficients relating the irradiance and windspeed to module temperature
AM_a	= air mass adjusted according to altitude
AOI	= angle between the sun and module (degrees)
B0–B5	= coefficients for the incident angle function, $f_2(AOI)$
C_0, C_1	= empirical coefficients relating I_{mp} to the “effective” irradiance
C_2, C_3	= empirical coefficients relating V_{mp} to the “effective” irradiance
E_b	= beam irradiance (W/m^2)
E_{diff}	= diffuse irradiance (W/m^2)
E_e	= “effective” irradiance
E_o	= reference irradiance, 1000 (W/m^2)
E_{POA}	= irradiance incident on the plane of the module (W/m^2)
$f_1(AM_a)$	= polynomial describing the spectral influence on I_{sc}
$f_2(AOI)$	= polynomial describing the effect of incident angle on I_{sc}
f_d	= fraction of diffuse irradiance used by module, 1 for non-concentrating modules
I_{mp}	= current at maximum power point (A)
I_{mp_o}	= maximum power current at $E = 1000 W/m^2$, $T_c = 25^\circ C$, $AM_a = 1.5$, and $AOI = 0$ (A)
I_{sc}	= short-circuit current (A)
I_{sc_o}	= short-circuit current at $E = 1000 W/m^2$, $T_c = 25^\circ C$, $AM_a = 1.5$, and $AOI = 0$ (A)
k	= Boltzmann’s constant, 1.380×10^{-23} (J/K·molecule)
n	= empirical diode factor
N_s	= number of cells in series in the module
P_{mp}	= power at maximum power point (W)
q	= elementary charge, $1.60218E-19$ (C)
T_m	= temperature on the back surface of a module ($^\circ C$)
T_{amb}	= ambient temperature ($^\circ C$)
T_c	= temperature of PV cell
T_o	= reference temperature, 25 ($^\circ C$)
V_{mp}	= voltage at maximum power point (V)
V_{mp_o}	= maximum power voltage at $E_e = 1$ and $T_c = T_o$ (V)
V_{oc}	= open-circuit voltage (V)
V_{oc_o}	= open-circuit voltage at $E_e = 1$ and $T_c = T_o$ (V)
WS	= wind speed (m/s)
$\alpha_{I_{mp}}$	= maximum power temperature coefficient normalized with respect to I_{mp_o} ($1/^\circ C$)
$\alpha_{I_{sc}}$	= short-circuit temperature coefficient normalized with respect to I_{sc_o} ($1/^\circ C$)
$\delta(T_c)$	= “thermal voltage” as a function of cell temperature
$\beta_{V_{mp}}$	= maximum power voltage temperature coefficient ($V/^\circ C$)
$\beta_{V_{oc}}$	= open-circuit voltage temperature coefficient ($V/^\circ C$)
ΔT	= temperature difference between cell and back of module at $1000 W/m^2$ ($^\circ C$)

REFERENCES

- [1] 2000, Sandia Photovoltaic Performance Model I-V Curve Tracer, Maui Solar Energy Software Corp., Haiku, HI.
- [2] Fanney, A.H., and Dougherty, B.P., 2001, "Building Integrated Photovoltaic Test Facility," ASME J. Solar Energy Engineering, **123**, pp. 194-199.
- [3] Fanney, A. H., Davis, M. W., and Dougherty, B. P., “Short-Term Characterization of Building Integrated Photovoltaic Panels,” *Proc of Solar 2002: Sunrise on the Reliable Energy Economy*, June, Reno, NV, ASME, New York.
- [4] Fanney, A.H., Dougherty, B.P., and Davis, M.W. 2001, "Measured Performance of Building Integrated Photovoltaic Panels," ASME J. Solar Energy Engineering, **123**, pp. 187-193.
- [5] Davis, M. W., Fanney, A. H., and Dougherty, B. P., 2000, “Prediction of Building Integrated Photovoltaic Cell Temperatures,” ASME Solar Energy Engineering, vol. 123, no. 3, pp 200-210.
- [6] King, D.L., Kratochvil, J.A., and Boyson, W.E, 1997, "Temperature Coefficients for PV Modules and Arrays: Measurement Methods, Difficulties, and Results", Proc. 26th IEEE Photovoltaic Specialists Conference, Anaheim, CA, pp. 1183-1186.
- [7] King, D.L., 1996, "Photovoltaic Module and Array Performance Characterization Methods for all System Operating Conditions", Proc. NREL/SNL Photovoltaics Program Review, AIP Press, Lakewood, CO, 347-368.
- [8] King, D.L., Kratochvil, J.A., and Boyson, W.E, 1997, Measuring Solar Spectral and Angle-of-Incidence Effects on Photovoltaic Modules and Solar Irradiance Sensors", Proc. 26th IEEE Photovoltaic Specialists Conference, Anaheim, CA, pp. 1113-1116.
- [9] King, D.L., Kratochvil, J.A., and Boyson, W.E, 1998, "Field Experience with a New Performance Characterization Procedure for Photovoltaic Arrays", Proc. 2nd World Conference and Exhibition on Photovoltaic Solar Energy Conversion, Vienna, Austria.
- [10] King, David L., “Sandia’s PV Module Electrical Performance Model (Version, 2000),” Sandia National Laboratories, Albuquerque, NM
- [11] 2000, PV-Design Pro, Solar Design Studio, v4.0, Maui Solar Energy Software Corp., Haiku, HI.
- [12] 2000, TRNSYS, v15, Solar Energy Laboratory, University of Wisconsin, Madison, WI.

EVALUATING BUILDING INTEGRATED PHOTOVOLTAIC PERFORMANCE MODELS

Mark W. Davis, A. Hunter Fanney, and Brian P. Dougherty
National Institute of Standards and Technology, Gaithersburg, MD 20899-8632

ABSTRACT

Predictive performance tools could accelerate the implementation of building integrated photovoltaics (BIPV). The National Institute of Standards and Technology (NIST) seeks to improve and validate previously developed computer simulation tools with experimental data collected in a building integrated photovoltaic "test bed." Twelve months of performance data has been collected for BIPV panels using four different cell technologies: crystalline, polycrystalline, silicon film, and triple-junction amorphous. Two panels using each cell technology were present, one without any insulation attached to its rear surface and one with insulation attached to its rear surface. Two predictive performance tools were investigated: IV Curve Tracer, a photovoltaic model developed by Sandia National Laboratories (SNL), and PHANTASM, a BIPV predictive tool developed by the Solar Energy Laboratory at the University of Wisconsin. The performance data associated with the eight panels in the BIPV "test bed", along with meteorological data, was compared to the predictions of the SNL and PHANTASM models.

INTRODUCTION

Predictive performance tools are an important factor in the success of any technology. An effective performance model would accurately predict the annual energy production given the orientation of the proposed photovoltaic system, typical weather conditions for the geographic region, the nominal performance of the specified BIPV technology, and the proposed coverage area of the BIPV application. The predicted energy production would subsequently be used to compute the energy and cost savings for different cell technologies and system orientations.

The National Institute of Standards and Technology created a building integrated photovoltaic test facility to evaluate predictive performance tools [1]. The facility includes a "test bed" for side-by-side testing of BIPV products. During the calendar year 2000, four different cell technologies, crystalline, polycrystalline, silicon film, and triple-junction amorphous, were present in the "test bed." Two panels of each cell technology were installed, one panel without backside insulation and one with insulation attached to the rear surface of the panel. The 102 mm (4 in) thick extruded polystyrene insulation has a nominal R-value of 3.5 m²·K/W (R-20). Twelve months of performance data was recorded at five min. intervals, including

peak power output, peak power voltage, peak power current, panel temperature, and meteorological data. A solar tracking facility is used to characterize the electrical performance of the panels used in the "test bed." A rooftop meteorological station measures the total horizontal, horizontal diffuse, and the direct beam irradiance; the outdoor ambient temperature; and the wind speed and direction. These facilities provide the measurements needed to evaluate BIPV predictive performance tools. The measured "test bed" performance [2,3] is compared to the performance predicted with two simulation programs: Sandia National Laboratories' IV Curve Tracer [4] and the University of Wisconsin's PHANTASM [5]. This paper describes the performance models and compares measured results to the model predictions.

SIMULATION MODELS

A number of publications have described the model developed by Sandia National Laboratories to predict the electrical output of photovoltaic panels [6,7,8,9]. The equations presented in this paper represent SNL's latest implementation of the model [10]. The premise of this performance model is that the I_{mp} , V_{oc} , and V_{mp} of a photovoltaic module can be described as functions of I_{sc} and the cell temperature. The short-circuit current is assumed to be dependant on the beam and diffuse irradiance, air mass, incident angle, and panel temperature. The effective irradiance compares the short-circuit current at any meteorological conditions with the short-circuit current at standard rating conditions. The remaining performance parameters (I_{mp} , V_{oc} , and V_{mp}) are predicted using the effective irradiance and several empirical coefficients, as well as the respective temperature coefficients.

A large number of performance parameters that are not provided by manufacturers are required. Temperature coefficients for the maximum power current and voltage, polynomials describing the effect of air mass and incident angle, and an empirical diode factor are a few of the less-common parameters that a system designer would need. The developers have provided these obscure values in a large database of parameters for a number of popular pre-fabricated panels. In the case of custom-fabricated BIPV panels, however, these parameters are not available. Once the parameters are acquired, the implementation of the model is simple, and several programs utilize the SNL model, including IV Curve Tracer [4] and PV-Design Pro [11].

The PHANTASM model, developed by the University of Wisconsin, requires fewer parameters than the SNL model, and most of the parameters are commonly provided by panel manufacturers, such as the electrical performance at standard rating conditions and the short-circuit current and open-circuit voltage temperature coefficients. The PHANTASM model approximates the photovoltaic cell with an electrical circuit that includes a current generator, diode, shunt resistor, and series resistor. For very high shunt resistances, assuming an infinite shunt resistance results in a simpler four-parameter model, as compared to the standard five-parameter model. An equation is derived to calculate the output current with respect to voltage for the four or five-parameter model. An iterative routine is used to find the combination of current and voltage that result in the maximum power output.

PHANTASM requires the transmittance of the glazing, absorptance of the PV cells, series resistance, shunt resistance, and the electron bandgap, which are not as readily available from cell or panel manufacturers. However, the series resistance can be calculated by the program for any panel using the temperature coefficients and the rating conditions. The shunt resistance is assumed to be the absolute value of the inverse slope of the I-V curve, which is commonly supplied with the panel specifications, at the short-circuit condition. A slope of nearly zero corresponds to a high shunt resistance, which indicates that the use of the four-parameter model is reasonable. In general, the five-parameter model is only used with amorphous PV technologies. The electron bandgap is given for crystalline silicon (1.12 eV), but it is not provided for other materials. With these parameters and others describing the orientation of the application, the energy output for a building integrated photovoltaic module can be predicted using PHANTASM.

MODEL PARAMETERS

The parameters used to model the panels in the BIPV “test bed” for the SNL model and the four and five-parameter PHANTASM model are shown in Table 1. As mentioned previously, many of these parameters are not readily available from module specification sheets. For the purpose of evaluating the performance models, the remaining parameters were determined by contacting the PV technology’s manufacturer or using measurement resources available at NIST.

The reference conditions, temperature coefficients, NOCT values, and the SNL model parameters ($f(\text{AMa})$, $f(\text{AOI})$, etc.) were measured using NIST’s solar tracking test facility [12] for each PV technology. The slope of the I-V curve at short-circuit conditions was computed with measured I-V curves from each panel. The electron bandgap was assumed to be 1.12 eV unless the manufacturer specified another value. Rauschenbach described a method to determine the series resistance of a module using two I-V curves measured at differing irradiance values [13]. This method was used to calculate the series resistance for each module. The resulting values closely matched those measured using a dark I-V procedure by

Table 1. SNL and PHANTASM Model Parameters

		Single Crystalline	Poly-crystalline	Silicon Film	Triple Junction Amorphous
Reference Conditions					
P_{mpo}	(W)	103.96	133.40	125.78	57.04
I_{sco}	(A)	5.11	4.37	4.25	4.44
V_{oco}	(V)	29.61	42.93	41.50	23.16
I_{mpo}	(A)	4.49	3.96	3.82	3.61
V_{mpo}	(V)	23.17	33.68	32.94	16.04
NOCT	(°C)	316.2	316.9	316.5	311.1
NOCT (Ins)	(°C)	337.9	340.1	338.6	328.5
Temperature Coefficients					
α_{isc}	(A/°C)	0.00468	0.00175	0.00238	0.00561
α_{imp}	(A/°C)	0.00160	-0.00154	0.00018	0.00735
β_{voc}	(V/°C)	-0.1300	-0.1524	-0.1528	-0.0931
β_{vmp}	(V/°C)	-0.1304	-0.1536	-0.1591	-0.0477
SNL Model Parameters					
$f(\text{AMa})$	Cnst	9.38E-01	9.36E-01	9.18E-01	1.10E+00
	Ama	6.22E-02	5.43E-02	8.63E-02	-6.14E-02
	AMa ²	-1.50E-02	-8.68E-03	-2.45E-02	-4.43E-03
	AMa ³	1.22E-03	5.27E-04	2.82E-03	6.32E-04
	AMa ⁴	-3.43E-05	-1.14E-05	-1.26E-04	-1.92E-05
$f(\text{AOI})$	Cnst	9.99E-01	1.00E+00	9.99E-01	1.00E+00
	AOI	-6.10E-03	-5.56E-03	-1.21E-02	-5.65E-03
	AOI ²	8.12E-04	6.55E-04	1.44E-03	7.25E-04
	AOI ³	-3.38E-05	-2.73E-05	-5.58E-05	-2.92E-05
	AOI ⁴	5.65E-07	4.64E-07	8.78E-07	4.70E-07
	AOI ⁵	-3.37E-09	-2.81E-09	-4.92E-09	-2.74E-09
C0		0.96	1.00	1.01	1.07
C1		0.04	0.00	-0.01	-0.10
C2		0.23	-0.54	-0.32	-1.85
C3		-9.43	-21.41	-30.20	-5.18
n		1.36	1.03	1.03	3.09
PHANTASM Parameters					
IV Slope @ Isc	(A/V)	-0.008	-0.004	-0.003	-0.020
Rs	(Ohm)	0.57	0.52	0.52	0.41
Bandgap	(eV)	1.12	1.12	1.14	1.60
$\tau\alpha$ Product		0.748	0.779	0.755	0.763
SNL Temperature Model Parameters					
Panel Type	Mount	a	b	ΔT	
Glass/Cell/Glass	Open	-3.473	-0.0595	2	
Glass/Cell/Glass	Close Roof	-2.976	-0.0471	3	
Glass/Cell/Tedlar*	Open	-3.562	-0.0786	3	

SNL for all four PV technologies except the triple-junction amorphous [14]. The product of glazing transmission measurements and bare cell absorptance measurements, each as a function of wavelength, were weighted according to the quantum efficiency of each module. The resulting value yields a transmittance-absorptance ($\tau\alpha$) product weighted according to its performance across the range of wavelengths that each module responds. The SNL temperature model parameters are used to predict the module temperature necessary for electrical performance predictions. The model developers provide values for three mounting scenarios. The “Glass/Cell/Tedlar” panel with an “open” mount was used to model the uninsulated panels, and the “Glass/Cell/Glass” panel with a “Close Roof” mount was used to model the insulated panels.

MODEL IMPLEMENTATION

In order to compare the measurements made by the BIPV “test bed” with those predicted by the SNL and PHANTASM models on an annual basis, both models are applied at five min. intervals over one year for eight different panels. IV Curve Tracer, which houses the SNL photovoltaic performance model, is used to trace a single I-V curve at specified input conditions. To simplify the use of the BIPV “test bed” meteorological data [2,3], the SNL model was implemented in a FORTRAN subroutine for

use in the TRNSYS [15] frontend. The predicted electrical output using the FORTRAN subroutine was compared to the predicted output using IV Curve Tracer. As expected, results from the TRNSYS subroutine matched those of IV Curve Tracer. The PHANTASM model is an extension of an existing TRNSYS subroutine for predicting the performance of photovoltaics. Therefore, the TRNSYS subroutine was used to calculate the predicted energy output for the eight BIPV panels in the “test bed.”

RESULTS

All three models (SNL, PHANTASM four-parameter, and PHANTASM five-parameter) were applied to the eight panels present in the BIPV “test bed” over the course of a year. The electrical output of the models are compared to the measured electrical output of each panel. The measured accumulated energy is compared to the predicted energy output directly, which is expressed as a positive

Table 2. Monthly Comparisons of Predicted and Measured Energy Outputs for Eight BIPV Panels

Uninsulated Single Crystalline						Insulated Single Crystalline						
PHANTASM-4			PHANTASM-5		SNL	PHANTASM-4		PHANTASM-5		SNL		
Month	Diff (%)	R ²	Diff (%)	R ²	R ²	Diff (%)	R ²	Diff (%)	R ²	R ²		
January	-0.1	0.914	-1.6	0.906	0.7	0.916	-3.7	0.928	-5.0	0.918	-3.0	0.932
February	-1.1	0.955	-4.9	0.948	0.6	0.959	-3.3	0.963	-6.5	0.955	-1.8	0.967
March	-3.7	0.968	-8.9	0.959	-1.4	0.971	-5.3	0.968	-10.0	0.958	-3.1	0.972
April	-8.4	0.968	-16.8	0.950	-5.0	0.973	-9.4	0.967	-17.4	0.948	-6.2	0.973
May	-9.5	0.957	-20.8	0.925	-6.3	0.964	-8.9	0.959	-19.9	0.929	-5.9	0.966
June	-8.2	0.956	-20.6	0.918	-5.3	0.962	-7.2	0.959	-19.4	0.923	-4.5	0.964
July	-8.5	0.933	-20.2	0.897	-5.7	0.939	-7.5	0.936	-19.0	0.902	-4.9	0.942
August	-7.0	0.944	-16.4	0.921	-2.8	0.948	-6.3	0.946	-15.4	0.925	-2.3	0.950
September	-4.5	0.937	-10.2	0.925	-1.4	0.940	-4.6	0.939	-9.8	0.926	-1.6	0.942
October	-1.3	0.973	-4.3	0.968	0.4	0.976	-1.2	0.977	-3.6	0.972	0.4	0.980
November	-1.7	0.937	-5.3	0.929	0.8	0.938	-3.1	0.946	-6.1	0.937	-0.7	0.949
December	1.2	0.933	-3.3	0.928	2.8	0.933	-2.1	0.945	-5.9	0.939	-0.8	0.948
Total	-3.4	0.945	-9.2	0.935	-1.1	0.947	-4.6	0.952	-9.9	0.941	-2.5	0.956

Uninsulated Polycrystalline						Insulated Polycrystalline						
PHANTASM-4			PHANTASM-5		SNL	PHANTASM-4		PHANTASM-5		SNL		
Month	Diff (%)	R ²	Diff (%)	R ²	R ²	Diff (%)	R ²	Diff (%)	R ²	R ²		
January	0.3	0.926	-2.9	0.921	0.6	0.919	-4.8	0.942	-7.5	0.936	-4.8	0.938
February	-5.0	0.961	-2.9	0.957	0.2	0.958	-8.7	0.969	-6.4	0.964	-4.1	0.967
March	-1.6	0.970	-5.9	0.966	-1.7	0.969	-5.4	0.969	-9.2	0.963	-5.8	0.969
April	-4.0	0.971	-11.1	0.963	-4.5	0.972	-8.1	0.967	-14.7	0.956	-9.0	0.968
May	-3.6	0.960	-13.1	0.948	-6.8	0.961	-6.7	0.959	-15.7	0.942	-10.4	0.957
June	-1.3	0.960	-11.8	0.946	-6.6	0.957	-4.4	0.960	-14.3	0.941	-10.2	0.952
July	-2.3	0.935	-12.1	0.921	-7.1	0.932	-5.1	0.936	-14.4	0.918	-10.4	0.930
August	-2.3	0.945	-10.1	0.936	-3.6	0.945	-5.0	0.946	-12.3	0.934	-6.8	0.945
September	-2.4	0.938	-7.1	0.932	-2.2	0.937	-5.0	0.940	-9.2	0.932	-5.3	0.939
October	-0.8	0.977	-3.3	0.974	-0.3	0.976	-2.6	0.981	-4.7	0.978	-2.4	0.981
November	-0.3	0.947	-3.4	0.943	1.1	0.943	-3.7	0.958	-6.3	0.953	-2.6	0.958
December	2.8	0.944	-1.1	0.942	3.0	0.939	-2.3	0.959	-5.6	0.955	-2.5	0.958
Total	-1.4	0.951	-5.8	0.947	-1.4	0.948	-5.0	0.959	-9.0	0.953	-5.4	0.958

Uninsulated Silicon Film						Insulated Silicon Film						
PHANTASM-4			PHANTASM-5		SNL	PHANTASM-4		PHANTASM-5		SNL		
Month	Diff (%)	R ²	Diff (%)	R ²	R ²	Diff (%)	R ²	Diff (%)	R ²	R ²		
January	13.4	0.905	7.3	0.909	7.9	0.918	9.3	0.938	4.0	0.936	3.1	0.948
February	14.0	0.935	7.6	0.942	6.7	0.954	11.2	0.951	5.6	0.954	3.1	0.965
March	14.0	0.944	5.3	0.955	4.6	0.965	11.3	0.954	3.4	0.960	1.2	0.969
April	15.5	0.949	1.4	0.965	3.6	0.970	12.6	0.957	-0.7	0.967	0.1	0.972
May	22.0	0.915	2.1	0.954	4.1	0.956	20.2	0.922	1.1	0.955	1.5	0.959
June	27.6	0.874	5.1	0.941	6.4	0.947	25.7	0.884	4.1	0.942	3.8	0.952
July	25.1	0.858	4.1	0.910	4.8	0.923	23.4	0.867	3.3	0.912	2.4	0.929
August	21.1	0.894	4.9	0.925	6.0	0.937	19.8	0.901	4.3	0.927	3.8	0.943
September	14.9	0.905	5.3	0.915	4.0	0.930	13.7	0.912	4.7	0.918	1.8	0.936
October	12.4	0.956	7.2	0.962	4.5	0.974	12.4	0.961	7.9	0.964	3.4	0.979
November	13.2	0.927	7.2	0.931	7.5	0.941	11.3	0.948	6.0	0.948	4.7	0.960
December	16.6	0.921	9.4	0.930	10.0	0.937	12.5	0.951	6.1	0.954	5.1	0.964
Total	16.2	0.925	6.2	0.935	6.2	0.945	14.0	0.943	4.6	0.949	3.0	0.960

Uninsulated Triple-Junction Amorphous						Insulated Triple-Junction Amorphous						
PHANTASM-4			PHANTASM-5		SNL	PHANTASM-4		PHANTASM-5		SNL		
Month	Diff (%)	R ²	Diff (%)	R ²	R ²	Diff (%)	R ²	Diff (%)	R ²	R ²		
January	-6.0	0.943	-10.4	0.933	-6.1	0.958	-5.6	0.939	-9.3	0.930	-6.1	0.953
February	-9.1	0.960	-13.9	0.946	-3.8	0.971	-9.4	0.959	-13.5	0.947	-4.3	0.971
March	-16.0	0.947	-22.6	0.919	-3.4	0.973	-16.9	0.943	-22.8	0.917	-4.5	0.973
April	-24.1	0.918	-33.9	0.863	-2.0	0.975	-25.1	0.913	-34.2	0.860	-3.0	0.976
May	-30.1	0.866	-42.8	0.766	0.5	0.968	-30.3	0.865	-42.6	0.769	0.5	0.968
June	-31.7	0.841	-45.8	0.707	2.7	0.961	-31.8	0.840	-45.6	0.710	2.9	0.962
July	-31.7	0.824	-45.1	0.702	0.8	0.943	-31.7	0.824	-44.7	0.706	1.1	0.943
August	-26.8	0.874	-38.0	0.795	3.0	0.949	-26.9	0.873	-37.7	0.798	3.0	0.950
September	-19.4	0.903	-26.6	0.868	-0.7	0.943	-19.5	0.904	-26.1	0.870	-0.9	0.944
October	-8.4	0.974	-12.6	0.963	-0.6	0.984	-8.5	0.973	-12.0	0.963	-1.1	0.983
November	-4.6	0.955	-9.2	0.946	0.2	0.967	-5.5	0.955	-9.3	0.945	-1.1	0.968
December	1.1	0.956	-4.4	0.951	1.2	0.970	0.1	0.954	-4.6	0.948	-0.2	0.968
Total	-14.8	0.938	-22.2	0.912	-1.0	0.967	-15.2	0.937	-22.0	0.911	-1.5	0.966

percent difference from the measured value if the predicted value is higher, Table 2. The expanded uncertainty of the measurements is $\pm 1.2\%$. A second method of comparison is the statistical correlation coefficient, R^2 . Unlike the comparison of accumulated energy, the correlation coefficient compares the predicted output at each five min. data point. This provides a clearer picture of the precision of the model.

It is clear from Table 2 that the SNL model outperforms the two PHANTASM models overall with respect to percent difference and R-squared. This is to be expected considering the number of parameters that are required for the SNL model. The greatest yearly percent difference is 6.2 % for the uninsulated silicon film panel, and the greatest monthly percent difference is -10.4 % for the insulated polycrystalline panel in May and July. The four-parameter PHANTASM model performed well (less than 5 % difference) for the single crystalline and polycrystalline panels, but large differences were observed during the months of April through September for the silicon film and triple-junction amorphous panels. Likewise, large differences were found using the five-parameter PHANTASM model for the single crystalline and triple-junction amorphous during these same months. The large differences tended to occur during months in which high incident angles (approximately 75° at solar noon in June) were accompanied by low values of incident irradiance. The magnitude of the differences varied between models for each panel. For example, the low irradiance values and high incident angles did not seem to affect the five-parameter model on the silicon film panel, but the exact same meteorological conditions produced large differences between the predicted and measured energy output for silicon film panels using the four-parameter PHANTASM model. The opposite trend occurred for the polycrystalline panel.

The five-Parameter PHANTASM model should perform the same or better than the four-parameter PHANTASM model, which is a simplification of the five-parameter model, for each panel. More importantly, the five-parameter model, which is intended for use on amorphous panels (steeper I-V slopes), should outperform the four-parameter PHANTASM model for the triple-junction amorphous panel. Six of the eight panels were more closely modeled using the four-parameter model than the five-parameter model, including the triple-junction amorphous. However, the silicon film panel, which has the second steepest slope at short-circuit conditions, was more closely modeled by the five-parameter PHANTASM model than the four-parameter.

CONCLUSION

The SNL model closely models the measured performance of all eight panels in the NIST BIPV "test bed." The PHANTASM model does not produce results consistent with its basic premise, which indicates that the complete five-parameter model should better predict PV performance than the simplified four-parameter model. Only two of the eight panels were better modeled by the five-parameter PHANTASM model than the four-parameter.

Future work will investigate the abnormalities found in the PHANTASM models.

REFERENCES

- [1] Fanney, A.H., and Dougherty, B.P., 2001, "Building Integrated Photovoltaic Test Facility," ASME J. Solar Energy Engineering, **123**, pp. 194-199.
- [2] Fanney, A.H., Dougherty, B.P., and Davis, M.W. 2001, "Performance and Characterization of Building Integrated Photovoltaic Panels," Proc. IEEE PVSC May 2002.
- [3] Fanney, A.H., Dougherty, B.P., and Davis, M.W. 2001, "The Measured Performance of Building Integrated Photovoltaic Panels," ASME J. Solar Energy Engineering, **123**, pp. 187-193.
- [4] 2000, Sandia Photovoltaic Performance Model I-V Curve Tracer, Maui Solar Energy Software Corp., Haiku, HI.
- [5] 1999, PHANTASM, Solar Energy Laboratory, University of Wisconsin, Madison, WI.
- [6] King, D.L., Kratochvil, J.A., and Boyson, W.E, 1997, "Temperature Coefficients for PV Modules and Arrays: Measurement Methods, Difficulties, and Results", Proc. 26th IEEE Photovoltaic Specialists Conference, Anaheim, CA, pp. 1183-1186.
- [7] King, D.L., 1996, "Photovoltaic Module and Array Performance Characterization Methods for all System Operating Conditions", Proc. NREL/SNL Photovoltaics Program Review, AIP Press, Lakewood, CO, 347-368.
- [8] King, D.L., Kratochvil, J.A., and Boyson, W.E, 1997, "Measuring Solar Spectral and Angle-of-Incidence Effects on Photovoltaic Modules and Solar Irradiance Sensors", Proc. 26th IEEE Photovoltaic Specialists Conference, Anaheim, CA, pp. 1113-1116.
- [9] King, D.L., Kratochvil, J.A., and Boyson, W.E, 1998, "Field Experience with a New Performance Characterization Procedure for Photovoltaic Arrays", Proc. 2nd World Conference and Exhibition on Photovoltaic Solar Energy Conversion, Vienna, Austria.
- [10] King, David L., "Sandia's PV Module Electrical Performance Model (Version, 2000)," Sandia National Laboratories, Albuquerque, NM
- [11] 2000, PV-Design Pro, Solar Design Studio, v4.0, Maui Solar Energy Software Corp., Haiku, HI.
- [12] Fanney, A. H., Davis, M.W., and Dougherty, B.P., 2002 "Short-Term Characterization of Building Integrated Photovoltaic Panels", Proc. Solar Forum 2002, Reno, NV
- [13] Rauschenbach, H.S., 1980, *Solar Cell Array Design Handbook*, Van Nostrand Reinhold Co., New York, pp 390-391.
- [14] King, D.L., et al, "Dark Current-Voltage Measurements of Photovoltaic Modules as a Diagnostic or Manufacturing Tool", Proc. 26th IEEE Photovoltaic Specialists Conference, Anaheim, CA
- [15] 2000, TRNSYS, v15, Solar Energy Laboratory, University of Wisconsin, Madison, WI

* Certain trade names and company products are mentioned in the text or identified in an illustration in order to adequately specify the experimental procedure and equipment used. In no case does such an identification imply recommendation or endorsement by the National Institute of Standards and Technology, nor does it imply that the products are necessarily the best available for the purpose.

MEASURED PERFORMANCE OF A 35 KILOWATT ROOF TOP PHOTOVOLTAIC SYSTEM

A. Hunter Fanney

National Institute of Standards and Technology
100 Bureau Drive, MS 8632
Gaithersburg, MD 20899-8632

P: 301-975-5864, F: 301-975-5433, hunter@nist.gov

Eric R. Weise

National Institute of Standards and Technology
100 Bureau Drive, MS 8632
Gaithersburg, MD 20899-8632

P: 301-975-6470, F: 301-975-5433, eweise@nist.gov

Kenneth R. Henderson

National Institute of Standards and Technology
100 Bureau Drive, MS 8632
Gaithersburg, MD 20899-8632

P: 301-975-6470, F: 301-975-5433, khenders@nist.gov

ABSTRACT

A 35-kilowatt roof top photovoltaic (PV) system has been installed at the National Institute of Standards and Technology (NIST) in Gaithersburg, Maryland. The system, located on the flat roof that connects NIST's Administration Building to its adjoining conference and cafeteria facilities, produced NIST's first site-generated renewable energy on September 14, 2001. In addition to providing electrical energy and reducing monthly peak electrical loads, the rear surface of each module is laminated to 51 mm of extruded polystyrene enhancing the thermal performance of the roof. A unique ballast system secures the photovoltaic system, eliminating the need for roof penetrations. An instrumentation and data acquisition package was installed to record the ambient temperature, wind speed, solar radiation, and the electrical energy delivered to the grid. Additional solar radiation instruments were installed after determining that the original solar radiation sensor was influenced by reflections from the south-facing wall of the Administration Building's tower.

NIST's electric utility billing schedule includes energy and peak demand charges. The generation charges vary significantly depending upon the time interval - off-peak, intermediate, and on-peak - during which the energy is consumed. The schedule is divided into summer billing months (June-October) and winter billing months (November-May). During the winter billing months, the distribution, transmission, and generation peak demand charges are based on the greatest power demand imposed by the site on the grid. During the summer billing months an additional demand

charge is imposed to capture electrical demand during the on-peak time interval.

This paper summarizes the monthly and annual measured performance of the photovoltaic system. The monthly energy produced by the system is tabulated. Conversion efficiencies - computed using solar radiation measurements from a single photovoltaic cell radiation sensor, four thermopile-based radiation sensors located around the perimeter of the photovoltaic array, and a remotely located thermopile-based radiation sensor, are presented. Using the electric utility's rate schedule, the monetary savings credited to the photovoltaic system is determined by combining the cost of the displaced energy with the reduction in peak demand charges attributable to the photovoltaic system. Finally, using utility provided data and the Environmental Protection Agency's (EPA) Environmental Benefits Calculator, estimates are made of the avoided emissions of the photovoltaic system over its projected life span.

INTRODUCTION AND SYSTEM DESCRIPTION

An agency of the U.S. Department of Commerce, NIST's mission is to promote U.S. economic growth by working with industry to develop and apply technology, measurements, and standards. Approximately 2500 of NIST's 2800 employees are located in Gaithersburg, Maryland, the site of the rooftop photovoltaic system described within this paper. The photovoltaic system is located on a roof section that connects the tower portion of NIST's Administration Building

to adjoining cafeteria and conference room facilities, Fig. 1. System components include an array of photovoltaic modules, a DC to AC inverter, a step-up transformer, and electrical switch gear. Performance of the system is monitored using two data acquisition systems and various meteorological instruments.

The photovoltaic array consists of 234 active modules. Six additional modules, not electrically connected, were included for aesthetic considerations. Each module consists of 72 single-crystalline photovoltaic cells connected in series. The cells are laminated between a multi-layered polymer back sheet and layers of ethylene-vinyl acetate (EVA) for environmental protection and electrical isolation. The outer glazing of each module consists of 6 mm low-iron tempered glass.

Each PV assembly is laminated to 51 mm high spacers that are in turn laminated to 51 mm thick sheets of extruded polystyrene insulation, Fig. 2. The extruded polystyrene insulation provides additional insulation, approximately 1.76 m² K/W (R-10 °F·ft²·h/Btu), to the portion of the roof covered by the photovoltaic modules. The insulation pieces are interlocked with surrounding pieces by means of a “tongue and groove” system.

The outer photovoltaic module assemblies are secured by means of a concrete ballast system. This mounting system results in an assembly that can resist the uplifting forces of wind and eliminates the need for roofing penetrations. Based upon wind tunnel tests and subsequent calculations commissioned by the manufacturer [1], the design can withstand a 3-second 63 m/s (140 mph) wind gust. For the particular NIST installation, the design condition is a 3-second wind gust of 45 m/s (100 mph) [2].

According to the photovoltaic module manufacturer [3], each module produces 150 watts at standard rating conditions

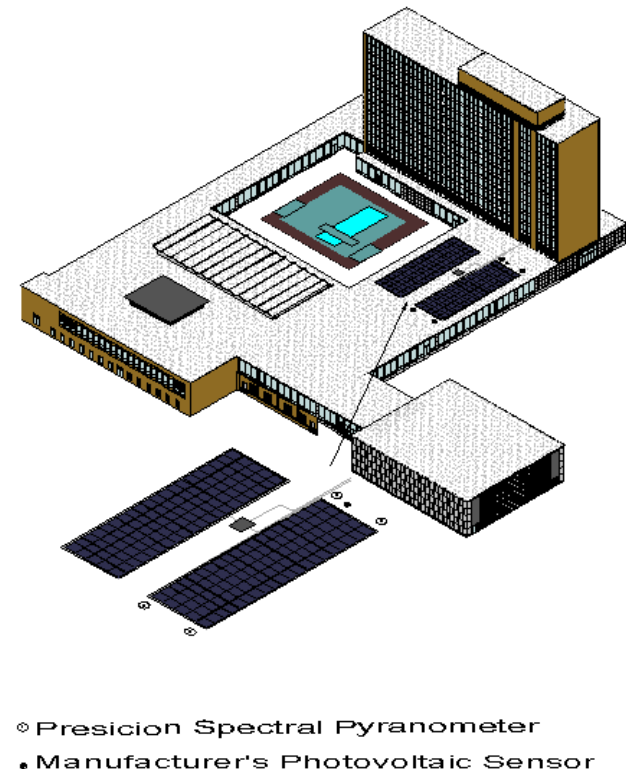


Figure 1 NIST’s Photovoltaic System

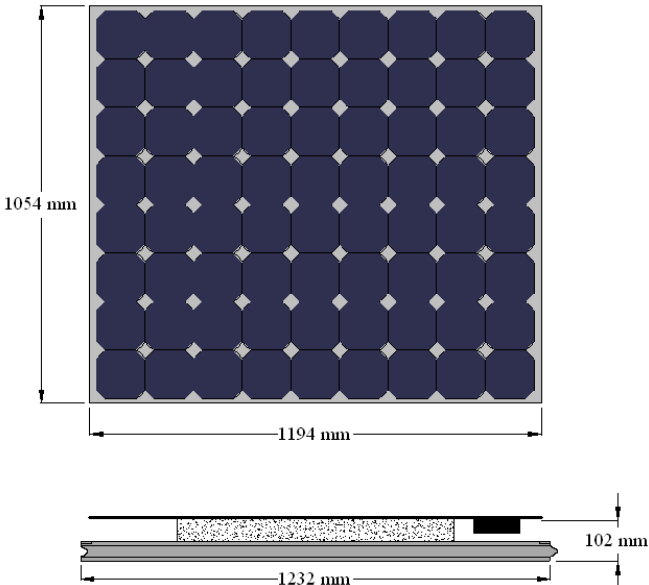


Figure 2 Photovoltaic Module

(1000 W/m², 25°C, and an absolute air mass value of 1.5). The 234 modules are electrically connected to form 18 strings, each string consisting of 13 modules in series. The eighteen strings are electrically connected in parallel. At standard rating conditions the photovoltaic array can produce 35 kW of direct current electrical power. Table 1 summarizes the electrical specifications associated with an individual module and the entire array.

The direct current from the photovoltaic array is converted to three-phase 208-volt alternating current by means of a grid-interconnected inverter. In addition to converting direct to alternating current, the inverter incorporates control logic that forces the photovoltaic array to operate at or near its maximum power point as well as providing several safety features. For example, if utility power is lost, the inverter automatically disconnects the photovoltaic system from the utility grid preventing the flow of electrical power into a possibly damaged grid system. Finally, a transformer

Table 1 – PV Module and System Array Specifications	
PV Module	Stabilized Power = 150 Wdc Open Circuit Voltage = 43.4 V Voltage at Peak Power = 34.0 V Short Circuit Current = 4.8 A Current at Peak Power = 4.4 A Dimensions = 1054 mm x 1194 mm
PV Array	No. of Modules in Series-Wired String = 13 No. of Parallel Strings in Source Circuit = 18 No. of Source Circuits = 1 Total Number of Modules = 234 Stabilized Power = 35 kW dc Open Circuit Voltage = 564 V Voltage at Peak Power = 442 V Short Circuit Current = 86 A Current at Peak Power = 79 A

is used to increase the 208-volt output from the inverter to 480 volts, the distribution voltage used within NIST facilities.

The manufacturer of the rooftop photovoltaic system installed a data acquisition system to measure ambient temperature, solar radiation, wind speed, and electrical power delivered to the grid. A silicon photovoltaic sensor provides the radiation measurement. Data is captured each minute and average or integrated, as appropriate, over 15-minute intervals. The amount of storage available for the minute and 15 minute data is limited to approximately two hours and two weeks, respectively.

On the rooftop of an adjacent building, NIST researchers maintain a separate meteorological station [4]. This meteorological station includes two precision spectral pyranometers (PSPs) that measure global horizontal radiation. From the start, the radiation measurements made using the manufacturer's supplied silicon photovoltaic sensor and the meteorological station's PSPs differed significantly. To help understand the cause of the discrepancy, four PSPs were installed in close proximity to the rooftop photovoltaic array. The outputs from these four pyranometers were measured and recorded by a separate data acquisition system every five minutes. This separate data acquisition system became operational in February 2002.

Prior to their deployment near the rooftop photovoltaic array, the four PSPs were placed next to the meteorological station's pyranometers for several days. The calibration factor for each of the four PSPs was adjusted slightly in an effort to match readings with one of the meteorological station's PSPs. The five PSPs agreed to within two percent of each other prior to adjusting the calibration coefficients. This procedure allowed direct comparisons between the solar radiation measured at the rooftop photovoltaic system versus the meteorological station.

VARIATION IN RADIATION MEASUREMENTS

A review of the photovoltaic system's performance one month after start-up revealed that the solar insolation measured at the array was substantially higher than the insolation recorded at the nearby meteorological station. Comparing the November 2001 total horizontal solar insolation values, for example, the manufacturer's supplied sensor recorded 95.5 kWh/m² versus 75.7 kWh/m² recorded by the meteorological station's PSP, a 26% difference. In order to rule out an instrumentation error, a precision spectral pyranometer was placed in close proximity to the manufacturer's silicon photovoltaic sensor.

During a limited comparison period, the manufacturer's sensor agreed within 3.6% of the pyranometer's reading. This agreement was well within the 5% accuracy stated by the manufacturer of the silicon photovoltaic sensor [5]. Both the precision spectral pyranometer and the photovoltaic system's sensor recorded readings approximately 26% greater than those recorded at the meteorological station. It was concluded that the large differences were not attributable to measurement errors but most likely due to reflections from the Administration Building's tower.

During the month of February 2002, four precision spectral pyranometers became available and were used to further explore discrepancies between the radiation measurements at the photovoltaic array's site and the nearby

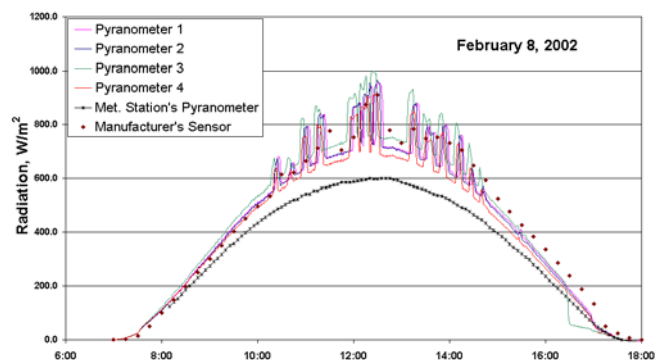


Figure 3 Solar Radiation Measurement Comparison

meteorological station. Initially the four sensors were positioned in close proximity to the manufacturer's sensor. The resulting data for the four pyranometers and the meteorological station's pyranometer are shown in Fig. 3 for a clear day (February 8, 2002). Data from the manufacturer's sensor, available every 15 minutes, are also displayed. The sensors located at the photovoltaic system's site recorded significantly higher values of solar radiation throughout the day. A very interesting phenomenon that occurs is the radiation spikes between 9:45 a.m. and 2:30 p.m. Visual observations on a subsequent day revealed that these solar radiation "spikes" were due to reflections from the vertical aluminum mullions associated with the Administration Building's curtain wall system.

In late March 2002, the four pyranometers were positioned at the four corners of the right photovoltaic sub-array as shown in Fig. 1. Figure 4 displays the monthly incident solar radiation measured by the manufacturer's sensor, the meteorological station's pyranometer and, commencing April 2002, the average of the four pyranometers. A comparison between the manufacturer's sensor and the meteorological station's pyranometers reveals an interesting trend. During the first five months, the solar radiation values recorded at the two locations differ by a significant amount. However, during the months of May, June and July, the readings at the two locations are in excellent agreement. During the months of August, September, and October the

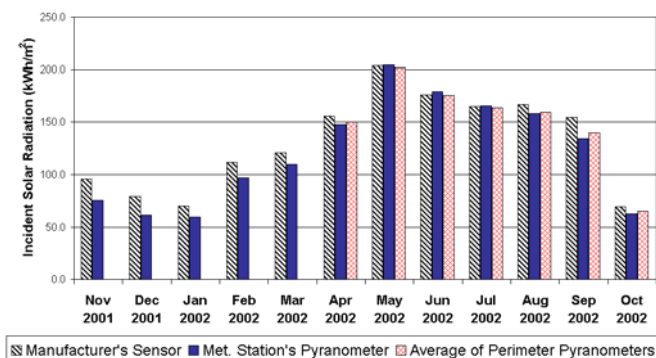


Figure 4 Monthly Incident Solar Radiation

manufacturer's sensor once again recorded higher values of incident solar radiation. This trend is due to the monthly variation in the sun's elevation. The sun's zenith angle for mid-June at solar noon is 16.2° compared to a zenith angle of 58° for November. The higher zenith angles, of the winter months, cause reflections from the Administration Building's tower and enhanced radiation on the manufacturer's supplied silicon photovoltaic sensor.

ELECTRICAL PERFORMANCE AND OVERALL SYSTEM EFFICIENCY

The electrical energy delivered by the photovoltaic system to the electrical grid for each billing cycle was computed by summing the 15-minute integrated values stored within the data acquisition system. Table 2 lists the monthly billing cycles and the energy supplied by the photovoltaic system. The efficiency of the solar photovoltaic system, including inefficiencies associated with the DC to AC inverter and the step-up transformer, in converting the incident solar energy into electrical energy delivered to the grid is computed using:

$$\eta_c = \frac{\int_{\tau_1}^{\tau_2} P \, d\tau}{A \int_{\tau_1}^{\tau_2} H_T \, d\tau} \quad (1)$$

where

A is a representative area, m²,
 H_T is the global incident solar radiation, W/m²,
 P is the system's alternating current electrical power output, W

and J_1 and J_2 correspond to the beginning and end of each billing cycle

The selection of an appropriate area and the source of the radiation measurement for computing the efficiency are somewhat subjective. Three different areas are used to present the efficiency results – cell area, module area, and footprint area. The cell area is the total number of active photovoltaic cells times the area of a single cell. The module area is defined as the glazed area of a single photovoltaic module times the number of electrically interconnected modules. Finally, the

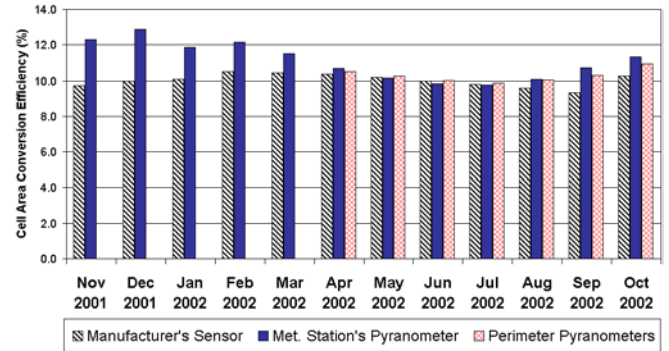


Figure 5 Cell Area Conversion Efficiencies

footprint area represents the total area of the roof installation, including the inactive modules, the perimeter curbing system, and the electrical interconnect boxes on the roof. The footprint area does not include the unoccupied space between the left and right arrays. The incident radiation measurement selected for computing the conversion efficiencies is also a subjective choice. At least three different choices are available – the radiation measurement provided by the silicon manufacturer's photovoltaic sensor, the meteorological station's precision spectral pyranometer or the average value measured by the four precision spectral pyranometers at the site of the photovoltaic installation.

Use of the manufacturer's sensor provides efficiency results that are available to the typical system owner. However, in this particular installation, the Administration Building's tower causes reflections on the manufacturer's sensor and a portion of the photovoltaic array. During time intervals in which solar radiation is reflected from the adjoining building tower, the efficiencies computed using the manufacturer's supplied sensor would be lower than efficiencies computed using radiation data from the meteorological station. The average value measured by the four precision pyranometers, during these time intervals, will yield higher efficiency results than those computed using the manufacturer's sensor and lower efficiencies than those computed using the meteorological station's pyranometer.

Table 2 – NIST Photovoltaic System Performance

Billing Period	Delivered Energy (kWh)	Conversion Efficiencies								
		Cell Area			Module Area			Footprint Area		
		Manufacturer's Sensor	Meteorological	Perimeter	Manufacturer's Sensor	Meteorological	Perimeter	Manufacturer's Sensor	Meteorological	Perimeter
Nov 01	2220.7	9.7	12.3	-	8.0	10.1	-	6.7	8.4	-
Dec 01	1896.2	10.0	12.9	-	8.2	10.6	-	6.9	8.9	-
Jan 02	1685.5	10.1	11.9	-	8.3	9.7	-	6.9	8.2	-
Feb 02	2800.1	10.5	12.2	-	8.6	10.0	-	7.2	8.4	-
Mar 02	3016.5	10.5	11.5	-	8.6	9.4	-	7.2	7.9	-
Apr 02	3777.6	10.4	10.7	10.5	8.5	8.8	8.6	7.1	7.4	7.2
May 02	4951.0	10.2	10.2	10.3	8.4	8.3	8.4	7.0	7.0	7.1
Jun 02	4202.5	10.0	9.8	10.0	8.2	8.1	8.2	6.9	6.8	6.9
Jul 02	3860.5	9.8	9.8	9.9	8.1	8.0	8.1	6.7	6.7	6.8
Aug 02	3826.0	9.6	10.1	10.1	7.9	8.3	8.3	6.6	6.9	6.9
Sep 02	3439.6	9.3	10.7	10.3	7.7	8.8	8.5	6.4	7.4	7.1
Oct 02	1702.0	10.3	11.3	11.0	8.4	9.3	9.0	7.1	7.8	7.5
Overall	35676.1	10.0	10.8	10.2	8.2	8.8	8.4	6.9	7.4	7.0

NOTE: Cell Area - 238.686 (m²); Module Area - 290.85 (m²); Footprint Area - 347.269 (m²)

The measured efficiency results for the photovoltaic system are given in Table 2. For each month the efficiencies are presented using cell, module, and footprint areas. For a given area, efficiencies are computed using solar radiation values measured by the manufacturer's sensor, the meteorological station's pyranometer, and the four pyranometers positioned around the photovoltaic array's perimeter. These efficiencies are respectively labeled as Manufacturer, Meteorological, and Perimeter in Table 2. Unlike module efficiencies reported at standard rating conditions, the Table 2 results include the effects of elevated operating temperature, the varying incident angle between the modules and sun, varying meteorological conditions, module soiling, and inverter and step-up transformer inefficiencies.

Efficiencies, computed using the cell area, are plotted for each month, using radiation measurements from the three available sources, Fig. 5. During the months that a large amount of solar radiation is reflected due to the high zenith angles (November 2001 - March 2002 and August 2002 - September 2002), efficiencies based on the manufacturer's sensor are significantly less than the efficiencies computed using the sensor. Based on the solar radiation measurements from the meteorological station, the overall conversion efficiencies for the entire monitoring period based on cell, module, and footprint areas are 10.8, 8.8, and 7.4%, respectively.

ECONOMIC SAVINGS

The total installed cost of the photovoltaic system, including the manufacturer's supplied data acquisition system, was \$239,945 or \$6.86 per DC watt at standard rating conditions. The photovoltaic system reduces NIST's electric utility bill by displacing electrical energy that would have been purchased and by lowering the site's peak electrical demand. The electric utility's energy and demand charges for large commercial customers like NIST, Table 3, are divided

Table 3-NIST Electric Utility Billing Schedule

		Summer Billing Jun-Oct		Winter Billing Nov-May	
Distribution Service Charge					
Customer		\$275.67	per mo	\$275.67	per mo
Kilowatt-hour Charge		0.590¢	per kwhr	0.590¢	per kwhr
Kilowatt Charge					
	On Peak	\$1.7738	per kw		
	Maximum	\$0.7350	per kw	\$0.7350	per kw
Transmission Service Charge					
Kilowatt-hour Charge		0.265¢	per kwhr	0.265¢	per kwhr
Kilowatt Charge					
	On Peak	\$0.7154	per kw		
	Maximum	\$0.2940	per kw	\$0.2940	per kw
Generation Service Charge					
Kilowatt-hour Charge					
	On Peak	3.994¢	per kwhr	3.265¢	per kwhr
	Intermediate	3.323¢	per kwhr	2.708¢	per kwhr
	Off Peak	1.745¢	per kwhr	1.438¢	per kwhr
Kilowatt Charge					
	On Peak	\$7.390	per kw		
	Maximum	\$3.040	per kw	\$3.040	per kw
NOTE:	On Peak (12 PM to 8 PM) Intermediate (8 AM to 12 PM) Off Peak (12 AM to 8 AM)				

Table 4 Economic Savings Associated with Photovoltaic System

Billing Period	Energy Savings	Max Peak Demand Savings	On-Peak Demand Savings	Thermal Savings	Total Savings
Nov 01	71.49	1.77	-	5.09	78.35
Dec 01	61.43	37.39	-	9.57	108.38
Jan 02	54.47	50.10	-	8.52	113.09
Feb 02	94.84	56.71	-	8.47	160.01
Mar 02	104.19	75.28	-	6.56	186.03
Apr 02	132.77	63.33	-	3.17	199.27
May 02	166.18	79.92	-	1.66	247.75
Jun 02	164.24	38.40	75.95	0.60	279.19
Jul 02	154.17	81.12	196.95	0.87	433.12
Aug 02	148.62	56.71	137.68	0.81	343.81
Sep 02	140.58	56.97	138.31	0.16	336.02
Oct 02	67.35	31.09	90.14	4.35	192.92
Total \$	1360.32	628.76	639.03	49.83	2677.94

into summer billing months (June-October) and winter billing months (November- May). Within a given billing month the charges are divided into distribution, transmission, and generation. The energy generation service charges are further divided into on-peak (12 p.m. to 8 p.m.), intermediate-peak (8 a.m. to 12 p.m.) and off-peak (12 p.m. to 8 a.m.) time intervals. The cost associated with a kWh of electricity can range from 4.85 cents during summer on-peak hours to a low of 2.29 cents during winter off-peak hours. During both winter and summer months, a maximum peak demand charge is imposed based upon the maximum thirty-minute power demand. During summer billing months, a second "on-peak" demand charge is assessed. This charge is based on the maximum thirty-minute demand recorded during the on-peak (12 p.m. to 8 p.m.) time interval. The maximum demand charge, including distribution, transmission, and generation is currently \$4.07 per kW. The additional summer month on-peak demand charge is \$9.88 per kW.

Electrical energy and power demand savings attributable to the photovoltaic system are given in Table 4 and Fig. 6 for each billing period. The savings associated with the energy displaced by the system is computed by multiplying the sum of the distribution, transmission, and generation charges, for the appropriate time interval, by the quantity of energy produced by the photovoltaic system during that time interval. The reduction in peak demand charges attributable to the

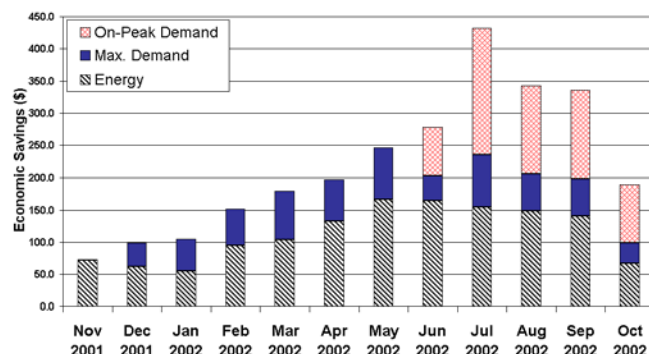


Figure 6 Economic Savings Associated with Solar Photovoltaic System

photovoltaic system are computed in the following manner. The date and time at which the maximum peak demand and, during the summer billing months, the on-peak demand charges occur are obtained from the electricity utility. The power output of the photovoltaic system during the utility's maximum peak demand and on-peak demand periods is obtained from the archived system performance data and subsequently multiplied by the sum of the appropriate distribution, transmission, and generation peak demand charges.

It is interesting to note, Fig. 6, that savings attributable to reducing NIST's power demand on the electric utility represents a significant fraction of the total economic savings associated with the photovoltaic system. In fact, during the months of July, August, and September 2002, the peak demand savings far exceed the energy displaced savings!

The 51-mm thick extruded insulation to which each PV module is laminated provides additional thermal insulation, approximately $1.76 \text{ m}^2\cdot\text{K}/\text{W}$ ($R\text{-}10 \text{ }^\circ\text{F}\cdot\text{ft}^2\cdot\text{h}/\text{Btu}$), to the portion of the Administration Building's roof occupied by the photovoltaic modules. The roof's original thermal resistance is assumed to be $4.05 \text{ m}^2\cdot\text{K}/\text{W}$ ($R\text{-}23.0 \text{ }^\circ\text{F}\cdot\text{ft}^2\cdot\text{h}/\text{Btu}$) [6]. This additional insulation reduces heat gains during months in which cooling is required and heat losses during months in which heating is required. The difference in heat transfer through the roof area occupied by the photovoltaic modules for each month was computed using the following equation,

$$Q = A \left[\frac{1}{R_o} - \frac{1}{R_{pv}} \right] \int_0^\tau (t_o - t_a) d\tau \quad (2)$$

where

t_o is the outdoor ambient temperature measured using the manufacturer's supplied sensor, $^\circ\text{C}$ ($^\circ\text{F}$)
 t_a is the $21.7 \text{ }^\circ\text{C}$ ($77 \text{ }^\circ\text{F}$) assumed indoor ambient temperature

A is the area of the roof occupied by the photovoltaic modules, m^2 (ft^2)

R_o is the thermal resistance of the original roof, $4.05 \text{ m}^2\cdot\text{K}/\text{W}$ ($R\text{-}23.0 \text{ }^\circ\text{F}\cdot\text{ft}^2\cdot\text{h}/\text{Btu}$)

R_{pv} is combined thermal resistance of the original roof and the PV system's insulation, $5.81 \text{ m}^2\cdot\text{K}/\text{W}$ ($R\text{-}33 \text{ }^\circ\text{F}\cdot\text{ft}^2\cdot\text{h}/\text{Btu}$).

and τ is the number of hours within each month (hr).

During months that cooling was required, the economic savings was computed by taking the difference between the heat gain associated with the original and enhanced roof section, dividing by the estimated overall efficiency of the mechanical chillers and associated distribution equipment [6], and finally multiplying by the appropriate electrical energy cost. The savings incurred during the heating season is computed by taking the difference between the heat loss associated with the original and enhanced roof, dividing by the estimated efficiency of the boilers and associated distribution equipment [6], and multiplying by the cost of natural gas used to fuel the boilers.

The savings attributed to the enhanced thermal insulation provided by the photovoltaic system are listed in Table 4. The monthly savings range from \$0.16 during the month of September 2001 to a high of \$9.57 computed for the month of

December 2001. The total savings due to the additional thermal insulation, \$49.83, is small in comparison to the displaced energy savings and peak demand reductions listed in Table 4. The small savings is partially attributable to the fact that the original roof was reasonably well insulated.

ENVIRONMENTAL IMPACT

The fuel mix of the electric utility providing service to the NIST site consists of 28.2% coal, 12.7% gas, 30% nuclear, and 28% oil [7]. Renewable energy sources account for approximately 1% of the current fuel mix. According to the utility [7], the quantity of sulfur dioxide, nitrogen oxides, and carbon dioxide associated with each megawatt hour (MWh) of electricity is approximately 4.8 kg, 1.4 kg, and 529 kg. Since November 1, 2001, the photovoltaic system has generated 35.7 MWh of electricity during its eleven months of operation. It is anticipated that the system will provide 1071 MWh over its expected 30-year life span. Thus, the projected 30 year lifetime avoided emissions for the photovoltaic system, based on the current fuel mix and air emissions per MWh of electricity, are 5141 kg of sulfur dioxide, 1499 kg of nitrogen oxides, and 566.6 metric tons of carbon dioxide.

A second means of estimating the avoided emissions is possible through the use of the Environmental Protection Agency's (EPA) web based solar calculator that computes emission reductions through the use of various solar technologies [8]. The web site requires that the user select the state in which the photovoltaic system is located and the power output of the photovoltaic array. The solar calculator predicts that 9630 kg of sulfur dioxide, 4020 kg of nitrogen oxide, and 1,579.4 metric tons of carbon dioxide will be avoided during the projected 30-year system lifespan from a 35 kW photovoltaic system in Maryland. The greater emission avoidance values projected by EPA's solar calculator are considerably greater than those projected using the information provided by the utility.

Reasons for the large discrepancies may include the fact that the EPA's solar calculator uses emissions data from all the electric utilities within the state of Maryland and assumes that the photovoltaic panels are tilted towards the sun at an angle that optimizes annual performance. Additionally, the EPA algorithm may also assume a conversion efficiency greater than the actual efficiency of the equipment used in this installation. Finally, it should be noted that neither methodology takes into account the reduced space conditioning loads resulting from the additional thermal insulation associated with the photovoltaic system.

SUMMARY

A 35-kilowatt roof top photovoltaic system has been installed at the National Institute of Standards and Technology in Gaithersburg, MD. The system became operational on September 14, 2001 and represents NIST's first on-site source of renewable energy. The total installed cost of the system was \$239,945.

During the past year the system has provided 35,676 kWh of electrical energy. In addition to displacing electrical energy that would have been purchased from the electric utility, the system has reduced the site's demand charges. During its first year of operation, the system has saved \$2678. To date, the savings in demand charges are essentially equivalent to

savings as a result of displaced energy. Annual savings attributable to the increased thermal resistance associated with the photovoltaic system amounted to \$49.83

Two different techniques were used to estimate the impact that the system will have on the electric utility's emissions. Using data provided by the electric utility, the avoided emissions associated with the system are 5141 kg of sulfur dioxide, 4499 kg of nitrogen oxides, and 566.6 metric tons of carbon dioxide. Using a tool included within EPA's Global Warming website, the projected avoided emissions are 9630 kg of sulfur dioxide, 4020 kg of nitrogen oxide, and 1,579.4 metric tons of carbon dioxide. The large discrepancy between the estimates in avoided emissions is currently being explored.

The area selected and the placement of the instrument used to measure solar radiation can have a significant impact on the reported conversion efficiency of a system. Annual conversion efficiencies of 10.8, 8.8, and 7.4 % were achieved using cell, module, and footprint areas, respectively. Reflected solar energy, from an adjacent building tower, resulted in computed efficiencies using the manufacturer's supplied radiation sensor significantly less than the efficiencies computed using a sensor that was not exposed to the reflected solar energy. The amount of reflected radiation, and thus the differences in computed efficiencies, varied based on the solar zenith angle. The greatest differences take place during the winter months when the highest zenith angles occur.

ACKNOWLEDGEMENTS

The authors would like to express their appreciation to Douglas Elznic, Mark Kuklewicz, and Ralph Whalen of NIST's Plant Division for providing the funding, engineering support, and system installation supervision in order to procure and install the photovoltaic system. The authors are also grateful to Tom Leyden and Lori Mitchell of the Power Light Corporation for providing guidance concerning the use of manufacturer's supplied data acquisition system. Merle Guyton is acknowledged for assisting in the calibration and installation of the solar radiation instruments used in this study. Sincere appreciation is extended to Paula Svincek for manuscript preparation.

REFERENCES

- [1] Neff, D.E., and Bienkiewicz, B., "Wind Tunnel Study of PowerGuard® RT Arrays," Final Report, PowerLight Corp., Berkeley, CA.
- [2] American Society of Civil Engineers, 7-98. (2000), "Minimum Design Loads for Buildings and Other Structures," Revision of ANSI/ASCE7-95.
- [3] Shell Solar Product Information Sheet, *Shell SP150-P, Photovoltaic Solar Module*, V2/SP150-P/05/02/US.
- [4] Fanney, A.H., Dougherty, B.P., Davis, M.W., 2000, "Building Integrated Photovoltaic Test Facility," *Proceedings of the, Solar 2000: Solar Powers Life, Share the Energy*, Conference, June 16-21, 2000, Madison WI.
- [5] LI-COR Radiation Sensors, <http://env.licor.com/Products/Sensors/rad.htm>.

[6] Personal communication with Mark Kuklewicz, Plant Division, NIST, December, 2002.

[7] Pepco-Environment Policy, Air Emissions, http://www.pepco.com/env_mdemis.htm.

[8] EPA Global Warming Site: Renewable Energy – Annual Emissions Avoided in Maryland, "<http://itdomino1.icfconsulting.com/epa/rew/rew.nsf/solar/impact?Open&MD1&1&35&&Photovoltaic>"

Energy Efficient and Affordable Small Commercial and Residential Buildings Research Program

*a Public Interest Energy Research Program
sponsored by the California Energy Commission*

Project 5.1 – Building Integrated Photovoltaics

Task 5.1.3c Economic Assessment of Building Integrated Photovoltaics in California

Vernon A. Smith, Architectural Energy Corporation
Fred W. Porter, Architectural Energy Corporation

September 2003

Prepared for
California Energy Commission

DISCLAIMER

This report was prepared as the result of work sponsored by the California Energy Commission. It does not necessarily represent the views of the Energy Commission, its employees or the State of California. The Energy Commission, the State of California, its employees, contractors and subcontractors make no warrant, express or implied, and assume no legal liability for the information in this report; nor does any party represent that the uses of this information will not infringe upon privately owned rights. This report has not been approved or disapproved by the California Energy Commission nor has the California Energy Commission passed upon the accuracy or adequacy of the information in this report.

Table of Contents

Introduction.....	4
Building Model Description	4
Building Integrated Photovoltaic Panels.....	5
PV Panels:.....	6
Inverters:	6
Climate Zones	6
Simulation Results	7
Baseline.....	7
Unshaded (Orientation A).....	7
Shaded (Orientation B)	8
First Cost Estimates	9
Conclusions.....	9
Recommendations.....	10

List of Figures

Figure 1 Sketch of Simulated Building.....	4
Figure 2 Plan View of Simulated Building Orientations	5

List of Tables

Table 1 Simulated Panel and PV Cell Characteristics	6
Table 2 General Inverter Characteristics for DOE 2.2 Simulations	6
Table 3 Climate Zones and Representative Cities	6
Table 4 Baseline Building Energy Simulation Results.....	7
Table 5 Economic Assessment Simulation Results	8
Table 6 Self-shading Degradation Limits for Orientation B.....	9

Introduction

Building integrated photovoltaics (BIPV) is a new alternative construction technology that serves as an exterior architectural finish and produces electric power from sunlight. Part of the promise of BIPV is to offset partially or wholly the PV cost by the cost of the replaced envelope material. BIPV assemblies are relatively new and there are few case studies with measured performance. There are, however, good modeling tools that should allow insight into the potential performance of BIPV in California.

This report documents a simulation study of BIPV on a small office building in four California climate zones. The following sections describe the key modeling assumptions, the BIPV characteristics, and the climate zones. The simulation results section compares the predicted energy savings against the baseline mode, followed by conclusion and recommendations sections.

Building Model Description

A 30,000 sf, three-story office building was selected as the assessment baseline building type. It has an “L” shaped floor plan with 10,000 sf per floor. The construction is structural steel with a typical curtain wall consisting of glazing and insulated opaque sections. Floor-to-floor height is 14 feet, with a 4-foot plenum section between each floor. The long sides of the “L” floor plate are 120 feet in length. Figure 1 is a 3-D rendering of the building.

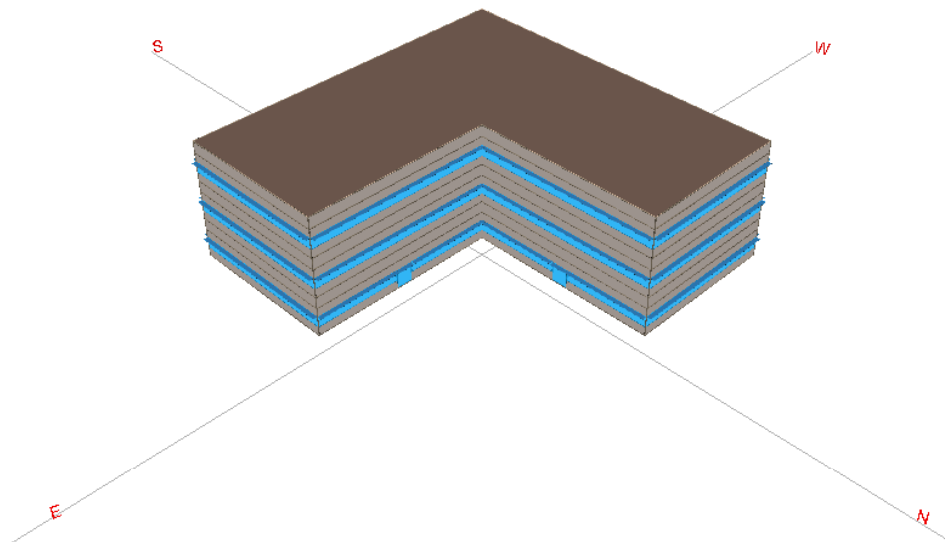


Figure 1 Sketch of Simulated Building

The envelope, lighting, and HVAC systems meet minimum Title 24 energy requirements. Occupancy was assumed to be from 8 am to 6 pm weekdays. The building is unoccupied on weekends and holidays. No parking lot or external lighting was assumed as part of the model.

The HVAC plant for the modeled building was assumed to have a water-cooled 120-ton centrifugal chiller and a 500,000 Btu/h boiler. The secondary distribution system was assumed to be a VAV system with hot water reheat.

Building Integrated Photovoltaic Panels

The simulated building has three levels of spandrel panels available for PV installation, each 120 feet long and 7 feet high. The windows are 3.75-feet high with the bottom edge located about 3 feet above the floor. The façade has 1.5-foot overhangs immediately above the windows on each floor. In the optimum orientation, one long side of the building faces directly south and all areas of all three spandrels are unshaded during all daylight hours (labeled “Orientation A” in Figure 2).

The PV panels were assumed to be three-feet in height and were arranged to fill the length of the south-facing side slightly above each window overhang.

An alternative building orientation was selected to explore the influence of self-shading. In this case the building is rotated 180° and the south facing spandrels are divided as shown in Orientation B of Figure 2. One section is in front, and will be unshaded all hours. The other section is "recessed" and will be shaded from direct sun for part of the day. See Figure 2 for the two orientations (the dashed blue line indicates the BIPV surfaces in plan view).

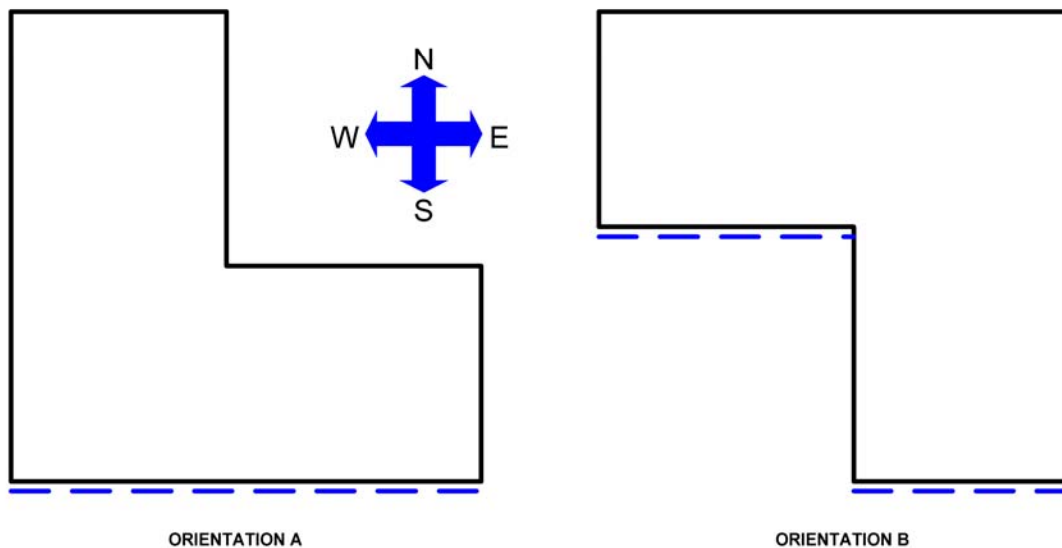


Figure 2 Plan View of Simulated Building Orientations

PV Panels:

The PV panels simulated were assumed to have conversion efficiency characteristics for the uninsulated panels described in the NIST paper titled *Measured Performance of Building Integrated Photovoltaic Panels*. Table 2 shows the assumed panel size, peak power output, total number of panels mounted on the curtain wall, and the power conversion efficiencies of each technology. The panels occupy about 1050 sf, or 21% of the total vertical surface area facing south (about 350 sf of PV panels per floor).

Table 1 Simulated Panel and PV Cell Characteristics

BIPV Type	Panel			Cell Conversion Efficiency %	
	Area (sf)	Rating (W)	Count	Uninsulated Backing	Insulated Backing
MonoC	17.5	133.4	20	10.3	9.9
PolyC	17.5	125.8	20	9.7	9.4
SiFilm	17.5	104.0	20	6.0	5.8
TripleJ	21.8	57.0	16	5.9	6.0

Inverters:

No specific inverter size, type, or electrical characteristics were specified. In a real installation, the size and voltage of panels, the fill factor, number of panels in series, and inverter characteristics will need to be coordinated to achieve reasonable performance. In order to minimize the effect of inverter and string variations on the results presented here, each PV system was modeled with *all panels in parallel*. A different virtual inverter was assumed for each PV panel type, with characteristics listed in Table

Table 2 General Inverter Characteristics for DOE 2.2 Simulations

Power	1.2 x sum of peak power
Max-track volts	1.0 x open circuit volts
Min-track volts	0.5 x max-track volts
Min operating volts	0.3 x open circuit volts

Climate Zones

Four climate zones representing large population centers in coastal and inland areas were selected for the parametric simulations. See Table 3.

Table 3 Climate Zones and Representative Cities

Climate Zone	Representative City
CZ-03c	Oakland
CZ-06c	Long Beach
CZ-10c	Riverside
CZ-12c	Sacramento

Simulation Results

Baseline

A set of simulations was run to create a baseline in each climate zone. The simulated building has 100 - 180 kW monthly peak demand, depending on location and time of year, with the peak set during the summer in all locations. The cost calculations were based on Pacific Gas & Electric Company's A10a rate schedule for all locations. This rate schedule was used to show representative costs, not predicted costs based on prevailing utility rates in each location since other utilities serve the selected cities. The value of saved energy using the PGE A10a rate is about \$0.145/kWh.

Table 4 Baseline Building Energy Simulation Results

Climate Zone	Representative City	Total kWh	Peak Demand	Energy \$	Demand \$	Total \$	kWh/sf-yr
CZ-03c	Oakland	385,497	139	\$53,082	\$ 6,612	\$60,594	12.85
CZ-06c	Long Beach	423,554	157	\$58,384	\$ 7,453	\$66,737	14.12
CZ-10c	Riverside	427,310	169	\$58,950	\$7,735	\$67,586	14.24
CZ-12c	Sacramento	413,247	176	\$57,387	\$7,807	\$66,094	13.77
	Averages	412,402	160	\$56,951	\$7,402	\$65,253	13.75

Unshaded (Orientation A)

Table 5 shows the results for each panel type by climate zone. As might be expected, higher conversion efficiency yields greater energy production. Also, climate zones with higher overall solar radiation (less cloudy) yield greater energy production, although the differences among the four selected climate zones is relatively small.

The overall energy savings range from 0.8% to 2.0% and the cost savings range from 0.7% to 1.8% annually. Demand savings for the south orientation are greatest in winter when the sun angle is low, due to higher direct radiation to the panels. The effect on peak demand is almost zero, since the sun angle is very high in summer when the peak is set and the south orientation with the vertical mounting produces the least amount of electricity. Roof-mounted panels that are horizontal or mounted at low angles have the greatest production during the summer, coincident with peak demand.

Table 5 Economic Assessment Simulation Results

		Module			Array		Annual Savings		Normalized Annual Savings		
Climate Zone	BIPV Type	Area (sf)	Rating (W)	Count	Area (sf)	Rating (kW)	Net Energy (kWh)	Value (\$)	kWh/sf	kWh/kW	\$/kWh
Ctz03 - Bay Area											
	MonoC	17.5	133.4	20	1051.1	8.0	7,290	1,052	6.9	911	0.144
	PolyC	17.5	125.8	20	1051.1	7.5	7,304	1,059	6.9	968	0.145
	SiFilm	17.5	104.0	20	1051.1	6.2	5,285	760	5.0	847	0.144
	TripleJ	21.8	57.0	16	1047.1	2.7	3,124	464	3.0	1,141	0.149
Ctz06 - South Coast											
	MonoC	17.5	133.4	20	1051.1	8.0	8,310	1,176	7.9	1,038	0.142
	PolyC	17.5	125.8	20	1051.1	7.5	8,356	1,188	7.9	1,107	0.142
	SiFilm	17.5	104.0	20	1051.1	6.2	6,213	876	5.9	996	0.141
	TripleJ	21.8	57.0	16	1047.1	2.7	3,786	556	3.6	1,383	0.147
Ctz10 - Riverside											
	MonoC	17.5	133.4	20	1051.1	8.0	8,607	1,174	8.2	1,075	0.136
	PolyC	17.5	125.8	20	1051.1	7.5	8,745	1,202	8.3	1,159	0.137
	SiFilm	17.5	104.0	20	1051.1	6.2	6,579	892	6.3	1,055	0.136
	TripleJ	21.8	57.0	16	1047.1	2.7	4,136	576	4.0	1,511	0.139
Ctz12 - Sacramento											
	MonoC	17.5	133.4	20	1051.1	8.0	7,189	1,023	6.8	898	0.142
	PolyC	17.5	125.8	20	1051.1	7.5	7,336	1,049	7.0	972	0.143
	SiFilm	17.5	104.0	20	1051.1	6.2	5,256	745	5.0	843	0.142
	TripleJ	21.8	57.0	16	1047.1	2.7	3,309	485	3.2	1,209	0.147

Shaded (Orientation B)

The current version of the DOE 2.2 program does not integrate the effect of shading on BIPV arrays by other building surfaces. The effect of modest shading fractions is highly dependent on panel type and array wiring layout and these characteristics are not defined in the program inputs at this time. For example, the power output of a group of panels wired in series will be diminished to a greater extent by the shading of one panel, than the power output from a group of panels in parallel (or with independent inverters). However, it is possible to bound the shading degradation effect from the simulation reports.

The lower spandrel panels will be shaded to a greater degree than the upper ones. See Table 1 for degradation limits. The minimum degradation is listed in the column titled “% of Unshaded Radiation, Total.” The maximum degradation is listed in the column titled “% of Mostly Unshaded (> 90% Direct Sun) Sunny Hours.”

For example, the PV panels located above the first floor windows will receive a maximum of 82% of the total available annual solar radiation. The reason for this 18% decrease is self-shading due to the angle of the sun during certain parts of the year and the building layout. The worst case for the first floor BIPV would be a design with all

panels wired in series and with 10% of the PV panel area shaded. In this case it is likely that there would be no electric power output during this condition. The first floor BIPV, due to its location and wiring arrangement, would be able to use only about 50% of the available solar radiation. This results in overall lower electrical output and has a significant adverse affect on the economics of installing BIPV.

Table 6 Self-shading Degradation Limits for Orientation B

	% of Unshaded Radiation		% of Mostly Unshaded (>90% direct sun) Sunny hours
	Direct	Total	Direct
1st Floor	85%	82%	50%
2nd Floor	92%	87%	65%
3rd Floor	99%	95%	80%

First Cost Estimates

We were able to obtain reliable total-cost installation estimates for large roof-mounted PV arrays. For rooftop systems with rated peak output of 30 kW and greater, the estimated cost ranges from \$7 to \$10 per peak watt. It is our opinion that smaller systems such as the ones simulated will be slightly more expensive, probably in the range of \$8 to \$12 per peak watt.

The range in installed costs for a 2.7 to 8.0 kW installed system with 1050 sf of surface area would be \$22,000 to \$96,000, assuming that the nominal cost per peak watt applies to all four of the simulated PV panel types. The nominal cost per square foot of installed PV surface would range between \$21 – 91/sf.

Conclusions

A vertical south-facing panel has a small effect on building or system peak demand. Maximum building peak demand reductions were in Riverside and were about 20% of the rated panel output. Other sites and systems were as low as 5%. Peak demand was set during the summer due to air conditioning loads. Rooftop and/or parking lot shading structures provide a better match for reducing peak demand.

Simple payback periods for all locations are from about 10 to 45 years with currently available utility or government rebate and tax credit programs. The cost of BIPV may be offset in California by utility or government rebate programs by as much as 50%, but it is clear that vertically mounted curtain wall BIPV is expensive relative to other distributed power generation options. Rooftop and parking structure PV systems have better payback periods due to higher power production and coincidence in peak power production with peak cooling loads.

Recommendations

For new construction, vertical BIPV should be considered when the cost of the installed BIPV is less than the initially specified curtain wall material. This may be the situation for show case office buildings.

For new construction and retrofit, BIPV in vertical curtain-walls may have public relations value. Although this may be an intangible benefit, it directly demonstrates the building owner's commitment to sustainable design.

Curtain-wall mounted BIPV should be considered when installing a rooftop or parking lot system to take advantage of its public visibility. A rooftop system is usually hidden from public view. Adding curtain-wall mounted BIPV to a rooftop system project would likely lower the marginal installed costs of the curtain-wall mounted panels and provide a public relations benefit.